Dissertation
submitted to the
Combined Faculties for the Natural Sciences and for Mathematics
of the Ruperto-Carola University of Heidelberg, Germany
for the degree of
Doctor of Natural Sciences

presented by
Diplom-Physiker: Christian Mathias Müller
born in: Berlin
Oral examination: 06.07.2005

Cosmological Models and Observation

Referees: Prof. Dr. Christof Wetterich
Prof. Dr. Michael G. Schmidt

Kosmologische Modelle im Vergleich mit Beobachtungen

Zusammenfassung

Wir diskutieren detailliert die zugrundeliegende Theorie und den derzeitigen Stand der Beobachtungen in der Kosmologie. Wir benutzen eichinvariante Störungsrechnung um die linearen Störungsgleichungen herzuleiten und verwenden einen Matrixformalismus um die Anfangsbedingungen für numerische Integration zu erhalten. Mit der Software CMBEASY können wir die Modellvorhersagen berechnen und mit experimentellen Daten vergleichen. Um kosmologische Modelle schnell und bequem einzuschränken verwenden wir Markov Chain Monte Carlo Simulation. Wir beschreiben die Theorie und die spezielle Implementation in CMBEASY. Diese Werkzeuge werden dann benutzt um ein ΛCDM-Modell sowie ein Modell mit einer nichtverschwindenden Zustandsgleichung der Dunklen Materie einzuschränken. Wir betrachten ebenfalls die Auswirkungen einer Änderung der fundamentalen Kopplungen auf die Elementhäufigkeiten und formulieren eine modellunabhängige Herangehensweise, die verwendet werden kann, um die Vorhersage für jedes Modell zu erhalten, welches die fundamentalen Kopplungen zueinander in Beziehung setzt.

Cosmological Models and Observation

Abstract

In this work we give a detailed discussion of the basic theory and current observational status of cosmology. We introduce gauge-invariant perturbation theory to derive the linear perturbation equations and use a matrix formalism to find suitable initial conditions for numerical integration. With the cosmological software package CMBEASY we compute model predictions and compare these with experimental data. For constraining cosmological models quickly and conveniently we employ Markov Chain Monte Carlo simulation. We describe both the theory and the specific implementation in CMBEASY. These tools are then used to constrain a standard ΛCDM cosmology and a model with a non-zero equation of state of dark matter. We also consider the effect of a variation of the fundamental couplings on primordial element abundances, introducing a model-independent formulation that may be used to obtain predictions for any given model that relates the fundamental couplings to each other.

The scientist does not study nature because it is useful;
he studies it because he delights in it,
and he delights in it because it is beautiful.

Jules Henri Poincaré

Contents

– 1 –

Introduction

And he showed to them a vision, giving to them sight where before was only hearing; and they saw a new World made visible before them, and it was globed amid the Void, and it was sustained therein, but was not of it.

J. R. R. Tolkien, The Silmarillion

Cosmology has been with us since the first humans looked at the stars and tried to fit what they saw into a larger framework. But before the 20th century this endeavour to understand the universe was mainly restricted to theological or philosophical considerations. While some physical theories were proposed, proper empirical evidence was lacking and so the only progress possible in this direction was by 'taking a shot in the dark'. Distances and timescales in the universe are so large that only recently it has been possible to build the powerful instruments necessary to obtain data to falsify some of the theories.

Surprisingly enough, it was before the first modern cosmological observations were conducted that the basic theory for the description of the universe was formulated. In 1917 Albert Einstein applied his theory of general relativity to cosmology [1]. Lacking experimental data, he proposed a static universe by introducing the cosmological constant. Then, in 1922 Aleksandr Friedmann found that general relativity allows for an expanding universe [2]. The first cosmological observation was performed by Edwin Hubble in 1929 with the measurement of the distance-redshift relation of galaxies [3]. These observations confirmed that the universe was expanding and marked the beginning of observational cosmology. A number of cosmological models have been proposed since then, and as more and more experimental data became available, the big bang model emerged as the generally accepted basic framework of cosmology.

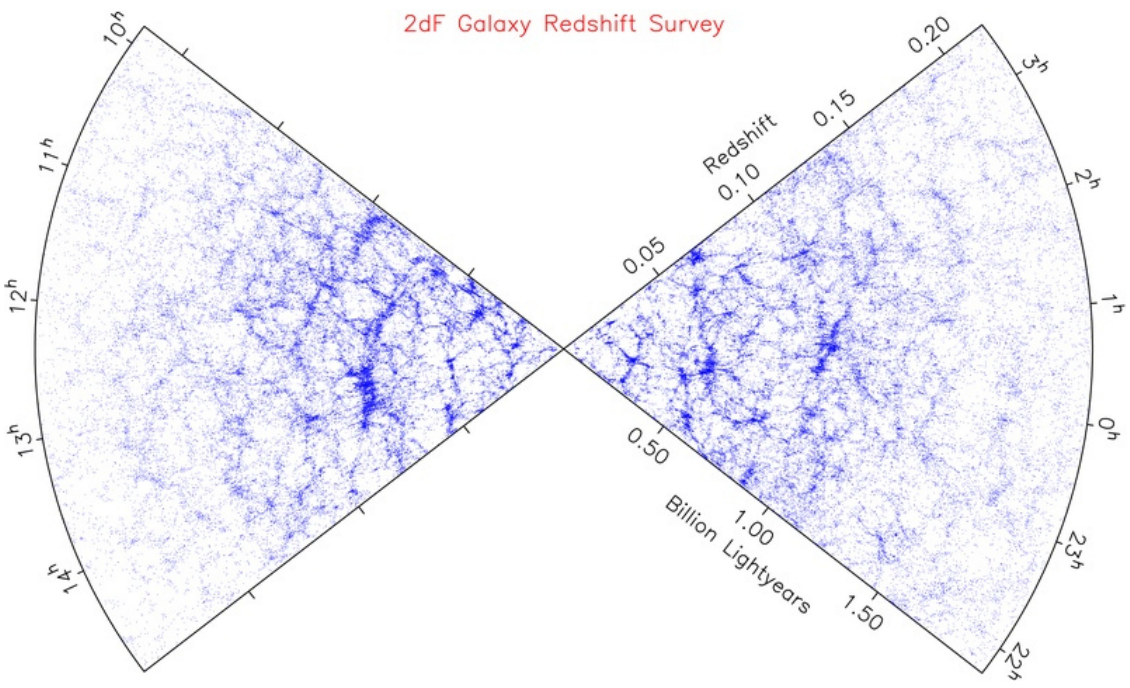

Figure 1.1: The final galaxy sample of the 2dFGRS survey. This is a slice of the universe with our galaxy at the center, each point represents one galaxy. The density of galaxies decreases with distance since the instruments can only resolve the bright objects.

During the last fifteen years cosmological observations have improved both in scope and precision. The first measurement of cosmic microwave background (CMB) anisotropies by the COBE satellite in 1992 [4] started a series of precision observations of the CMB, culminating with the unmatched accuracy of the WMAP measurements [5]. At the same time, powerful telescopes such as the Hubble telescope made it possible to look ever deeper into the cosmic past. Hundreds of supernovae have been measured and the quality of data has improved to a level where it can be used to determine the expansion history of the universe [6]. The Hubble parameter, known to a precision of about 50 % only a few years ago, has now been determined to within a few percent of error [7]. Galaxy surveys, observing hundreds of thousands of galaxies [8, 9], have given us an image of the distribution of matter in the local universe (see figure 1.1) making it possible to extract information with ever lower statistical error. All these probes have achieved a level of accuracy that enables us to rigorously constrain cosmological models.

Old problems were resolved, but more profound ones showed up and some surprising new discoveries were made. The existence of dark matter was more or less accepted two decades ago and observations indicated that matter (baryons

and cold dark matter) cannot make up more than $\approx 30\%$ of the energy content of the universe. As a consequence the consensus was that the universe was open, matter dominated and expansion was expected to slow down. Contrary to expectations it was discovered in 1998 that the expansion of the universe was accelerating instead [10–13]. Measurements of the cosmic microwave background anisotropies in 2000 showed that the spatial geometry of the universe is essentially flat. However, a flat matter dominated universe is too young to be consistent with observations. In addition, large scale structure measurements were incompatible with flat CDM model predictions where the matter anisotropies collapsed too quickly. Based on these findings, the present belief is that there is another energy component in the universe, quite fittingly termed 'dark energy'. Two main 'explanations' were suggested. The dark energy could be due to vacuum energy, termed the cosmological constant, or due a scalar field, termed quintessence [14, 15]. Since quintessence is a very versatile theory it cannot be easily ruled out, but the cosmological constant can if the equation of state of dark energy turns out to be different from -1. At present, however, both explanations agree with observation.

The amount and precision of the available data has ended the days of 'order of magnitude' estimation of cosmological parameters[1]. We have entered the era of precision cosmology. The amount and complexity of data and models have made it necessary to create tools for efficient and accurate computation of model predictions and compare them with experimental data. Advances in algorithms have made it possible to create software that can compute model predictions fast and accurately [16–18]. Comparison with data can be achieved in a variety of ways. Since the prediction is a non-trivial function of the model parameters, one has to resort to numerical computation. The grid approach simply discretizes the parameter space and computes the likelihood of each observational data set given the parameter set at each point. While this approach is simple, it is also computationally expensive since the available parameter space grows exponentially with the number of parameters. A better way to obtain useful and robust constraints from the data within an acceptable time frame and without use of excessive computing resources is by using Markov Chain Monte Carlo simulation [19]. The time and effort needed to create a software that contains all necessary routines and data sets is substantial, therefore it would be beneficial to have this software freely available.

This work intends to introduce such a tool – the CMBEASY software and its integrated ANALYZETHIS! package, the latter of which has been developed by the author in cooperation with Michael Doran [18, 20]. This software includes the necessary routines to compute model predictions for ΛCDM and quintessence

[1] Or, as Michael S. Turner put it: "The 'go-go' junk bond days of cosmology are over".

models, and can be easliy modified to accomodate other theoretical models. It contains an optimized Markov Chain Monte Carlo routine for constraining parameters. Most current cosmological data sets are included for convenience along with the likelihood computation routines. In addition, there is a graphical user interface for quick data analysis, all in one integrated software. With this, one can constrain cosmological models easily and quickly. We would like to add that we will be concerned exclusively with 'late' cosmology here, $T \lesssim 1$ MeV, and we will not discuss issues of early cosmology such as baryogenesis.

We will start with the basic description of cosmology in chapter 2. Assuming that the universe is homogeneous and isotropic, we derive some important equations needed later. We also describe the 'energy mix' of the universe from the perspective of the standard ΛCDM model. At this stage one already has all theoretical input that is needed to use current supernovae data. The homogeneous case is also the starting point for cosmological perturbation theory, presented in chapter 3. There we introduce gauge-invariant perturbation theory, which enables us to compute the model prediction for cosmic microwave background anisotropies and the large scale structure power spectrum. The initial conditions are derived using a matrix formalism. In chapter 4 we describe and discuss all the current experimental data sets which are included in the CMBEASY software. We briefly introduce other probes which are not yet implemented in CMBEASY, but will become increasingly important in the future such as Lyman-α forest and weak gravitational lensing observations. The theory of Markov Chain Monte Carlo simulation is described in chapter 5 along with the optimized implementation in our software. This method gives accurate and robust constraints on model parameters while being computationally inexpensive. We have then all the tools we need to constrain models. For illustrative purposes, we constrain a ΛCDM cosmology using these techniques. In chapter 6 we investigate a cosmological model which contains dark matter with a constant non-zero equation of state. In constrast to previous investigations, we also consider a negative equation of state. We show that this model, while tightly constrained, is not ruled out. Somewhat out of the main line of our treatment we discuss the effects of a variation in fundamental couplings on predictions of primordial element abundances. We provide an integrated approach that can be adapted to any model relating fundamental couplings to each other. We finish with our conclusions in chapter 8, some additional material can be found in the appendices. The work presented in section 3.3 was in collaboration with M. Doran, G. Schäfer and C. Wetterich, chapter 5 in collaboration with M. Doran and chapter 7 with G. Schäfer and C. Wetterich. The investigation of the model discussed in chapter 6 was suggested by C. Wetterich.

– 2 –

The Homgeneous Universe

There is a theory which states that if ever anybody discovers exactly what the Universe is for and why it is here, it will instantly disappear and be replaced by something even more bizarre and inexplicable. There is another theory which states that this has already happened.

Douglas Adams, The Hitchhiker's Guide to the Galaxy

In this chapter we will introduce the basic framework of cosmology, beginning with the homogeneous and isotropic universe. While this may seem too simplifying at first, it is nevertheless a good description at large scales. We will expand on this treatment in subsequent chapters and make frequent use of the equations and quantities defined here.

2.1 Basic Equations

The starting point for our considerations are the Einstein equations which relate the energy-momentum tensor to the geometric properties of spacetime[1],

$$G_{\mu\nu} = R_{\mu\nu} - \frac{1}{2} g_{\mu\nu} R = M_{\bar{p}}^{-2} T_{\mu\nu}. \tag{2.1}$$

Usually, these equations are difficult to solve for a given energy-momentum tensor, but in cosmology we can make use of symmetry. Measurements of the cosmic microwave background (CMB) by the COBE and WMAP satellites [26, 27] indicate that the CMB is isotropic to a large degree[2]. Large scale structure surveys

[1] For an introduction to the general theory of relativity and cosmology see [21–25].

[2] After the removal of the dipole contribution due to the motion of the solar system with respect to the cosmic rest frame, the anisotropies in the CMB are at a level of about 10^{-5}.

such as the SDSS and the 2dFGRS [8, 9] also show that galaxies are evenly distributed and that there seems to be no prefererred direction on the sky. From these observations one may conclude that, at least on very large scales, the universe is isotropic. Since we may assume that our place in the universe is in no way special this also means that the universe is homogeneous. These basic assumptions are also called the cosmological principle.

The most general form of the metric of a four-dimensional space-time which respects these symmetries is the Friedmann-Robertson-Walker metric

$$ds^2 = -dt^2 + a(t)^2 \left(\frac{dr^2}{1 - Kr^2} + r^2 d\theta^2 + r^2 \sin^2 \theta \, d\phi^2 \right), \tag{2.2}$$

where $K = -1, 0$ or $+1$ if the spatial geometry of the universe is open, flat or closed. The dynamics of the metric is contained in the scale factor $a(t)$. Observations indicate that the universe is most probably flat [5], which is in line with most theories of inflation. We will therefore consider only spatially flat universes in all that follows and set $K = 0$. We will also use conformal time τ from now on, which is defined by

$$d\tau = dt/a(t), \tag{2.3}$$

and all derivatives are with respect to conformal time. The metric we use for the homogeneous and isotropic, spatially flat universe is therefore

$$ds^2 = a(\tau)^2(-d\tau + d\mathbf{x}^2), \tag{2.4}$$

$$\text{i.e. } g_{\mu\nu} = \text{diag}\,(-a^2, a^2, a^2, a^2). \tag{2.5}$$

The scale factor $a(\tau)$ is normalized such that the scale factor today $a_0 = 1$, and we will use the shorthand notation $\mathcal{H} \equiv a'/a$ where $a' \equiv da/d\tau$. $\mathcal{H}$ is related to the normal Hubble parameter $H = \dot{a}/a$ by $\mathcal{H} = aH$ with $\dot{a} \equiv da/dt$.

Let us now turn to the right-hand side of equation (2.1), the energy-momentum tensor. Here, we will work exclusively from a fluid perspective and describe all forms of energy in the universe as fluids. The energy-momentum tensor for an ideal fluid with energy density ρ, pressure p and four-velocity u_μ is given by

$$T_{\mu\nu} = (\rho + p)u_\mu u_\nu + p g_{\mu\nu}, \tag{2.6}$$

or, with four-velocity $u^\mu = (a^{-1}, 0, 0, 0)$ in the cosmic rest frame:

$$T^\mu{}_\nu = \text{diag}\,(-\rho, p, p, p). \tag{2.7}$$

There is no net energy or momentum flow in the cosmic rest frame, since this would violate the isotropy and homogeneity requirement. Using energy-momentum conservation

$$T^\mu{}_{\nu;\mu} = 0, \tag{2.8}$$

yields then

$$\rho' + 3\mathcal{H}(\rho + p) = 0. \tag{2.9}$$

It is worthwhile to pause a litte at this point. This equation applies to the total energy density and the total pressure of the universe. But there is a variety of different forms of energy, e.g. photons, neutrinos, baryons and so on. If one species x interacts only gravitationally with the rest then eq. (2.9) applies for this species alone as well, since the energy-momentum tensor for this species is conserved separately.

We need to relate pressure p and energy density ρ. This is most conveniently done by the equation of state w_x of a component x, defined by

$$w_x \equiv p_x/\rho_x. \tag{2.10}$$

For relativistic particles (e.g. photons) $w_\gamma = 1/3$, and for non-relativistic particles such as baryons $w_b = 0$.

To determine the dynamics of the scale factor $a(\tau)$, we insert the FRW metric (2.4) and the energy-momentum tensor (2.7) into the Einstein equations (2.1) and find the Friedmann equation in flat space:

$$3M_{\bar{p}}^2\mathcal{H}^2a^{-2} = \rho(\tau). \tag{2.11}$$

The energy density today is given by

$$3M_{\bar{p}}^2H_0^2 = \rho^{(0)}, \tag{2.12}$$

with H_0 the Hubble constant. One frequently expresses energy densities relative to the total energy density as

$$\Omega_x \equiv \frac{\rho_x}{3M_{\bar{p}}^2\mathcal{H}^2a^{-2}}\ , \tag{2.13}$$

so that $\Omega_x^{(0)} = \rho_x^{(0)}/\rho_{\rm tot}^{(0)}$. Since we only consider spatially flat universes, we must have $\sum_x \Omega_x = 1$. If one can determine the contributions to the energy density, the equation of state of every component in the universe and their interactions, one has, essentially, a complete description of the past and future of the universe. See [28] for the currently known (and unknown) contributions.

Another very important quantity is the redshift z which is given by the measured wavelength λ_1 of a source relative to the laboratory wavelength λ_0

$$\frac{\lambda_0}{\lambda_1} \equiv 1 + z. \tag{2.14}$$

It is straightfoward to relate the redshift to the scale factor

$$\frac{1}{a} = 1 + z. \tag{2.15}$$

2.2 The Constituents of the Universe

We skipped over the problem of determining the constituents of the universe in the previous section. There are many cosmological observations that have led to the establishment of the so-called concordance model. Even though we will consider these observations later in this work, this may be a good point to discuss what is believed to be the 'energy mix' of the universe. We need to remember that this changes over time, and what we would like to discuss is the distribution of energy today. We would also like to emphasize that most of the numerical values here are model-dependent. We have taken the values from the SDSS team plain vanilla ΛCDM model [29] (see appendix B.2 for details). Frequently, we will employ the symbol h which is defined such that $H_0 = 100\ h\,\mathrm{km\,sec^{-1}\,Mpc^{-1}}$. From measurements of the local Hubble flow one finds $h = 0.72 \pm 0.08$ [7], for numerical values we have used $h = 0.7$ in this section. The temporal evolution of the 'energy mix' of the universe for this ΛCDM model is depicted in Fig. 2.1.

2.2.1 Photons

When we refer to photons we mean relic photons from the big bang. In the early universe, photons were the dominant part of the energy budget along with neutrons. During the era of recombination all interactions of photons with matter essentially ceased and these relic photon have been traveling through the universe ever since, redshifting as the universe expands. What we see as the cosmic microwave background is a redshifted image of the surface of last scattering. From the measured temperature of the CMB black body spectrum $T = 2.725 \pm 0.002$ K as determined by COBE [30] we can conclude that the energy density of photons today is negligible: $\Omega_\gamma = (2.471 \pm 0.004) \times 10^{-5}/h^2$. But at early times radiation was the dominating form of energy. Since photons are fully relativistic, their equation of state is $w_\gamma = 1/3$.

2.2.2 Baryons

Baryons are 'ordinary' matter such as protons and neutrons and their nuclear bound states. Suprisingly enough, observations of the CMB and primordial element abundances from the big bang nucleosynthesis show that the amount of baryons can only make a contribution of $\Omega_B = 0.0228/h^2$, or about 5% of the energy inventory. Since baryons are non-relativistic at temperatures considered in this work one takes their equation of state to be $w_B = 0$.

2.2.3 Neutrinos

Another well-known ingredient are relic neutrinos. They are believed to couple only weakly at the energies considered here. Consequently, when the expansion rate of the universe exceeded the weak reaction rates at $T \sim 1$ MeV, neutrinos have essentially ceased to interact and have been free streaming ever since. This transition is also referred to as 'decoupling'. In our calculation we take the neutrinos to be massless $w_\nu = 1/3$, though recent experimental evidence of neutrino oscillations suggests that neutrinos have mass. In fact, one may even use cosmological probes to set upper limits on the sum of the neutrino masses [5, 31–36]. The current upper limit if the mass may not be neglected is $\Omega_\nu < 0.04$ [29]. If the mass may be neglected, then $\Omega_\nu = 1.68 \times 10^{-5}/h^2$.

2.2.4 Dark Matter

The contribution of baryons to the total energy budget is, as we have seen, rather small. Present theory assumes that the matter density flucuations visible in the CMB spectrum grow to form clusters and galaxies, but the amount of baryons is insufficient to form the structures we see today. Also, from the rotation curves of galaxies one can deduce that the visible mass is much too small to account for the observed rotation. There needs to be another, invisible form of energy that can cluster. The existence of this so-called 'dark matter' was first postulated by Zwicky [37] and has been reinforced by recent observational evidence such as gravitational lensing. The common assumption is that dark matter is a form of weakly interacing massive particle (WIMP) [38]. There is a number of direct dark matter searches such as EDELWEISS [39], CRESST [40], CDMS [41] and DAMA [42], but so far there has been no direct detection of a WIMP[3]. Every bit of evidence for the existence of dark matter is of astrophysical or cosmological origin. Given these facts, one may wonder whether dark matter is a particle at all. We will discuss this point in chapter 6. In the concordance model, dark matter is assumed to be cold (the CDM in ΛCDM), hence $w_{DM} = 0$. The contribution to the total energy budget is $\Omega_{DM} = 0.123/h^2$, or about 25 %.

2.2.5 Dark Energy

As mentioned before, CMB measurements indicate $\Omega_{tot} = 1$, but so far we have only $\approx 30\%$ of that. Also, by observing the expansion history through the luminosity distance of supernovae [10–12] it was found that the expansion of the universe has accelerated recently, which requires a total equation of state $w < -1/3$. A spatially flat matter dominated universe is ruled out due to its low age which

[3] We do not wish to discuss the reported claim of a deteced annual modulation by DAMA [42].

is in conflict with observation. Further, large scale structure growth would be too fast. As a consequence, one introduces a new form of energy. It does not seem to cluster, but rather appears to be homogeneously distributed in the universe, and has been termed 'dark energy'. In the concordance model, the dark energy is assumed to be the cosmological constant Λ, originally introduced by Einstein to make the universe static [1]. It can be thought of as vacuum energy and has equation of state $w_\Lambda = -1$. As good as this looks at first sight, there are uncomfortable theoretical problems associated with this [43]. First, from a quantum field perspective one would expect the energy density of Λ to be precicely zero due to some unknown symmetry or at the order of $\sim M_{\bar{p}}^4$. However, from eq. (2.12) and the measurement of the Hubble parameter we obtain $\rho_\Lambda \sim 10^{-64}\text{GeV}^4$ which is a long way from $M_{\bar{p}}^4 \sim 10^{73}\text{GeV}^4$. Furthermore the energy density of Λ is constant throughout the history of the universe, necessitating strong fine tuning in order that it become important just today. As a consequence, there is a large number of possible alternative models for dark energy such as scalar field dark energy [14, 15, 44], topological defects [45] and modifications to gravity [46, 47] to name just a few. Models with $w_{DE} < -1$, so-called phantom cosmologies, have also been proposed [48]. In this work we will only concern ourselves with quintessence and the cosmological constant as models of dark energy. In the concordance model, the dark energy makes up most of the current energy density of the universe, $\Omega_\Lambda \approx 0.6 - 0.7$. For a review of the experimental evidence for dark energy see [49] and references therein.

2.2.6 Gravitational Waves

A very important ingredient for setting constraints on models of inflation are primordial gravitational waves which are believed to have been generated during inflation [50]. These gravitational waves contribute to the CMB anisotropy. In contrast to Thomson scattering which creates only E-mode polarization, the gravitational waves generate also B-mode polarization. Detection of B-mode polarization in the CMB may thus be used to identify gravitational waves[4]. At present, no gravitational wave signature has been identifed in the CMB, the upper limit is $\Omega_{GW} \lesssim 10^{-10}$, but this number is a bit misleading – this is already the level of the perturbation, and hence their impact on the CMB is expected to be detectable with near future CMB experiments such as PLANCK [52].

[4]Weak lensing of the CMB by large scale structure also generates B-mode polarization. It is therefore important to distinguish these two sources of polarization [51].

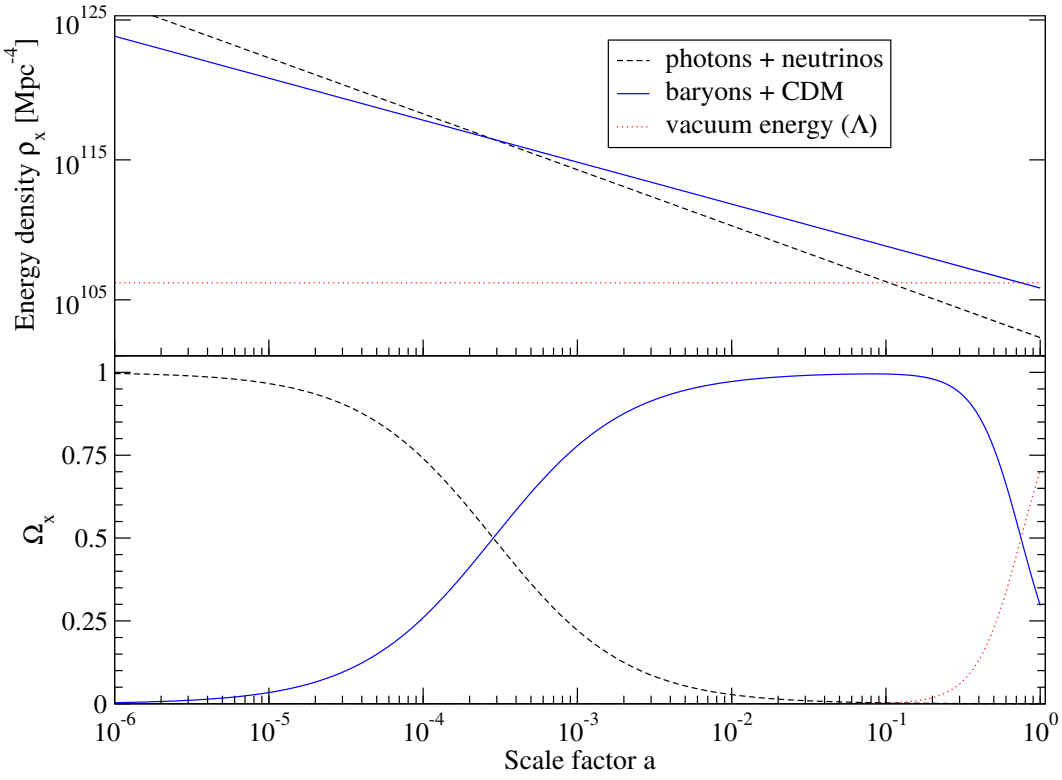

Figure 2.1: Evolution of the different contributions to the total energy density of the universe. Absolute contribution in terms of energy density (top) and relative to the total energy density (bottom) of radiation (dashed, black), matter (straight, blue) and vacuum energy (dotted, red). Parameters as in the ΛCDM plain vanilla model of [29] (see also appendix B.2).

2.2.7 The Rest

There are some more contributions, such as cosmic rays and magnetic fields, post-stellar radiation and more. These are not relevant for our purposes since they are subdominant and have no noticable impact on current cosmological probes and will not be treated here. The interested reader is referred to [28] for a review.

2.3 Quintessence

In the previous section we mentioned scalar field dark energy as a possible alternative to model dark energy. The basic idea is to postulate the existence of a scalar field χ with a self-interacting potential $U(\chi)$. This form of dynamical dark energy has been termed quintessence. Unfortunately, the specific form of the potential can – at present – only be postulated. Since quintessence was first intro-

duced [14, 15, 53–55] a number of different models have been proposed. Many of these models feature tracking behaviour, that is, their evolution is largely insensitive to the initial conditions [56]. As a consequence, there is no excessive fine tuning involved which makes quintessence an attractive alternative to the cosmological constant. Scalar fields appear in many advanced theories of physics and quintessence is therefore well motivated. This section introduces a few basic equations and specific models. We will not discuss quintessence models that interact non-gravitationally with other forms of energy [57] or scalar-tensor theories [58]. There are other scalar field models such as k-essence [59] and phantom energy [48], but these will not be treated here.

The action for a quintessence field χ that is minimally coupled to gravity is given by

$$S = \int d^4x\sqrt{-g}\left(\frac{M_{\bar{p}}^2}{2}R - \frac{1}{2}\partial_\mu\chi\partial^\mu\chi - U(\chi)\right) + S_{matter}. \tag{2.16}$$

with some self-interacting potential $U(\chi)$ and the Ricci scalar R. The associated energy-momentum tensor is given by

$$T^\mu_{(Q)\nu} = \partial^\mu\chi\partial_\nu\chi - \delta^\mu_\nu\left(\frac{1}{2}\partial^\alpha\chi\partial_\alpha\chi + U(\chi)\right). \tag{2.17}$$

In a homogeneous universe the quintessence field depends only on time, $\chi = \phi(\tau)$, so that all spatial derivatives vanish. Energy density and pressure of the homogeneous field are then given by

$$\rho_Q = \frac{1}{2a^2}\phi'^2 + U(\phi) \qquad \text{and} \qquad p_Q = \frac{1}{2a^2}\phi'^2 - U(\phi). \tag{2.18}$$

The term $\frac{1}{2a^2}\phi'^2$ is commonly referred to as 'kinetic term' and $U(\phi)$ as 'potential term'. It is clear that the equation of state of quintessence will usually be non-constant and is bounded $-1 < w_Q < 1$. Since the quintessence field interacts with other forms of energy only gravitationally, the energy-momentum tensor is conserved separately $T^\mu_{(Q)\nu;\mu} = 0$. From this one can derive the equation of motion for the homogeneous field, or alternatively by starting from the action (2.16). In either case one obtains

$$\phi'' + 2\mathcal{H}\phi' + a^2U_{,\phi} = 0, \tag{2.19}$$

which is commonly referred to as Klein-Gordon equation. We will now introduce a few of the most important models.

2.3.1 Exponential Potential

The exponential potential model was introduced by Wetterich and Ratra & Peebles [14, 15] and features tracking behaviour:

$$U(\chi)_{EXP} = M_{\bar{p}}^4 \exp(-\lambda\chi/M_{\bar{p}}). \tag{2.20}$$

The contribution to the energy budget is completely determined by λ, the only parameter of this model, as $\Omega_Q = 3/\lambda^2$. The equation of state of this quintessence model is the same as that of the total equation of state of the universe, hence it can never be negative and thus is unable to account for the accelerated expansion of the universe. In order to overcome this deficit, the leaping kinetic term model has been introduced.

2.3.2 Leaping Kinetic Term

In an alternative formulation of the action (2.16) one introduces a kinetic term $k(\chi)$ [60]:

$$\mathcal{L}_Q = -k(\chi)^2 \partial_\mu\chi\partial^\mu\chi - M_{\bar{p}}^4 \exp(-\chi/M_{\bar{p}}). \tag{2.21}$$

By redefining the scalar field $\chi \rightarrow \varphi$ one can obtain a canonical kinetic term $k(\varphi) = 1$ by inverting the expression $d\varphi/d\chi = k(\chi)$. This transformation will alter the exponential potential term and thus allow for a negative equation of state. A specific form for the kinetic term has been proposed by Wetterich and Hebecker [60][5]:

$$k(\chi) = k_{min} + \tanh[\sigma(\chi - \chi_1)/M_{\bar{p}}] + 1. \tag{2.22}$$

The effect of this term is to 'kick' the scalar field out of the tracking behaviour at $\chi \approx \chi_1$. The parameter σ controls the steepness of this transition. The parameter k_{min} determines the amount of early quintessence – a non-negligible amount of dark energy during last scattering and structure formation [61]. This model is very versatile and is consistent with supernovae and large scale structure observations.

2.3.3 Inverse Power Law

This very popular model has originally been introduced by Ratra and Peebles [15, 62] and has the potential

$$U(\chi)_{IPL} = A\left(\frac{\chi}{M_{\bar{p}}}\right)^{-\alpha}, \tag{2.23}$$

[5] We have added the parameter σ which was not present in the original paper.

where A and α are parameters. This model is of the tracking type. When confronted with recent observations, this model appears to need fine-tuning in the parameter A in order to be consistent since $\alpha < 2.5$ [63].

2.3.4 Other Models and Parametrizations

There is a large number of other models such as modified exponentials [64, 65], SUGRA inspired models [66], double exponentials [67] and others [68, 69]. Instead of specifiying a specific model, one may also formulate a parametrization of the equation of state w_Q. In fact, the evolution of the scalar field can be completely derived from w_Q using Eqs. (2.9), (2.11) and (2.18):

$$\phi' = M_{\bar{p}}\mathcal{H}\sqrt{3\Omega_Q(a)[1+w_Q(a)]}, \tag{2.24}$$

$$U(\phi) = \frac{3}{2}M_{\bar{p}}^2\mathcal{H}^2a^{-2}\Omega_Q(a)[1-w_Q(a)], \tag{2.25}$$

where

$$\Omega_Q(a) = \Omega_Q^{(0)}H_0^2a^{-1}\mathcal{H}^{-2}\exp\left(3\int_a^1 w_Q(\tilde{a})d\ln\tilde{a}\right). \tag{2.26}$$

Parametrizations are therefore often used for comparison with observations. An equation of state of dark energy different from -1 would indicate that the cosmological constant cannot be the dark energy[6]. Unfortunately there is no entirely obvious way to parametrize the equation of state. One can do a polynomial fit in redshift space [70,71], logarithmic expansions [72] or multi-parameter fits [73,74].

2.4 Expansion and Horizons

A very important concept in cosmology is that of the horizon. Since light speed is finite and the universe has been expanding and has been in existence a finite time, it follows that there is a certain length scale beyond which no causal contact is possible. This 'particle horizon' L_H changes over time and is determined by

$$L_H = \int_0^t dt'/a = \int_0^\tau d\tau' = \tau. \tag{2.27}$$

The horizon size is thus determined by the conformal time. It is useful to introduce the comoving wavenumber k/h defined by

$$L = 2\pi(k/h)^{-1}, \tag{2.28}$$

[6] At least not all of it. It might be that dark energy consists of the cosmological constant and dynamical dark energy, but we will not discuss this possibility further.

	horizon [Mpc]	k/h [Mpc^{-1}]	scale factor a
at matter-radiation equality	1.09×10^2	5.72×10^{-2}	2.85×10^{-4}
at last scattering	2.71×10^2	2.32×10^{-2}	8.82×10^{-4}
today	1.39×10^4	4.51×10^{-4}	1.00

Table 2.1: Particle horizon size, corresponding comoving k/h and scale factor a for the plain vanilla ΛCDM model of [29] at different times.

where L is some length scale. We can relate the horizon size to the Hubble parameter. First, we note that the solution to the Friedmann equation (2.11) is

$$a \propto \tau, \tag{2.29}$$

for a radiation dominated universe and

$$a \propto \tau^2, \tag{2.30}$$

for a matter dominated universe. For a purely matter dominated universe we have then $\mathcal{H} = 2/\tau$ and thus $L_H = 2/H_0$. For a universe containing a mixture of radiation, matter and dark energy there is no such simple solution, but we can say that the particle horizon today is of the order of the inverse Hubble constant.

$$L_H \sim H_0^{-1}. \tag{2.31}$$

In order to get a feeling for the typical particle horizon sizes we give the values for the concordance model in table 2.1. Scales that are much larger than the horizon $k \ll \mathcal{H}$ are referred to as super horizon sized while scales much smaller $k \gg \mathcal{H}$ are called sub horizon sized.

The horizon at last scattering corresponds to a scale of $\sim 1°$on the sky today, yet the CMB is isotropic to a high degree over the entire sky. How can this be? In the horizon size computation we did not include inflation which is believed to be responsible for the high degree of homogeneity and for the spatial flatness of the universe. Also, the perturbations were probably seeded by inflation, see [25] for a thorough treatment.

Another important quantity is the luminosity distance of an object of absolute luminosity $\mathscr{L}$ and measured flux $\mathcal{F}$ defined by

$$d_L^2 \equiv \frac{\mathscr{L}}{4\pi\mathcal{F}}. \tag{2.32}$$

This quantity can be measured if $\mathscr{L}$ is known. Interestingly, one may extract the expansion history from d_L since

$$d_L = (1+z)\int_0^z \frac{d\tilde{z}}{H(\tilde{z})}. \tag{2.33}$$

This concludes our treatment of the homogeneous universe. In the next chapter we will discuss linear perturbation theory, one of the most important tools in cosmology.

– 3 –

The Perturbed Universe

Of course a certain number of scientists have to go mad, just to keep the tradition alive.

Matt Ruff, Fool on the Hill

We already mentioned before that the universe appears to be almost homogeneous on large scales. But it is not entirely homogeneous and that enables us to extract a lot of information from the observation of inhomogeneities. In order to be able to do that we must first consider linear perturbation theory in cosmology. The concept is quite simple: we take the homogeneous universe to be a solution of zeroth order of the Einstein equations (2.1), add perturbations of first order and drop all terms of higher order in subsequent calculations. But in general relativity there is freedom in the choice of coordinates, and this leads to the difficulty of distinguishing genuine physical effects from artifacts that may be removed by a suitable coordinate transformation. One possibility to cope with this problem is to fix the coordinates from the beginning – commonly referred to as fixing the gauge. There are some gauges that do not completely fix the coordinates, such as the harmonic and synchronous gauge, and as a consequence unphysical artifacts – so-called gauge modes – may appear. The other possibility, and the one we are going to use here, is to formulate all quantities in a gauge-invariant way, which means they do not change under gauge transformation. This approach was pioneered by Bardeen [75], see [76–78] for a review.

3.1 Gauge Invariant Variables

We will use the notation of Kodama & Sasaki [76] in what follows. The starting point is to decompose the metric and the energy-momentum tensor into parts

that transform as scalars, vectors and tensors under spatial coordinate transformations. As it turns out, the Einstein equations keep this separation intact. To first order, scalar parts of the metric are only connected to scalar parts of the energy momentum tensor, the same holds for vector and tensor parts, respectively. As an example for the decomposition of a vector into scalar and vector parts consider the well-known decomposition of a vector **B** into the divergence of a scalar function ϕ and divergence-free rotational vector **C**:

$$\mathbf{B} = \text{grad}\,\phi + \text{rot}\,\mathbf{C}. \tag{3.1}$$

In the same manner a tensor may be decomposed into scalar, vector and tensor parts. We can then fourier expand these quantities.

Scalar quantities may be expanded by a complete set of scalar harmonic functions $Y(k)$ satisfying[1]

$$\left(\Delta + k^2\right) Y = 0. \tag{3.2}$$

Scalar type components of vectors may be expanded by

$$Y_i \equiv -k^{-1} Y_{,i}\,, \tag{3.3}$$

and those of tensors by

$$Y_{ij} \equiv \left(k^{-2} Y_{,ij} + \frac{1}{3}\delta_{ij} Y\right). \tag{3.4}$$

Similarly, we may introduce vector and tensor harmonic functions. Since we will not consider vector and tensor perturbations here, we refer the reader to [76] for a full treatment. Vector modes decay and are not generated through interactions, so they do not contribute and may be neglected[2]. The scalar part of the full metric $\tilde{g}_{\mu\nu}$ may be decomposed as

$$\begin{aligned}
\tilde{g}_{00} &= -a^2[1 + 2AY], && (3.5)\\
\tilde{g}_{0j} &= -a^2 B Y_j, && (3.6)\\
\tilde{g}_{ij} &= a^2[\delta_{ij} + 2H_L Y \delta_{ij} + 2H_T Y_{ij}], && (3.7)
\end{aligned}$$

and the inverse metric $\tilde{g}^{\mu\nu}$ to first order is

$$\begin{aligned}
\tilde{g}^{00} &= -a^{-2}[1 - 2AY], && (3.8)\\
\tilde{g}^{0j} &= -a^{-2} B Y^j, && (3.9)\\
\tilde{g}^{ij} &= a^{-2}[\delta_{ij} - 2H_L Y \delta^{ij} - 2H_T Y^{ij}], && (3.10)
\end{aligned}$$

[1] We will suppress the argument of Y in what follows.

[2] In second order perturbation theory the Einstein equations mix scalar, vector and tensor modes and vector modes may therefore be generated by scalar and tensor modes. But in linear perturbation theory, we may safely neglect vector modes. A possible contribution of vector modes is discussed in [79].

with scalar functions A, B, H_L and H_T. The scalar part of the energy-momentum tensor is

$$\begin{aligned}
\tilde{T}^0_{\ 0} &= -\rho[1+\delta Y], && (3.11)\\
\tilde{T}^0_{\ j} &= (\rho+p)(v-B)Y_j, && (3.12)\\
\tilde{T}^j_{\ 0} &= -(\rho+p)vY^j, && (3.13)\\
\tilde{T}^i_{\ j} &= p[\delta^i_j+\pi_L\delta^i_j+\pi_T Y^i_{\ j}]. && (3.14)
\end{aligned}$$

We may interpret δ as the energy density peturbation, π_L as the pressure perturbation, v as the velocity and π_T as the anisotropic stress. However, we will later see that there are problems with this way of interpreting these quantities. In order to construct gauge-invariant quantities, we need to consider how $A, B, \delta, \pi_L \ldots$ change under a gauge transformation. The scalar part of a general coordinate transformation $x_\mu \to \overline{x}_\mu$ is

$$\begin{aligned}
\overline{\tau} &= \tau + T\,Y, && (3.15)\\
\overline{x}^j &= x^j + L\,Y^j, && (3.16)
\end{aligned}$$

with L and T scalar functions of τ. Under a gauge transformation the metric changes according to

$$\overline{\tilde{g}}_{\mu\nu}(\tau, x^j) = \frac{\partial x^\alpha}{\partial \overline{x}^\mu}\frac{\partial x^\beta}{\partial \overline{x}^\nu}\tilde{g}_{\alpha\beta}(\tau - T\,Y, x^j - L\,Y^j). \qquad (3.17)$$

Note that the transformed metric $\overline{\tilde{g}}_{\mu\nu}$ is evaluated at the same space-time coordinates. Expanding to first order, this gives the following transformation properties:

$$\begin{aligned}
\overline{A} &= A - T' - \mathcal{H}T, && (3.18)\\
\overline{B} &= B + L' + kT, && (3.19)\\
\overline{H_L} &= H_L - \frac{k}{3}L - \mathcal{H}T, && (3.20)\\
\overline{H_T} &= H_T + kL. && (3.21)
\end{aligned}$$

The transformation properties of the energy-momentum tensor may be obtained along similar lines

$$\begin{aligned}
\overline{\delta} &= \delta + 3(1+w)\mathcal{H}T, && (3.22)\\
\overline{v} &= v + L', && (3.23)\\
\overline{\pi_L} &= \pi_L + 3\frac{c_s^2}{w}(1+w)\mathcal{H}T, && (3.24)\\
\overline{\pi_T} &= \pi_T, && (3.25)
\end{aligned}$$

where we defined the background sound speed

$$c_s^2 \equiv p'/\rho'. \tag{3.26}$$

The transformation properties (3.18) – (3.25) make it obvious why we need gauge-invariant variables. Take the energy density perturpation δ as an example. This quantity has no absolute physical meaning, since δ transforms non-trivially under a gauge transformation, or in other words: δ in one coordinate system is not identical to δ in another coordinate system. Only the anisotropic stress π_T has a coordinate-free meaning. But by forming suitable linear combinations we may define variables that do not change under gauge transformations. There is no unique way to combine these variables but one very convenient definition is

$$V \equiv v - k^{-1}H_T', \tag{3.27}$$

as the gauge-invariant velocity. Let us also define

$$\Delta \equiv \delta + 3(1+w)\left[H_L + \frac{1}{3}H_T\right], \tag{3.28}$$

as the gauge-invariant energy density. As mentioned before, the anisotropic stress is already gauge-invariant

$$\Pi \equiv \pi_T, \tag{3.29}$$

while the gauge-invariant pressure perturbation may be defined by

$$P_L \equiv \pi_L + 3\frac{c_s^2}{w}(1+w)\mathcal{H}k^{-1}\sigma_g, \tag{3.30}$$

with

$$\sigma_g \equiv k^{-1}H_T' - B. \tag{3.31}$$

Another quantity of interest is the entropy production rate [80] defined by

$$\Gamma \equiv \pi_L - \frac{c_s^2}{w}\delta, \tag{3.32}$$

which, roughly speaking, measures the difference between background sound speed $c_s^2 = p'/\rho'$ and adiabatic sound speed defined by[3]

$$c_{ad}^2 \equiv \frac{p}{\rho}\frac{\pi_L}{\delta}. \tag{3.33}$$

The metric variables may also be combined to form gauge-invariant quantities

$$\Phi \equiv H_L + \frac{1}{3}H_T - k^{-1}\mathcal{H}\sigma_g, \tag{3.34}$$

$$\Psi \equiv A - k^{-1}\mathcal{H}\sigma_g - k^{-1}\sigma_g'. \tag{3.35}$$

[3]Note that c_{ad}^2 is not gauge-invariant whereas c_s^2 is.

One may verify from the equations (3.18) – (3.25) that the gauge-invariant quantities do not change under a gauge transformation.

How do we interpret these quantities? The simplest possiblity to see the physical meaning is to choose a set of hypersurfaces, this is the same as choosing a gauge. For instance, the synchronous gauge choice corresponds to a transformation such that

$$A = B = 0. \qquad \text{(synchronous gauge)} \tag{3.36}$$

In this case, we have chosen the hypersurface of free falling observers. A more convenient choice is the conformal Newtonian gauge with the requirement

$$\sigma_g = 0. \qquad \text{(Newtonian gauge)} \tag{3.37}$$

Here we have chosen hypersurfaces of isotropic expansion rate perturbation. The interpretation of the quantities Φ and Ψ on this kind of hypersurfaces is surprisingly simple:

$$\tilde{g}_{\mu\nu}^{Newton} = a^2 \,\mathrm{diag}(-1-2\Psi Y, 1+2\Phi Y, 1+2\Phi Y, 1+2\Phi Y). \tag{3.38}$$

It will be shown later that if we have vanishing anisotropic stress $\Pi = 0$ then $\Phi = -\Psi$. The metric is then the same as in the Newtonian approximation, hence Φ may be interpreted as Newtonian potential[4].

In Newtonian gauge P_L is the physical pressure perturbation as can be seen from setting $\sigma_g = 0$ in eq. (3.30).

The quantity Δ is best interpreted in a frame where $H_L + 1/3H_T = 0$, which is the hypersurface where the perturbation of the scalar curvature of constant time hypersurfaces vanishes. There, $\Delta = \delta$ and so on this set of hypersurfaces Δ is the energy density perturbation. In conformal Newtonian gauge it takes the form

$$\Delta = \delta^{Newton} + 3(1+w)\Phi. \tag{3.39}$$

We would like to emphasize again that the interpretation of these variables is tied to a certain set of hypersurfaces; on different ones the interpretation may also be different. For later it will be convenient to formulate the entropy production rate (3.32) in terms of gauge-invariant variables:

$$\Gamma = P_L - \frac{c_s^2}{w}[\Delta - 3(1+w)\Phi]. \tag{3.40}$$

A scalar field perturbation $\chi = \phi + \tilde{\chi}$ transforms as a scalar and is given by

$$\overline{\tilde{\chi}} = \tilde{\chi} - \phi' T. \tag{3.41}$$

[4]Hence the name 'Newtonian gauge'.

The expression

$$X \equiv \tilde{\chi} - k^{-1}\sigma_g\phi', \tag{3.42}$$

is gauge invariant and has the interpretation of the scalar field perturbation in conformal Newtonian gauge. Having defined our variables we can now proceed and obtain the evolution equations for the perturbations.

3.2 Perturbation Equations and the CMB

The way to obtain the perturbation equations is clear: insert the perturbed metric and energy-momentum tensor into the Einstein equations and combine to form gauge-invariant quantities – we want the resulting equations to be manifestly gauge-invariant. Since the calculation is rather lengthly and not very instructive, we will present only the final results. First, one obtains algebraic relations for Φ and Ψ:

$$-M_{\bar{p}}^2 k^2(\Phi + \Psi) = a^2 p\Pi, \tag{3.43}$$

$$a^2\rho\Delta = 2M_{\bar{p}}^2 k^2\Phi - 3a^2\rho(1+w)(k^{-1}\mathcal{H}V - \Phi). \tag{3.44}$$

The dynamical equation is

$$a^2(\rho + p)V = 2M_{\bar{p}}^2 k(\mathcal{H}\Psi - \Phi'). \tag{3.45}$$

Using energy-momentum conservation one obtains

$$\Delta' + 3(c_s^2 - w)\mathcal{H}\Delta + kV(1+w) + 3\mathcal{H}w\Gamma = 0, \tag{3.46}$$

for the energy density perturbation and

$$V' = \mathcal{H}(3c_s^2 - 1)V + k(\Psi - 3c_s^2\Phi) + \frac{c_s^2 k}{1+w}\Delta + \frac{wk}{1+w}\left(\Gamma - \frac{2}{3}\Pi\right), \tag{3.47}$$

for the velocity. The equation of motion for the scalar field perturbation is

$$X'' = \phi'(\Psi' - 3\Phi') - 2a^2 U(\phi)_{,\phi}\Psi - \left[a^2 U(\phi)_{,\phi\phi} + k^2\right] X - 2\mathcal{H}X'. \tag{3.48}$$

So far, we have not split these equations into the various different forms of energy. Any such splitting will need to take into account the non-gravitational interactions between the various species. For the concordance model the only important interaction for our purposes is Thomson scattering of photons by electrons. This entrails solving the Boltzmann equation for the baryon-photon system. Unfortunately, the derivation is rather lengthly and since we will not need the result directly subsequently, we will not perform the derivation here. Instead, we

give a short sketch on how to obtain the result. For more information the reader is referred to the literature [81, 82]. The starting point is the general relativistic Boltzmann equation for the photon distribution function [83]. One then connects the temperature perturbation to the perturbed distribution function. The temperature perturbation is then expanded in spherical harmonics[5] [86]. At this point one may integrate the equations and find the CMB spectrum. However, there is a further simplification which speeds up computation tremendously. The resulting equations may be formally integrated over τ, along the photon past light cone [16, 87]. The benefit of this is that instead of solving a coupled system of $\sim$ 2000 differential equations, we only need to solve $\sim$ 20. This has made it possible to compute models quickly and efficiently for comparison with observations using dedicated numerical packages such as CMBFAST [16], CAMB [17] and CMBEASY [18]. The computation of the effect of tensor modes on the CMB temperature and polarization spectrum follows along similar lines [88–90].

Assuming that the distribution of perturbations is Gaussian, the complete information contained in the CMB can be expressed by the respective cross correlations of the spherical harmonics coefficients a_{lm}^X of each observational quantity X

$$C_l^{XY} = \frac{1}{2l+1} \sum_m \langle a_{lm}^{X*} a_{lm}^Y \rangle, \tag{3.49}$$

where the variables X and Y are T for the temperature, E for E-mode polarization and B for B-mode polarization. We will discuss the two polarization types in section 4.2.1. The expression given above is for extracting the power spectrum from experimental data. The brackets indicate that we should average over different independent experiments, but there is only sky we can observe. In other words, we observe a particular realization of the statistical distribution of the coefficients a_{lm}. For high multipoles this is not a problem since we sum over m and the variance of C_l will be small. But for low multipoles we have to take into account that we measure only a particular realization for the computation of likelihoods, a problem commonly called 'cosmic variance'. The variance of C_l is largest for the quadrupole, C_2. The WMAP experiment has already measured close to the cosmic variance limit in the low multipoles, so improvements in this regime will not be possible due to lack of statistics.

For illustrative purposes we give the theoretical expression for the scalar part of the C_l^{TT} power spectrum. In order to be able to do that one needs to know how the perturbations are distributed over the scales k. This is where the initial power spectrum $P_g(k)$ comes in. It is defined by

$$\langle \xi^*(\mathbf{k_1}) \xi(\mathbf{k_2}) \rangle = P_g(k) \delta(\mathbf{k_1} - \mathbf{k_2}), \tag{3.50}$$

[5]For the polarization, the decomposition is into spin-weighted spherical harmonics. Alternatively, one may use a generalized expansion if one employs the angular momentum method of [84, 85].

where $\xi(\mathbf{k})$ is a random variable characterizing the initial amplitude of the mode and the average is again taken over different realizations. Note that we have assumed $\xi(\mathbf{k})$ to be a Gaussian random variable, as a consequence all information is contained in the power spectrum. From inflation one expects the power spectrum of the initial scalar perturbations to follow a power law [25]

$$P_g(k) \propto k^{n_s-4}. \tag{3.51}$$

The quantity n_s is called the scalar spectral index[6]. This is referred to as scale-invariant power spectrum, or Harrison-Zeldovich spectrum [91, 92]. The case $n_s > 1$ is called a blue tilted spectrum whereas $n_s < 1$ is a red tilted spectrum. There is a corresponding expression for the power spectrum of tensor perturbations and an associated tensor spectral index, but we will not discuss this here. The prediction of slow-roll single-field inflation is $n_s \approx 1$.

We are now ready to give the the part of C_l^{TT} coming from scalar perturbations[7]. After a lot of computation one arrives at the expression

$$C_l^{TT} = (4\pi)^2 \int k^2 dk P_g(k) \left[\int_0^{\tau_0} d\tau S_T(k,\tau) j_l(k(\tau_0 - \tau)) \right]^2. \tag{3.52}$$

where $j_l(x)$ is the spherical Bessel function of order l and $S_T(k,\tau)$ is a source term containing a combination of temperature and polarization perturbation moments and their derivatives. These need to be computed by using the Boltzmann equations. The benefit of formally integrating over τ first is apparent in eq. (3.52). We only need to solve the Boltzmann hierarchy for the sources $S_T(k,\tau)$, and these are no more than $\sim$ 20 equations, depending on the desired level of accuracy. Afterwards, one can integrate the above equation for every l and obtain the power spectrum. In contrast, without this integration over τ we would have to solve the hierarchy containing as many equations as we want to have multipoles, usually in the range $\sim$ 2000. This is why one uses this formal integration, also called the line-of-sight method [16]. From a practical point of view, since C_l^{XY} is a smooth function of l it is not evaluated at every multipole l but at suitable intervals. The full function is then obtained by interpolating. The resulting savings in computing time are substantial while the error compared to full-fledged Boltzmann codes is minimal [93]. We will discuss the observational status of the CMB in section 4.2.

[6]Sometimes one encounters the expression $\Delta^2(k)$ which is related to $P_g(k)$ by $P_g(k) = 2\pi^2\Delta^2(k)/k^3$.

[7]There is also a contribution to C_l coming from tensor perturbations as well, but this case is not covered here.

3.3 Initial Conditions for Quintessence Universes

In order to be able to solve the perturbation equations we need to know the initial conditions. Single-field inflation predicts that the initial conditions are adiabatic and observations of the CMB seem to confirm this expectation. However, from a theoretical point of view there is a large number of different initial conditions possible, but not all of them are important. All those who decay will not be relevant if constant or growing modes are present. We can make this a bit clearer and determine the suitable initial conditions by an approach that employs eigenvectors and eigenvalues. The approach we describe here is an abridged version of [94]. Suppose that the vector $\mathbf{U}$ contains all interesting dynamical variables for which we want to find the initial conditions. The evolution equations follow a matrix equation

$$\frac{d}{d\ln x}\mathbf{U} = A(x)\mathbf{U}, \tag{3.53}$$

where the matrix $A(x)$ encodes the evolution equations and $x \equiv k\tau \ll 1$ is small – we are considering super horizon sized contributions only. As we will show in a moment, to leading order one may consider a constant matrix A_0 if we take the super horizon limit $x^2 \to 0$. The task of finding the appropriate initial conditions boils down to finding the eigenvectors to the largest eigenvalues of the matrix A_0. Suppose we have found the eigenvalues λ_i and corresponding eigenvectors $\mathbf{U}^{(i)}$. The evolution of a general perturbation vector $\mathbf{U}$ to leading order is given by

$$\mathbf{U}(x) = \sum_i c_i \left(\frac{x}{x_0}\right)^{\lambda_i} \mathbf{U}^{(i)}. \tag{3.54}$$

The coefficients c_i specify the initial contribution towards the general perturbation $\mathbf{U}$. As time progresses, components corresponding to the largest eigenvalues Re λ_i will dominate ('dominating modes') while those with smaller eigenvalues will decay ('decaying modes'). Therefore, if we are not interested in the early time behaviour it is sufficient to specify the initial contribution c_i of dominant modes. We will now proceed to find the eigenvalues and eigenvectors of these dominant modes. We will be very brief, for a more thorough treatment see [94, 95].

Since the initial conditions will be set deep in the radiation dominated era, we can take $a = \tau$, and we can use the fact that baryons and photons are tightly coupled which simplifies the expressions considerably. We define reduced velocity $\tilde{V} = V/x$ and reduced shear $\tilde{\Pi} = \Pi/x^2$.

Quintessence

By perturbing the energy-momentum tensor for quintessence one finds that there are no spatial off-diagonal components and hence

$$\Pi_Q = 0. \tag{3.55}$$

By comparing the perturbed energy-momentum tensor of quintessence with the definition of Δ and V one obtains the gauge-invariant expression [76,96] in terms of the scalar field variables:

$$\Delta_Q = (1+w_Q)\left[3\Phi - \Psi + \frac{X'}{\phi'}\right] + XU(\phi)_{,\phi}\rho_Q^{-1}, \tag{3.56}$$

and

$$V_Q = k\frac{X}{\phi'}. \tag{3.57}$$

Taking the time derivatives of these equations and using the equation of motion (3.48) one obtains

$$\Delta_Q' = (1+w_Q)\left[\frac{2a^2U(\phi)_{,\phi}}{\phi'}\left(\frac{\Delta_Q}{1+w_Q} - 3\Phi\right) + \left(\frac{6aa'U(\phi)_{,\phi}}{k\phi'} - k\right)V_Q\right] + \frac{w_Q'\Delta_Q}{1+w_Q}, \tag{3.58}$$

$$V_Q' = k\left[\frac{\Delta_Q}{1+w_Q} - 3\Phi + \Psi\right] + 2\mathcal{H}V_Q. \tag{3.59}$$

These equations depend on the specific quintessence model through $U(\phi)$ and ϕ'. We can, however, make progress if w_Q is constant. Many quintessence models have solutions for which ϕ approaches an attractor solution irrespective of its initial value. For these tracking quintessence models [14,15,56] the equation of state of quintessence w_Q is nearly constant during radiation domination. We will use this tracking behaviour to simplify eq. (3.58). Taking the derivative of eq. (2.24) one obtains

$$\frac{\phi''}{\phi'} = \frac{d}{d\tau}\ln\phi' = \frac{1}{2}\frac{\Omega_Q'}{\Omega_Q} + \frac{\mathcal{H}'}{\mathcal{H}}. \tag{3.60}$$

where we have set $w_Q' = 0$ in accordance with the tracking assumption. Taking $\mathcal{H} = \tau^{-1}$ for radiation domination and inserting the resulting expression (3.60) into the Klein-Gordon equation (2.19) one finds

$$\frac{a^2U(\phi)_{,\phi}}{\phi'} = -\frac{3(1-w_Q)}{2\tau}. \tag{3.61}$$

Thus, for the radiation dominated universe and a tracking quintessence model the relevant evolution equations are

$$\Delta_Q' = 3(w_Q-1)\frac{k}{x}\left[\Delta_Q - 3(1+w_Q)\Phi + \left(3 - \frac{x^2}{3(w_Q-1)}\right)(1+w_Q)\tilde{V}_Q\right], \tag{3.62}$$

and for the reduced velocity

$$\tilde{V}_Q' = \frac{k}{x}\left[\frac{\Delta_Q}{1+w_Q} - 3\Phi + \Psi\right] + \frac{k}{x}\tilde{V}_Q. \tag{3.63}$$

Dark Matter

Setting $c_s^2 = w = \Gamma = 0$ in equations (3.46) and (3.47) we obtain

$$\Delta_c' = -kx\tilde{V}_c, \tag{3.64}$$

$$\tilde{V}_c' = \frac{k}{x}(-\tilde{V}_c + \Psi). \tag{3.65}$$

Neutrinos

The multipole expansion of the neutrino distribution function can be truncated beyond the quadrupole at early times [86, 97]. It is given by

$$\Delta_\nu' = -\frac{4}{3}kx\tilde{V}_\nu, \tag{3.66}$$

$$\tilde{V}_\nu' = \frac{k}{x}\left(\frac{1}{4}\Delta_\nu - \tilde{V}_\nu - \frac{1}{6}x^2\tilde{\Gamma\Pi}_\nu + \Psi - \Phi\right), \tag{3.67}$$

$$\tilde{\Gamma\Pi}_\nu' = \frac{k}{x}\left(\frac{8}{5}\tilde{V}_\nu - 2\tilde{\Gamma\Pi}_\nu\right). \tag{3.68}$$

Photons and Baryons

Tight coupling between photons and baryons leads to $V_b = V_\gamma$ and the evolution equations become [76, 98]

$$\Delta_\gamma' = -\frac{4}{3}kx\tilde{V}_\gamma, \tag{3.69}$$

$$\tilde{V}_\gamma' = \frac{k}{x}\left(\frac{1}{4}\Delta_\gamma - \tilde{V}_\gamma + \Psi - \Phi\right), \tag{3.70}$$

$$\Delta_b' = -k\,x\,\tilde{V}_\gamma. \tag{3.71}$$

Potentials

There is no anisotropic stress for quintessence and the photon quadrupole, and all higher multipoles are suppressed due to tight coupling, it follows that only the anisotropic stress of the neutrinos is not negligible:

$$\Phi = -\Psi - \Omega_\nu\tilde{\Gamma\Pi}_\nu, \tag{3.72}$$

and the potential is given by

$$\Phi = \frac{\sum\limits_{\alpha=c,b,\gamma,\nu,Q}\Omega_\alpha\left(\Delta_\alpha + 3(1+w_\alpha)\tilde{V}_\alpha\right)}{\sum\limits_{\alpha=c,b,\gamma,\nu,Q}3(1+w_\alpha)\Omega_\alpha + \frac{2x^2}{3}}, \tag{3.73}$$

where the index α runs over all species.

Rewriting these evolution equations (3.62) – (3.73) in terms of $d/d\ln x$ and replacing Φ by means of (3.72) we obtain the following set of equations

$$\frac{d}{d\ln x}\Delta_c = -x^2\tilde{V}_c, \tag{3.74}$$

$$\frac{d}{d\ln x}\tilde{V}_c = -2\tilde{V}_c + \Psi, \tag{3.75}$$

$$\frac{d}{d\ln x}\Delta_\gamma = -\frac{4}{3}x^2\tilde{V}_\gamma, \tag{3.76}$$

$$\frac{d}{d\ln x}\tilde{V}_\gamma = \frac{1}{4}\Delta_\gamma - \tilde{V}_\gamma + \Omega_\nu\tilde{\Pi}_\nu + 2\Psi, \tag{3.77}$$

$$\frac{d}{d\ln x}\Delta_b = -x^2\tilde{V}_\gamma, \tag{3.78}$$

$$\frac{d}{d\ln x}\Delta_\nu = -\frac{4}{3}x^2\tilde{V}_\nu, \tag{3.79}$$

$$\frac{d}{d\ln x}\tilde{V}_\nu = \frac{1}{4}\Delta_\nu - \tilde{V}_\nu - \frac{1}{6}x^2\tilde{\Pi}_\nu + \Omega_\nu\tilde{\Pi}_\nu + 2\Psi, \tag{3.80}$$

$$\frac{d}{d\ln x}\tilde{\Pi}_\nu = \frac{8}{5}\tilde{V}_\nu - 2\tilde{\Pi}_\nu, \tag{3.81}$$

$$\begin{aligned}\frac{d}{d\ln x}\Delta_Q &= 3(w_Q-1)\Big[\Delta_Q + 3(1+w_Q)\\ &\quad\times(\Psi+\Omega_\nu\tilde{\Pi}_\nu) + \left(3 - \frac{x^2}{3(w_Q-1)}\right)(1+w_Q)\tilde{V}_Q\Big],\end{aligned} \tag{3.82}$$

$$\frac{d}{d\ln x}\tilde{V}_Q = 3\Omega_\nu\tilde{\Pi}_\nu + \frac{\Delta_Q}{1+w_Q} + \tilde{V}_Q + 4\Psi. \tag{3.83}$$

From the structure of these equations one can see that they may be formulated as a matrix equation as in (3.53) with a perturbation vector $\mathbf{U}$ given by

$$\mathbf{U}^T \equiv (\Delta_c, \tilde{V}_c, \Delta_\gamma, \tilde{V}_\gamma, \Delta_b, \Delta_\nu, \tilde{V}_\nu, \tilde{\Pi}_\nu, \Delta_Q, \tilde{V}_Q). \tag{3.84}$$

The matrix $A(x)$ may be read off from equations (3.74) – (3.83). We find that in the limit $x^2 \to 0$ the matrix A has a fourfold degenerate eigenvalue $\lambda = 0$, independent of Ω_c, Ω_b and Ω_Q[8]. One may check numerically that there are no larger eigenvalues present. This means that these modes remain constant during radiation domination in the super-horizon regime. We must now find the eigenvectors corresponding to the four eigenvalues $\lambda = 0$. In the super horizon limit in a radiation dominated universe the matrix $A(x)$ may be taken to be constant $A(x) \approx A_0$ if we ignore the evolution of the small components $\Omega_b \propto \Omega_{dm} \propto x$.

[8]For $w_Q = 1$ we find another eigenvalue with $\lambda = 0$. We will ignore this special case in what follows.

Quintessence has either equation of state $w_Q = 1/3$, implying its contribution remains constant, or it is small at early times and may be neglected[9]. Further, assuming that A_0 does not diverge in the limit $x \to 0$ we may conclude that

$$\mathbf{U}(x) = \mathbf{U}_0. \tag{3.85}$$

Using the fact that we want the eigenvectors to the eigenvalue 0 we obtain the leading order equation

$$A_0 \mathbf{U}_0^{(i)} = 0. \tag{3.86}$$

Neglecting the very small contributions of baryons and cold dark matter to the energy budget and taking the superhorizon limit we set $\Omega_c = \Omega_b = x^2 = 0$. Then equations (3.74), (3.76), (3.78) and (3.79) are automatically satisfied. The remaining equations (3.75), (3.77), (3.80), (3.81), (3.82) and (3.83) give nontrivial contstraints on $\mathbf{U}_0^{(i)}$. Note that for quintessence, only w_Q appears in these equations. There is no dependence on the scalar field or the potential as long as we are in the tracking regime with constant equation of state.

While any basis for the subspace spanned by the eigenvectors with an eigenvalue $\lambda = 0$ can be used to specify the initial conditions, it is still worthwhile to use a basis that is physically meaningful. Following the existing literature, we use the gauge-invariant entropy perturbation [76]

$$S_{\alpha:\beta} \equiv \frac{\Delta_\alpha}{1+w_\alpha} - \frac{\Delta_\beta}{1+w_\beta}, \tag{3.87}$$

between two species α and β. The first perturbations one would try to find are adiabatic perturbations, which are specified by the adiabaticity conditions $S_{\alpha:\beta} = 0$ for all pairs of components. In our case, this results in eleven constraints[10] for the ten components of $\mathbf{U}_0^{(i)}$. It is a priori not clear that this has a solution, so we will not include the quintessence component in the adiabaticity requirement. Requiring adiabaticity between CDM, baryons, neutrinos and photons

$$\Delta_\nu = \Delta_\gamma = \frac{4}{3}\Delta_c = \frac{4}{3}\Delta_b, \tag{3.88}$$

[9] An expanded treatment that covers the case of $w_Q < 1/3$ and gives the contribution of first order as well can be found in [94, 95].

[10] We have six constraining equations plus four constraints from the adiabaticity requirement plus one constraint from the overall normalization, which is fixed by choosing a specific value for Δ_γ.

and using the six constraint equations we obtain the adiabatic initial conditions

$$\begin{pmatrix} \Delta_c \\ \tilde{V}_c \\ \Delta_\gamma \\ \tilde{V}_\gamma \\ \Delta_b \\ \Delta_\nu \\ \tilde{V}_\nu \\ \tilde{\Pi}_\nu \\ \Delta_Q \\ \tilde{V}_Q \end{pmatrix}_{\text{adiabatic}} = C \begin{pmatrix} 3/4 \\ (-5/4)\,\mathcal{P} \\ 1 \\ (-5/4)\,\mathcal{P} \\ 3/4 \\ 1 \\ (-5/4)\,\mathcal{P} \\ -\mathcal{P} \\ 3(1+w_Q)/4 \\ (-5/4)\,\mathcal{P} \end{pmatrix}, \tag{3.89}$$

where $\mathcal{P} = (15+4\Omega_\nu)^{-1}$ and C is an arbitrary constant. From $\Delta_Q/\Delta_\gamma = 3(1+w_Q)/4$ we conclude that quintessence is automatically adiabatic if CDM, baryons, neutrinos and photons are adiabatic, independent of the quintessence model as long as we are in the tracking regime.

The remaining three eigenvectors may be determined using another condition that makes use of the curvature perturbation ζ on hyper surfaces of uniform total energy density [99–101] [11]

$$\zeta = \frac{\sum_\alpha \Delta_\alpha \Omega_\alpha}{\sum_\alpha 3(1+w_\alpha \Omega_\alpha)}. \tag{3.90}$$

If $\zeta = 0$, energy density perturbations do not generate curvature. Such a perturbation is a perturbation in the local equation of state. These modes are referred to as 'isocurvature modes' in the literature [103, 104]. They have been investigated for the case of universes containing quintessence previously [105, 106] but our treatment differs in approach and interpretation. A somewhat similar investigation for the case of quintessence and one fluid was carried out in [107]. Isocurvature modes may be generated by multi-field inflation or curvaton models [108]. In order to distinguish different isocurvature modes from one another we require that all species except one and quintessence are adiabatic with respect to each other. For the neutrino isocurvature mode we require

$$\zeta = 0, \qquad \Delta_c = \Delta_b = \frac{3}{4}\Delta_\gamma. \tag{3.91}$$

[11] The definition given here is different from that of [77]. It coincides in the super horizon limit for a spatially flat universe [102].

In combination with the constraint equations we obtain

$$\begin{pmatrix} \Delta_c \\ \tilde{V}_c \\ \Delta_\gamma \\ \tilde{V}_\gamma \\ \Delta_b \\ \Delta_\nu \\ \tilde{V}_\nu \\ \tilde{\Pi}_\nu \\ \Delta_Q \\ \tilde{V}_Q \end{pmatrix}_{\text{neutrino iso.}} = C \begin{pmatrix} 3/4 \\ \Omega_\gamma \mathcal{P} \\ 1 \\ \left(\Omega_\gamma + \Omega_\nu + \frac{15}{4}\right) \mathcal{P} \\ 3/4 \\ -\Omega_\gamma/\Omega_\nu \\ -\frac{15}{4}\,\mathcal{P}\,\Omega_\gamma/\Omega_\nu \\ -3\,\mathcal{P}\,\Omega_\gamma/\Omega_\nu \\ 0 \\ \Omega_\gamma \mathcal{P} \end{pmatrix}. \tag{3.92}$$

Here, quintessence is not adiabatic with respect to the rest of the species, so we could have labled this mode 'quintessence isocurvature' as well. The remaining two modes are CDM isocurvature

$$\zeta = 0, \qquad \Delta_\gamma = \Delta_\nu = \frac{4}{3}\Delta_b, \tag{3.93}$$

which gives

$$\mathbf{U}^T_{\text{CDM iso.}} = C(1,0,0,0,0,0,0,0,0,0), \tag{3.94}$$

and baryon isocurvature, defined by the requirements

$$\zeta = 0, \qquad \Delta_\gamma = \Delta_\nu = \frac{4}{3}\Delta_c, \tag{3.95}$$

yielding

$$\mathbf{U}^T_{\text{baryon iso.}} = C(0,0,0,0,1,0,0,0,0,0). \tag{3.96}$$

All these vectors are linearly independent. We have therefore identified the four dominating modes. Arbitrary initial conditions may therefore be represented by projecting a perturbation $\mathbf{U}$ at initial time onto the subspace spanned by the four aforementioned vectors, as this is the part of the initial perturbations which will dominate as time progresses. Interestingly one sees here that adding quintessence does not increase the number of modes. This is due to the fact that none of the perturbation equations for quintessence (3.82) and (3.83) equate to zero in the super horizon limit; this holds for non-tracking quintessence models as well.

There are various studies that set constraints on the presence of isocurvature modes based on observations [109–113]. At present, there is no indication that the initial conditions are not adiabatic, and we will therefore only use adiabatic initial conditions in what follows.

– 4 –

Cosmological Probes

Very strange people, physicists – in my experience, those who aren't dead are in some way very ill.

Douglas Adams, The long dark tea-time of the soul

In this chapter we will give a thorough discussion of all observational data sets implemented in the ANALYZETHIS! package of the CMBEASY software. We will briefly describe how the χ^2 statistic is computed for each data set. More complete treatments can be found in the relevant papers of the experimental results. We will also mention other cosmological probes such as weak lensing surveys and Lyman-α forest data which are not yet implemented in CMBEASY.

4.1 Likelihood Computation

Before we delve into the different cosmological probes it is worthwhile to discuss how one compares these data sets with models. Usually one uses the χ^2 statistic for describing 'goodness of fit'. If a set of measured variables y_i^{exp} is Gaussian distributed with known covariance matrix $V_{ij} = \mathrm{cov}[y_i^{exp}, y_j^{exp}]$ and we want to compare with a theoretical model y_i^{th} then the χ^2 statistic is given by [114]

$$\chi^2 = \sum_{i,j} \left(y_i^{exp} - y_i^{th}\right) V_{ij}^{-1} \left(y_j^{exp} - y_j^{th}\right). \tag{4.1}$$

The likelihood of obtaining the data x given the parameters θ of the model is then

$$L(x|\theta) = \exp(-\chi^2/2). \tag{4.2}$$

The covariance matrix V_{ij} is usually unknown and one needs other estimators to determine it. Sometimes the distribution of variables is non-Gaussian and is taken to be a lognormal distribution. In such a case one performs a variable transformation in order to find the likelihood. Another important concept is that of the window function. Usually instruments have limited resolution or there is a different weighting of data. In such a case one needs to convolve the theoretical prediction y_i^{th} with the experimental window functions w_{ij} before computing the χ^2 statistic

$$y_i^{th,conv.} = \sum_j w_{ij} y_j^{th}. \tag{4.3}$$

Sometimes there is also an uncertainty in absolute calibration (for instance in ground-based CMB experiments), which is taken care of by considering this as a 'nuisance parameter' and looking for the calibration for which the χ^2 statistic is minimal. Fortunately, when using the ANALYZETHIS! package one need not worry about these details and constraining models becomes very easy.

4.2 CMB Experiments

Perhaps the most stringent constraints on cosmological parameters come from observations of the anisotropies of the cosmic microwave background. These anisotropies were first discovered by the COBE satellite [4] in 1992 and are at a level of tenths of micro Kelvin. The experimental resolution was restricted to the low multipoles, but already a lot of information could be extracted. With the detection of the first acoustic peak by BOOMERANG and MAXIMA [115–117] which indicated the universe to be spatially flat and the detection of the second peak [118,119] in the CMB TT-spectrum the age of precision measurements of the CMB was inaugurated. E-mode type polarization was first detected in the CMB by the DASI experiment in 2002 [120]. The analysis of the CMB was pushed to a new level by the observations of the WMAP satellite [121, 122] which measured the TT and TE spectrum to unprecedented accuracy. At present, there is a large number of ground based CMB experiments such as VSA [123], CBI [124] and ACBAR [125] with even more planned. The PLANCK satellite [52], sheduled to launch in 2007 will measure the TT spectrum even more accurately than WMAP, maybe even detecting B-mode polarization which would make it possible to constrain inflation.

4.2.1 Different Types of CMB Spectra: C_l^{TT}, C_l^{EE}, C_l^{BB} and C_l^{TE}

We will shortly describe the different forms of spectra and the difference between E-Mode and B-Mode polarization. There is an extensive literature on how to

physically interpret the form of the TT spectrum and how it depends on cosmological parameters [126–129]. For model comparison one has to solve the perturbation equations for photons in order to determine the different spectra as discussed in section 3.2. As mentioned earlier there are two distinct polarization types. The reader may be familiar with the usual description of polarization by Stokes' parameters I, Q, U, and V [130]. In cosmology it is advantageous to use their linear combinations in order to reduce to scalar quantities B and E by using spin-weighted spherical harmonics that differ by their transformation with respect to space inversion (parity) [87,131,132]. E type polarization has even parity whereas B type polarization has odd parity. It follows that there is no cross correlation between B and T or B and E if there are no parity-violating interactions since T has even parity. This leaves us with the four spectra $C_l^{TT}, C_l^{TE}, C_l^{EE}$ and C_l^{BB}. What is interesting is that B type polarization can not be generated by Thomson scattering. But gravitational waves can lead to B type polarization of the CMB and so one may infer information about primordial gravitational waves from measurements of C_l^{BB}. Since inflation generates these gravitational waves one may constrain models of inflation once the C_l^{BB} spectrum has been measured. At present, no experiment has been able to detect B type polarization.

4.2.2 CBI, VSA and ACBAR

In CMBEASY we have implemented the latest data sets of the experiments giving the most stringent constraints on the CMB. These are the Very Small Array (VSA) [123] on Tenerife, the Cosmic Background Imager (CBI) [124] in the Chilenian Andes and the Arcminute Cosmology Bolometer Array Receiver (ACBAR) [125] at the South Pole. The latest data of all three experiments is displayed in Fig. 4.1. All of this data is implemented in CMBEASY. If we use the WMAP data as well, we cannot use all the data. WMAP uses the entire sky for measurements, and if we want to have independent data sets[1] we need to exclude the l region that is covered by WMAP $l \sim 2 - 700$. But since the WMAP measurements are so accurate, this is not a problem. Since the measurements in the extremely high-l region $l \sim 2000 - 3000$ do not give good constraints on models and since their computation takes an unjustified amount of time, we limit the data set to $l < 2000$ for efficient and fast model comparison. We use the procedures for likelihood computation described by the VSA, ACBAR and CBI collaborations, with window functions and calibration uncertainty.

[1]The ground-based observations only measure the CMB anisotropy in patches on the sky. Since there is only one sky, if one experiment takes measurements from all of it we cannot use other experiments if we want to have independent data sets.

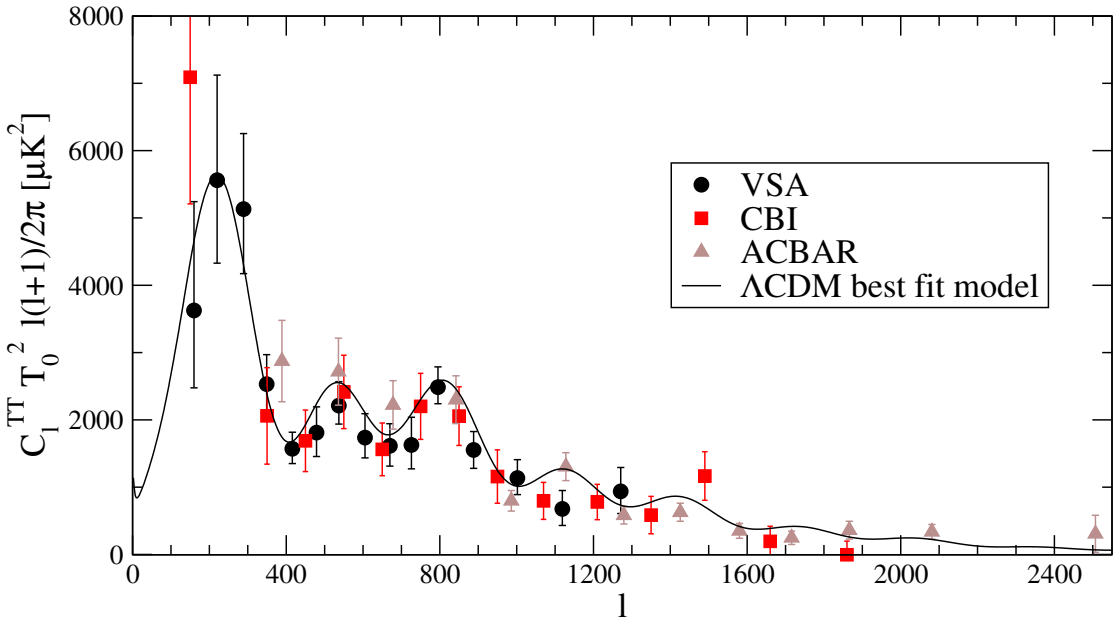

Figure 4.1: A compilation of the latest ground-based CMB measurements. VSA [123] (circles, black), CBI [124] (squares, red) and ACBAR [125] (triangles, brown), all even binning. We have also included the concordance model prediction for comparison.

4.2.3 WMAP

The Wilkinson Microwave Anisotropy Probe (WMAP) is a satellite situated at the second Lagrange point at a distance of about 1.5 million km. Its measurements of the low to intermediate multipole region ($l \sim 2 - 700$) of the CMB are at present the most accurate available. We display the first year WMAP data TT power and TE cross correlation spectrum [121, 122] in fig. 4.2. Looking at this figure, it becomes clear why the WMAP measurements were such a large step in observational cosmology. The first acoustic peak is clearly visible as is the second. We also display the data points from ground-based CMB experiments that we include for constraining models (see section 4.2.2). The WMAP χ^2 computation routines are slightly modified C++ ports of the likelihood code [133] available at the LAMBDA web site [134][2]. When computing the χ^2 statistic we take the amplitude of the power spectrum giving the optimal fit. In other words, we marginalize over the amplitude of the power spectrum.

[2]It was found that the likelihood code provided by the WMAP team is inaccurate for very low multipoles [135]. However, since the impact on parameter constraints is negligible we will use the WMAP procedure.

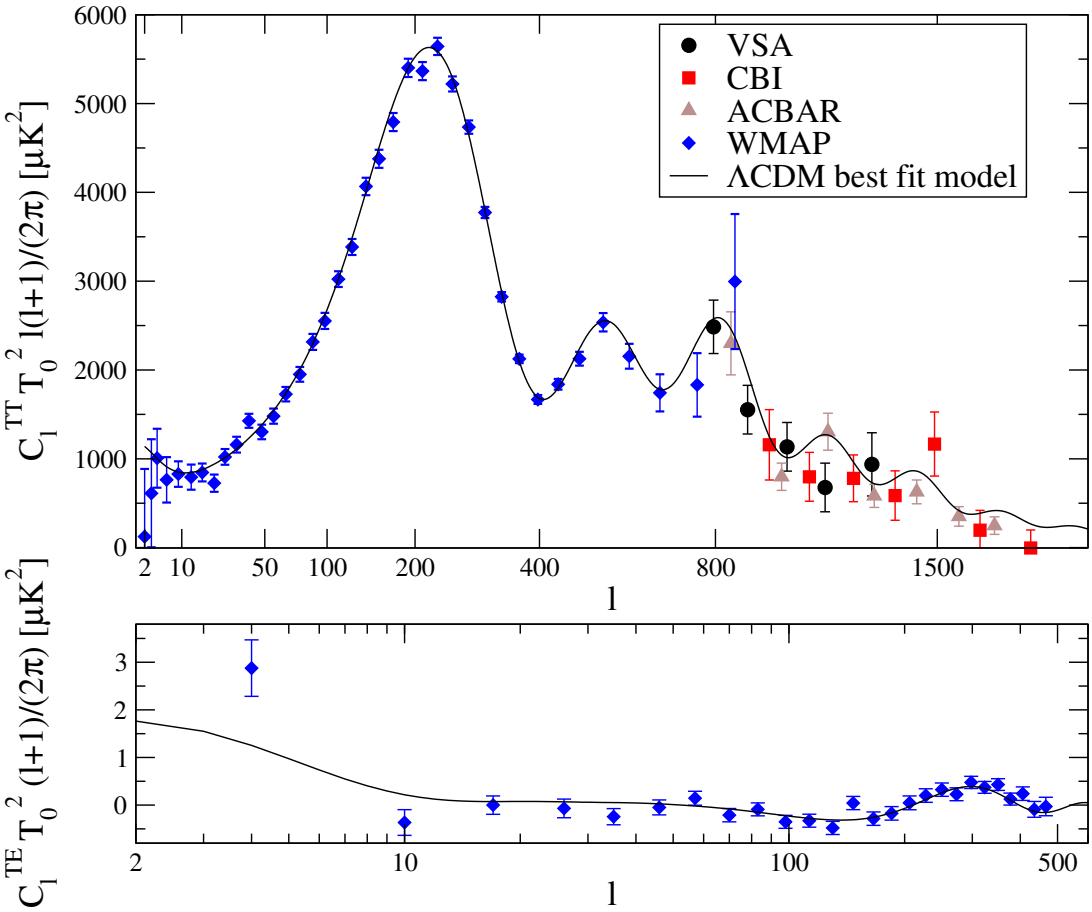

Figure 4.2: The data set of CMB experiments used for constraining models. We have displayed the binned TT and TE spectrum of WMAP [121, 122] (diamonds, blue) and a selection of measurements in the high-l region $l \sim 700 - 2000$ from VSA [123] (circles, black), CBI [124] (squares, red) and ACBAR [125] (triangles, brown). The concordance model prediction is shown for comparison.

4.3 SDSS and 2dFGRS

Observations of the CMB tell us something about the distribution and amplitude of anisotropies when the primordial photons last interacted with free electrons. This was at a redshift of $z \approx 1100$. But we can also measure the distribution of anisotropies today and by doing so we may infer something about the growth of these anisotropies between $z \approx 1100$ and $z = 0$. One way to measure the distribution of anisotropies today is by large scale structure observations. One observes objects such as galaxies and measures their redshift. This data may then be condensed into a power spectrum $P(k)$ that is somewhat alike to the CMB power

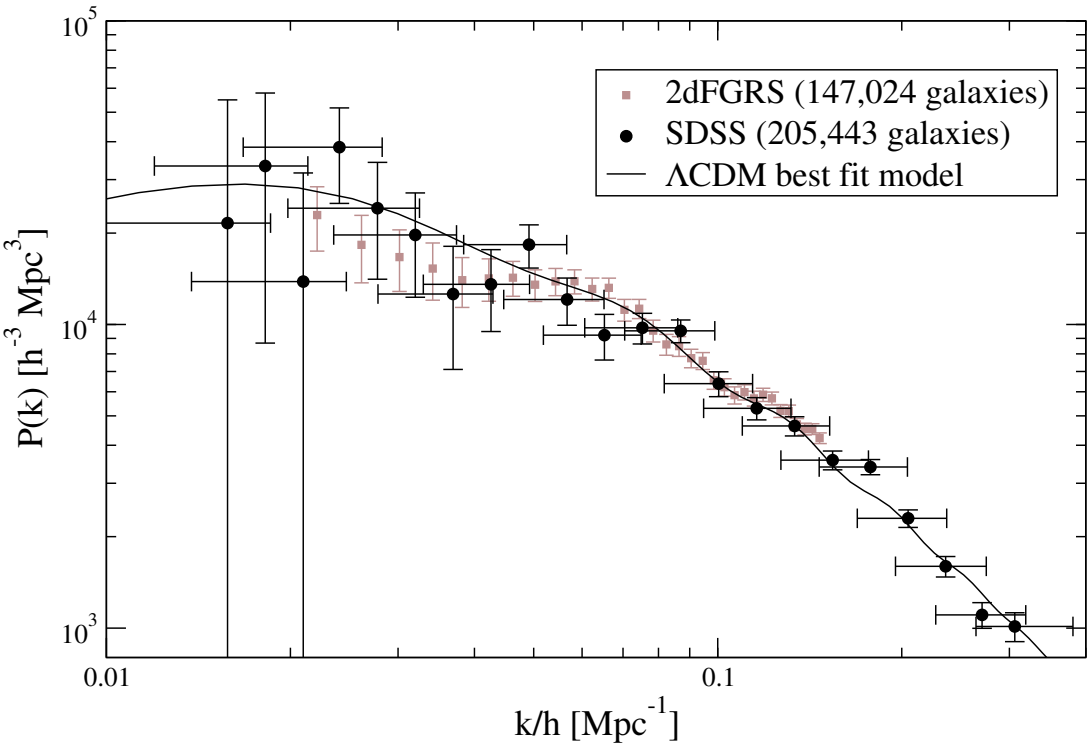

Figure 4.3: The galaxy power spectrum as measured by the large scale structure surveys 2dFGRS [8] (squares, brown) and SDSS [9] (circles, black) and the prediction of the concordance ΛCDM model without window functions and bias (see text). The nonlinear regime starts at $k/h \gtrsim 0.15\ \mathrm{Mpc}^{-1}$.

spectrum and is defined to be the fourier transform of the two-point correlation function of the energy density perturbation

$$\langle \delta(\mathbf{x})\delta(\mathbf{x}+\mathbf{r})\rangle \equiv \int d^3\mathbf{k} P(k) \exp(i\mathbf{k}\cdot\mathbf{r}). \tag{4.4}$$

Assuming that the anisotropies are Gaussian distributed all information is contained in this spectrum as there are no higher correlation moments. Unfortunately, the situation is a bit more complicated – it turns out that perturbation theory is no longer valid on all scales; for instance, the structures at small scales we see today are no longer small perturbations in the energy density. Also, gravitational collapse of the anisotropies leads to the formation of galaxies and makes the distribution of anisotropies non-Gaussian. But fortunately, on the largest scales perturbation theory is still valid as is our assumption of Gaussianity (see [136] for a full treatment). There are two major collaborations that measure the distribution of the galaxies: the two-degree Field Galaxy Redshift Survey (2dFGRS) [8] and the Sloan Digital Sky Survey (SDSS) [9] whose current results we display in

figure 4.3. What these experiments measure is the galaxy power spectrum $P_G(k)$, but what we really would like to have is the CDM power spectrum $P_{CDM}(k)$. It was found that there is a bias $b \equiv P_G(k)/P_{CDM}(k)$ between these two spectra that is independent of scale for large scales and that the non-linear regime starts at about the same scale where one has scale dependent bias [137, 138][3]. Therefore we may use these galaxy power spectrum measurements for constraining models in a linear perturbation theory setting if we only use the data at scales where the anisotropies are linear, $k/h \lesssim 0.15$ Mpc^{-1}. In order to compare the theoretical power spectrum with the data one must compute the power spectrum at the effective redshift of the survey, $z = 0.17$ for the 2dFGRS and $z = 0.10$ for the SDSS. In CMBEASY we use the window functions and marginalize over bias, alternatively the bias may be taken as another parameter.

4.4 Supernovae Ia

Another very important cosmological probe are measurements of the expansion history $\mathcal{H}(z)$. It is directly connected to the constituents of the universe by the Friedmann equation (2.11). One method to do this is by measuring the luminosity distance d_L of objects at different redshifts z and comparing with predictions of the expansion history via eq. (2.33). For a ΛCDM cosmology, d_L takes the form

$$d_L H_0 = (1+z)\int_0^z \left[\Omega_{rad}^{(0)}(1+\tilde{z})^4 + \Omega_{mat}^{(0)}(1+\tilde{z})^3 + \Omega_\Lambda^{(0)}\right]^{-1/2} d\tilde{z}. \qquad (4.5)$$

For models with a quintessence component one has to replace $\Omega_\Lambda^{(0)}$ with the expression for a variable equation of state:

$$\Omega_Q^{(0)}(1+z)^3 \exp\left[3\int_0^z \frac{w_Q(\tilde{z})}{1+\tilde{z}} d\tilde{z}\right]. \qquad (4.6)$$

In order to be able to determine d_L from eq. (2.32) one needs 'standard candles', objects whose absolute luminosity $\mathscr{L}$ is known. It seems that supernovae Ia (SNe Ia) are such standard candles, they have about the same absolute luminosity, there is little evolution over cosmological time scales and they are very bright, making it possible to observe them over cosmological distances. The absolute luminosity of SNe Ia is commonly determined by light-curve fitting. Observations of SNe Ia

[3] We would like to add that in transforming the measured galaxy power spectrum from redshift to real space one needs a cosmological reference model for the background. Using the galaxy power spectrum for constraining a model that differs significantly with respect to the expansion history of the assumed reference model $z \lesssim 0.2$ one will get biased results. For the models we are considering in this work we may assume that there is no problem since they are close to a ΛCDM model at late times.

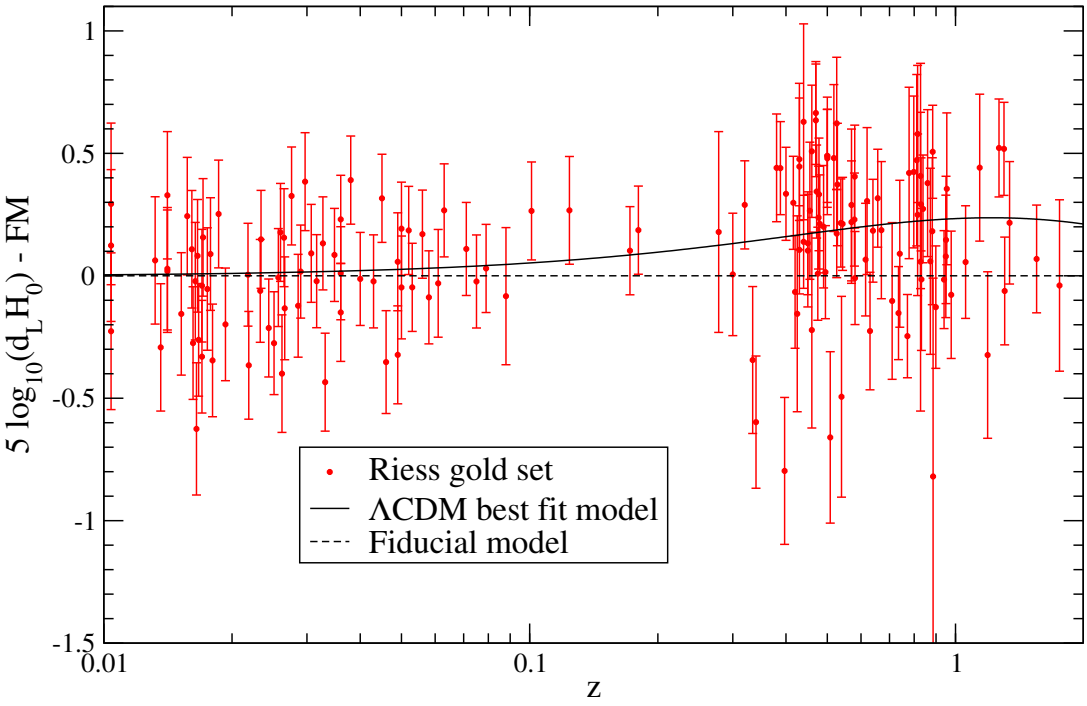

Figure 4.4: The supernovae Ia compilation of Riess et al. [6]. We have plotted the logarithm of the luminosity distance minus a fiducial model (FM) of a spatially flat universe that neither accelerates nor decelerates, see section 4.4 for details. As a reference we also display the luminosity distance for the ΛCDM concordance model with $\mathcal{M} = 25.18$.

have frequently been used to constrain the equation of state of dark energy ever since measurements first indicated that there is such a component in the universe [10–12, 139]. The most complete available data set of SNe Ia is the compilation of Riess et al. [6]. In Fig. 4.4 we display the logarithm of the luminosity distance minus a fiducial model (FM). We have chosen a spatially flat universe that neither accelerates nor decelerates as fiducial model, where d_L is given by

$$d_L H_0 = (1+z)\ln(1+z). \tag{4.7}$$

This corresponds to a universe that contains only one fluid with equation of state $w = -1/3$. We have also subtracted a constant factor $C = 43.34$ so that at $z = 0$ the difference $5\log_{10}(d_L H_0) - 5\log_{10}([1+z]\ln(1+z)) - C = 0$. Constraints from SNe Ia require only the background cosmology and do not require solving the perturbation equations.

The χ^2 statistic for this dataset is determined as follows. First, defining

$$\mu \equiv 5\log_{10}(d_L H_0), \tag{4.8}$$

we obtain

$$\chi^2_{SNeIa} = \frac{\sum_i (\mu_i^{exp} + \mathcal{M} - \mu_i^{theor})^2}{\sigma_i^2}, \tag{4.9}$$

where $\mathcal{M}$ is a nuisance parameter describing the absolute luminosity of the SNe Ia. By minimizing χ^2 with respect to $\mathcal{M}$ we can remove this parameter. When using SNe Ia for setting constraints on models, we will only use the 'gold' set as described in [6] with minimization with respect to $\mathcal{M}$ for each model[4].

4.5 Lyman-α Forest

We will now turn to cosmological probes that are not yet implemented in CMBEASY. We have seen in section 4.3 that we may use the CDM power spectrum at scales $k/h \lesssim 0.15\ \mathrm{Mpc}^{-1}$ where we are still in the linear regime. One interesting way to extend this range to smaller scales is by measuring the power spectrum at high redshift. Today the perturbations at a given scale may be non-linear, but at early times the gravitational collapse may not yet have progressed far enough for the perturbations to become non-linear. As a consequence they may be computed with linear perturbation theory. The problem is to measure the matter distribution at high redhift. Since the objects grow fainter with increasing redshift, it is no longer feasible to measure the spectra of a large number of galaxies. But there are very bright objects whose spectra may be measured: quasars. From a special part of their spectrum, the so-called Lyman-α forest one can extract information about the matter distribution in hydrogen gas clouds and as a consequence, one may determine a power spectrum. The spectrum of a quasar is essentially flat at shorter wavelengths than the Lyman-α wavelength. Since the radiation from a quasar redshifts as it travels towards us, there will be absorption lines appearing in this flat spectrum from the hydrogen clouds the radiation encounters on its way towards us. These absorption lines depend on the density of the gas clouds and on the position in redshift space. Redshifts of $z \approx 3.8$ have been reached using this technique. At present, power spectra have been determined from quasars measured by the SDSS [140] and the 2dFGRS [141]. The problem is that hydrodynamical simulations are needed to determine the resulting power spectrum and it may depend strongly on the assumed cosmology. Also, there is still some uncertainty concerning systematic effects. Nevertheless the Lyman-α forest has already successfully been used to constrain models [142] and will be an important cosmological probe in the near future.

[4] In CMBEASY it is also possible to use the full ('silver') data set.

4.6 Weak Gravitational Lensing

Instead of determining the power spectrum just today, we may also endeavour to measure it at different redshifts. In this way we will get information on the evolution of the anisotropies and thus it will be possible to constrain models, especially the evolution of the equation of state of dark energy w_{DE} if present. This may be accomplished by weak gravitational lensing surveys [143]. The idea is to measure the shapes of distant galaxies that have been distorted by gravitational lensing of massive structures that are between us and the galaxy. From the shapes one may extract the shear field and, eventually, the power spectrum at large redshifts $z \approx 1$. One survey that is presently taking data is the cosmic lens all-sky survey (CLASS) [144, 145]. The data is not yet competitive with other cosmological probes but will become so in the future as a number of dedicated weak lensing surveys are planned or currently taking data such as the CFHTLS [146]. For a review of the theory and experimental technique see [147, 148].

4.7 Primordial Element Abundances

One very restrictive cosmological probe are primordial element abundances. The amount of the light elements such as ^{4}He, deuterium and lithium that were generated during big bang nucleosynthesis (BBN) sets limits on the expansion history at times $z \sim 10^{10}$. This corresponds to limits on the energy density at that time through the Friedmann equation. If one can measure the amount of light elements that were generated during BBN one may learn something about the composition of the universe. Based on observations one may, for instance, compute the number of neutrino species, as more species lead to faster expansion. Primordial element abundances are also useful in restricting models of early dark energy [14, 61]. Unfortunately the measurements of abundances are plagued by various systematic effects. The elements in question are also generated by thermonuclear reactions within stars and therefore contaminate the measurements, other systematic effects also play a role. As a result, the reported abundances vary across the groups. For instance, Izotov and Thuan [149] quote two different values for the primordial ^{4}He abundance for two different equivalent width samples of spectra. The one is $Y_{\mathrm{He}} = 0.2421 \pm 0.0021$ and the other $Y_{\mathrm{He}} = 0.2444 \pm 0.0020$. Another estimate was obtained by Fields and Olive [150] $Y_{\mathrm{He}} = 0.238 \pm 0.002$ (statistic) ± 0.005 (systematic). This discrepancy is most likely attributable to unknown or underestimated systematic effects. At present, there is some strain between experiment and theory, the theory consistently predicting higher abundances for ^{4}He and lithium. We will consider this point thoroughly in chapter 7. Current experimental limits on the primordial element abun-

dances may be found in [151].

5

Markov Chain Monte Carlo Simulation

The probability of the bread falling buttered side down is directly proportional to the price of the carpet.

Murphy's Laws

In the previous chapter we described a variety of cosmological probes that may be used to constrain theoretical models. In this chapter we want to discuss how one obtains these constraints. There is a number of numerical tools, such as CMBFAST [16], CAMB [17] and CMBEASY [18] for calculating the prediction of a given model for the observational data. Once we have done so we can compute the χ^2 statistic for each observational data set. For each model we need a set of parameters. Suppose we have a cosmological model M with n parameters $\theta^{(i)}$ and we would like to obtain the distributions of these parameters for estimating confidence regions and means. One could use the naive approach and perform a grid computation: discretize each parameter range into a points and evaluate the likelihood of the model M at each point in the resulting lattice.

The problem is that the grid approach quickly becomes computationally unfeasable. For a grid of n parameters subdivided into a points we have to evaluate a^n models, so computing time grows exponentially with the number of parameters. Furthermore, many models computed in this way may have negligible weight due to low likelihood.

Markov Chain Monte Carlo (MCMC) simulation offers an alternative to this brute-force approach. Using this technique, we can directly draw samples from the underlying distribution and the computational effort increases only linearly

with the number of parameters. Obtaining the statistical properties of the parameters is then a straightfoward excercise.

MCMC simulation has been widely used since it was first introduced [19, 152] for constraining various models [63, 133, 153, 154]. There are some software packages that can set up MCMC simulations such as COSMO-MC [155] or ANALYZETHIS! [20]. We will now describe the general idea of Markov Chain Monte Carlo simulation and then turn to the specific implementation in the ANALYZETHIS! package of the CMBEASY software.

5.1 Bayesian Inference and Markov Chains

We will give a short introduction to Bayesian inference and Markov Chains in this section. For a more thorough treatment the reader is referred to the existing literature [156–159]. Suppose we have a set of observed data $x = (x_n, \ldots, x_0)$ with all of the x_i independent and a model with parameter vector θ containing all parameters of the model. The probability of obtaining x given parameters θ is called the likelihood $L(x|\theta)$. We may also have some knowledge of the distribution of the parameters before x was observed. For instance, some regions of parameter space may be excluded for physical reasons (such as a negative energy density) or there have been other observations giving us some idea about the distribution of θ. This knowledge prior to observing x is encapsulated in the prior distribution $P(\theta)$ of θ. Then the probability distribution of θ given observations x and a prior $P(\theta)$, the so-called posterior distribution $\pi(\theta|x)$, is given by Bayes' theorem:

$$\pi(\theta|x) = \frac{P(\theta)L(x|\theta)}{\int P(\theta)L(x|\theta)d\theta}. \tag{5.1}$$

In the following, we will write $\pi(\theta)$ for the posterior distribution, it being understood that x has been observed. From the posterior $\pi(\theta)$ we may then obtain the marginalized distribution of parameter $\theta^{(i)}$ by

$$\pi(\theta^{(i)}) = \int \pi(\theta^{(1)}, \ldots, \theta^{(n)}) d\theta^{(-i)}, \tag{5.2}$$

where the integration is over all parameters except $\theta^{(i)}$. The mean of a function $f(\theta)$ is given by

$$E[f(\theta)] = \frac{\int f(\theta)\pi(\theta)d\theta}{\int \pi(\theta)d\theta}. \tag{5.3}$$

We will now turn towards MCMC simulation itself, starting with Markov Chains in general. The general idea is to directly draw samples from the posterior distribution $\pi(\theta)$. The statistical properties of $\pi(\theta)$ such as confidence regions may

then be estimated using this sample[1]. A way to directly draw samples from $\pi(\theta)$ is by using a Markov Chain. Suppose we generate a series of random variables from a state space S (in our case, different parameter vectors), $(\theta_0, \theta_1, \ldots, \theta_n)$, such that the next state $\theta_{n+1} \in S$ in this sequence is sampled from a distribution $P_T(\theta_{n+1}|\theta_n)$ that depends only on the present state θ_n of the series. This sequence is then called a Markov Chain. If the transition probability between two states does not depend on n the chain is said to be homogeneous. A fundamental concept of Markov Chains is the stationary distribution $D(y)$. A distribution $D(y)$ is said to be a stationary distribution of a chain with transition probabilities $P_T(z|y)$ if

$$D(y) = \int_{-\infty}^{\infty} D(z) P_T(y|z) dz. \tag{5.4}$$

From this equation it is clear why this is called the stationary distribution: once the chain reaches a stage where $D(y)$ is the distribution of the chain, the chain retains this distribution in all subsequent stages. One can show that if the Markov Chain has certain properties then the stationary distribution will be reached irrespective of the initial distribution of the chain [157, 160]. So D will be reached as $n \to \infty$. In this sense, it is also referred to as the limiting distribution. The task is now to find an algorithm for the Markvo Chain that satisfies the requirements for the existence of the limiting distribution and gives us the posterior $\pi(\theta)$ as the limiting distribution. We can then let the chain run until it has reached the stationary distribution[2], the chain points are then samples of the posterior $\pi(\theta)$ and we can constrain our model parameters. One such algorithm is the Metropolis algorithm.

5.2 The Metropolis Algorithm

If we generate a Markov Chain using the Metropolis-Hastings algorithm then the limiting distribution exists and is identical to the posterior $\pi(\theta)$ [161, 162]. In this algorithm the transition probability P_T between two states θ_{i-1} and θ_i is given by

$$P_T(\theta_i, \theta_{i-1}) = \min \left[1, \frac{L(x|\theta_i) P(\theta_i) q(\theta_i, \theta_{i-1})}{L(x|\theta_{i-1}) P(\theta_{i-1}) q(\theta_{i-1}, \theta_i)} \right], \tag{5.5}$$

where $q(\theta_{i-1}, .)$ is a proposal distribution. If the proposal distribution is symmetric $q(y, z) = q(z, y)$ then this is called the Metropolis algorithm [162]. If we use flat priors $P(\theta)$ on the parameters the algorithm works as follows [133]:

[1] For instance, one can infer the mean of parameter $\theta^{(i)}$ from the sample of parameter values $\theta_1, \ldots, \theta_n$ (the ergodic average): $E[\theta^{(i)}] = \frac{1}{n} \sum_{j=1}^{n} \theta_j^{(i)}$

[2] In practice the stationary distribution is reached after a finite number of steps which makes it possible to use the chain output after a certain number of steps as a sample of the stationary distribution.

1. Choose randomly a starting parameter vector θ_0 within the flat prior $P(\theta)$
2. Compute the likelihood $L_0(x|\theta_0)$ of observing the experimental data given the parameters θ_0.
3. Obtain a new parameter vector by sampling from a proposal distribution $q(\theta_i, \theta_{i-1})$ (see section 5.3).
4. Compute the likelihood $L_i(x|\theta_i)$.
5. If $L_i > L_{i-1}$ save θ_i as a new point in the chain ('take the step') and go to (3).
6. If $L_i < L_{i-1}$ generate a random variable u from the flat distribution $[0, 1]$. If $u < L_i/L_{i-1}$ take the step as in (5). If $u > L_i/L_{i-1}$ reject θ_i, save θ_{i-1} as new point in the chain and go to (3).

If we end up with a parameter outside the prior in step (3), we assign likelihood zero to this point. The algorithm is illustrated in figure 5.1.

The resulting chain is then a sample of $\pi(\theta)$ once the chain has reached the stationary distribution. The points of the chain may then be used to estimate confidence regions of the parameters. We will now discuss the specific implementation of this algorithm in the ANALYZETHIS! package of the CMBEASY software.

5.3 Convergence and the Proposal Distribution

In the above discussion we skipped over two important details: how do we know that the chain has reached the stationary distribution, that is, when has a chain converged? And how do we choose the proposal distribution such that the convergence is optimized?

5.3.1 Convergence Testing

A chain has converged when the chain points constitute a sample from the posterior. In particular, there should be no dependence on the starting points. Our task then, is to find the point in the chain where we can assume that we are sampling from the posterior and delete all points prior to that (the so-called 'burn-in') from the chain to eliminate any dependence of our parameter estimates on the starting points.

This task can be made much easier by running more than one chain with different starting positions and then comparing the distribution of points of each chain. If they all give the same distribution we can assume that they all have converged and remove the burn-in from all chains to obtain the distribution of our parameters.

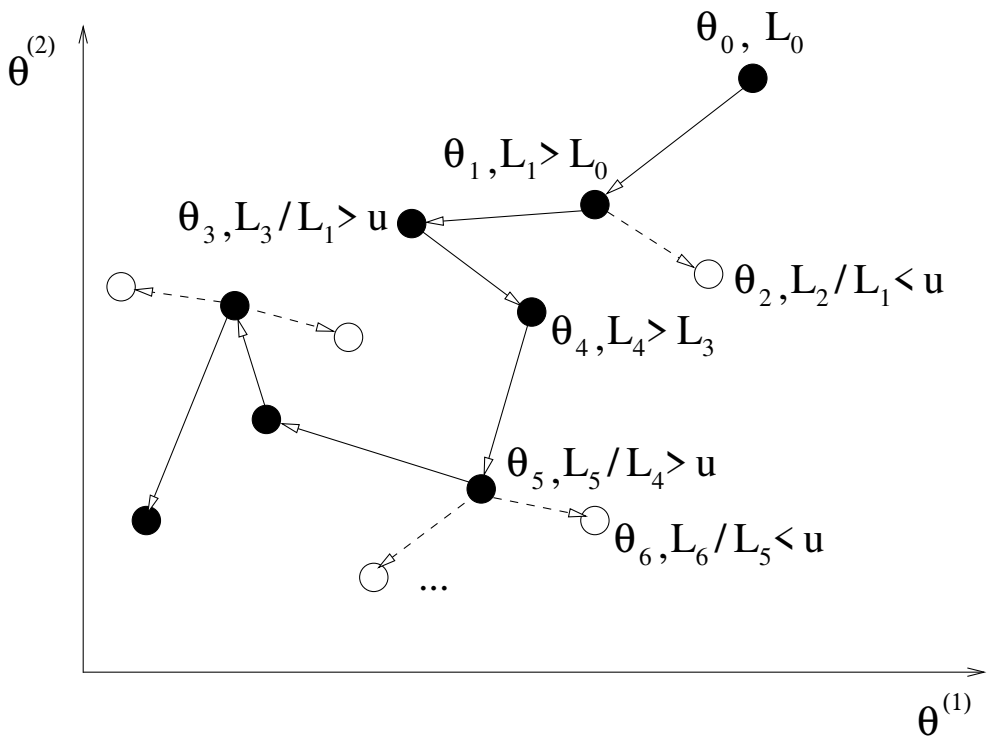

Figure 5.1: Illustrating the Metropolis algorithm with flat priors for two parameters. Filled circles represent points belonging to the chain, empty circles are proposed but rejected points not belonging to the chain. In this example, the chain would be $[\theta_0, \theta_1, \theta_1, \theta_3, \theta_4, \ldots]$

The convergence test used in the ANALYZETHIS! package is due to Gelman and Rubin [163]. The idea is to run multiple chains and compare the variance of the parameters within one chain with the variance between the chains. To be precise, consider using the last n points of each of m chains for the test. Let ψ_{ij} label one entry of the parameter vector θ at point $j = 1, \ldots, n$ in chain i with $\overline{\psi}_i$ the mean for chain i and $\overline{\psi}$ the mean of all chains. The variance between chains B and the within-chain variance W are then given by

$$B = \frac{n}{m-1} \sum_{i=1}^{m} \left(\overline{\psi}_i - \overline{\psi}\right)^2, \tag{5.6}$$

$$W = \frac{1}{m} \sum_{i=1}^{m} s_i^2, \quad \text{where} \quad s_i^2 = \frac{1}{n-1} \sum_{j=1}^{n} \left(\psi_{ij} - \overline{\psi}_i\right)^2, \tag{5.7}$$

and the quantity

$$R = \frac{[(n-1)/n]W + (1/n)B}{W}, \tag{5.8}$$

should converge to one. In a realistic situation, the numerator is an overestimate whereas the denominator is an underestimate of the variance of the stationary distribution of ψ. Gelman and Rubin suggest that a value of $R < 1.2$ for all parameters indicates that the chain is sampling from $\pi(\theta)$, but one may take more stringent constraints [133][3]. From this point onwards one may use the chain points for parameter estimates. This is not a mathematically stringent method to determine convergence but it nevertheless works well in practical applications which is why this convergence testing criterion is used in ANALYZETHIS!.

5.3.2 Optimizing the Proposal Distribution

Having described our convergence test we can now address the issue of choosing the proposal distribution $q(\theta_{i-1}, \theta_i)$ such that the burn-in is minimized. In principle, the proposal distribution can have any form as long as we can reach the entire parameter space with it. However, for optimal convergence $q(\theta_{i-1}, \theta_i)$ should be as close as possible to the likelihood surface of the posterior $\pi(\theta)$. Of course, the distribution of the posterior is not known a priori and hence we must resort to estimation procedures. Based on previous MCMC simulations we can assume that most of the parameters have approximately a Gaussian distribution. A first step in obtaining a good proposal distribution is therefore to use such a Gaussian distribution as proposal distribution with variances σ_i for each parameter. Before we can use this proposal distribution, we have to specify the variances σ_i for each parameter. We can make a guess and then use an adaptation scheme during the run to optimize the acceptance of proposed points; for instance, we can estimate the σ_i's from the points of the chain.

This 'naive Gaussian sampler' approach will work fine, but it can still be improved. There may be a degeneracy between the parameters, e. g. if one increases $\theta^{(1)}$ and decreases $\theta^{(2)}$ by a suitable amount one may obtain the same likelihood for the resulting model. In this case, our sampler will not be as good as it could be as illustrated in figure 5.2. So instead of sampling from a Gaussian distribution for each parameter separately we can sample from a multivariate Gaussian with covariance matrix estimated from the previous points in the chain. By taking into account the full covariance matrix we essentially approximate the likelihood contour in extent and orientation – the Gaussian samples are taken along the principal axis of the likelihood contour. Writing $\theta_{i-1} - \theta_i = \mathbf{u}_i$ for notational convenience, the proposal distribution we use for the steps is

$$q(\theta_{i-1}, \theta_i) \sim N \exp\left[-\frac{1}{2}\mathbf{u}_i^T \mathbf{S}^{-1} \mathbf{u}_i\right], \tag{5.9}$$

[3] In our implementation the value of R at which we assume the chains to have converged may be chosen freely.

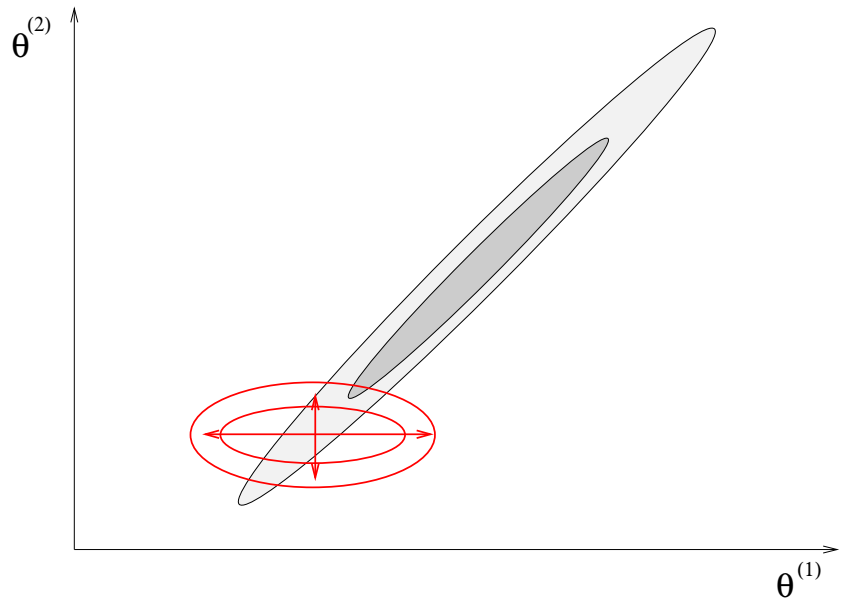

Figure 5.2: The naive Gaussian sampler for two partially degenerate parameters. The (unknown) true likelihood surface is shown along with the proposal distribution with arrows (stylized). This proposal distribution does not take into account the degeneracy among the parameters $\theta^{(1)}$ and $\theta^{(2)}$, leading to slow mixing.

where $N = (2\pi)^{-K/2} (\det \mathbf{S})^{-1/2}$ and $\mathbf{S}$ is the covariance matrix

$$\mathbf{S} = \begin{pmatrix} \sigma_1^2 & \rho_{12} & \cdots & \rho_{1K} \\ \rho_{21} & \sigma_2^2 & \cdots & \rho_{2K} \\ \vdots & & \ddots & \vdots \\ \rho_{K1} & \cdots & \rho_{K-1K} & \sigma_K^2 \end{pmatrix}. \tag{5.10}$$

The sampling is most easily performed by diagonalizing the covariance matrix

$$\mathbf{T}^T \mathbf{S}\, \mathbf{T} = \mathbf{D} \Longleftrightarrow \mathbf{T}^T \mathbf{S}^{-1} \mathbf{T} = \mathbf{D}^{-1}, \tag{5.11}$$

where $\mathbf{T}$ is an orthogonal matrix and $\mathbf{D}$ a diagonal matrix with entries $\tilde{\sigma}_i$. Then equation (5.9) becomes

$$q(\theta_{i-1}, \theta_i) \sim N \exp\left[-\mathbf{u}_i^T \mathbf{T}\mathbf{T}^T \mathbf{S}^{-1}\, \mathbf{T}\mathbf{T}^T \mathbf{u}_i\right] \tag{5.12}$$

$$= N \exp\left[-\frac{1}{2} \mathbf{v}_i^T \mathbf{D}^{-1} \mathbf{v}_i\right], \tag{5.13}$$

where $\mathbf{v}_i \equiv \mathbf{T}^T \mathbf{u}_i$. Thus, the procedure for obtaining a sample $\mathbf{u}_i$ is as follows:

1. Find the eigenvalues $\tilde{\sigma}_j^2$ and eigenvectors of $\mathbf{S}$. Construct the transformation matrix $\mathbf{T}$ from the eigenvectors.

2. Draw Gaussian samples with variances $\tilde{\sigma}_j^2$, thereby obtaining the vector $\mathbf{v}_i$.
3. Then $\mathbf{u}_i = \mathbf{T}\mathbf{v}_i$ is the desired sample from the multivariate Gaussian with covariance matrix $\mathbf{S}$.

The convergence can be further improved by scaling the covariance matrix $\mathbf{S}$ with a variable factor β. Using β, we can cope better in situations where the projected likelihood takes on banana shapes such as in [154]. It also improves the convergence during the early stages when the low number of points available limits the estimate of the covariance matrix $\mathbf{S}$. Using this method, convergence is speeded up considerably relative to the naive Gaussian sampler method[4].

There is a caveat, though. One can show that modifying the proposal distribution based on previous chain data during the run may lead to a wrong stationary distribution $\pi'(\theta)$ [157,159]; after all, the requirement that each point in the chain only depend on the previous point would be violated and we would no longer have a Markov Chain. Therefore we only apply the dynamical strategy of finding an optimal step proposal during the early stages of the simulation. When the R-criterion for convergence is satisfied we 'freeze in' the proposal distribution, that is, the covariance matrix $\mathbf{S}$ is fixed from then on. All chain points before this freeze in should be discarded.

5.4 Model Analysis Example: ΛCDM

5.4.1 Model & Used Data Set Specification

In order to make the whole procedure a bit clearer, we will constrain a ΛCDM cosmology using MCMC simulation. The model has five parameters: the reduced baryon and matter densities $\Omega_b h^2$ and $\Omega_m h^2$, the Hubble parameter $h = H_0/(100 \text{ km s}^{-1}\text{Mpc}^{-1})$, the optical depth to the last scattering surface τ and the spectral index of the initial power spectrum n_s. The flat priors and initial stepsizes used are displayed in table 5.1. The limits of the parameter ranges are chosen in accordance with previous results [27,29]. The cosmological constant Λ is the dark energy component and we limit ourselves to a spatially flat universe. We neglect any tensor contributions and we marginalize over the amplitude of the initical power spectrum, the bias b of the CDM power spectrum $P_{CDM}(k)$ and the absolute luminosity of the supernovae $\mathcal{M}$. The data used for constraining the model was WMAP, ACBAR, CBI and VSA as displayed in figure 4.2, the SDSS data with $k/h < 0.15 \text{ Mpc}^{-1}$ and the SNe Ia 'gold set' data of Riess (see the previous chapter for relevant details and references). In order to discuss the influence of the

[4] A different proposal distribution, applicable to the local Metropolis algorithm as used in the CAMB code has been suggested in [164].

Parameter	Min	Max	stepsize σ
$\Omega_b h^2$	0.016	0.03	0.00136
$\Omega_m h^2$	0.05	0.3	0.0144
h	0.60	0.85	0.032
τ	0	0.9	0.068
n_s	0.8	1.2	0.037

Table 5.1: Flat priors on the parameters and initial stepsizes used in our MCMC simulation for all three runs.

different data sets on the parameter constraints, we will run three simulations with CMB only, CMB + SNe Ia and with CMB + SNe Ia + LSS ('full set') data combined. The MCMC simulations were set up using four chains, with adaptive stepsize using the full covariance matrix that freezes is as soon as convergence is reached. The requirement for convergence was set to be $R < 1.1$. In the full set simulation, convergence was reached after ≈ 1000 models, the stepsize adaptation was then frozen in. After burn-in removal the total number of chain points used for analysis was 55,548, the numbers for the two other simulations were at the same order of magnitude. In order to illustrate convergence we have plotted the value of h for two chains in figure 5.3 for the first 1000 models.

5.4.2 Output Analysis

We have integrated a graphical user interface (GUI) in the CMBEASY software that allows one to quickly and conveniently process and analyze the raw chain data files generated in a MCMC simulation. One can also plot and print directly from the GUI.

For plotting one-dimensional marginalized distributions we fit the histograms extracted from the chains using a fit with seven parameters a_i

$$f_{1D}(x) = \exp\left(\sum_{i=0}^{6} a_i x^i\right), \tag{5.14}$$

while for plotting the two-dimensional distributions we fit the histograms using a fifteen parameter function in two dimensions

$$f_{2D}(x,y) = \exp\left(\sum_{0\le i+j\le 4} b_{ij} x^i y^j\right). \tag{5.15}$$

The one-dimensional marginalized distributions for the five parameters are depicted in figure 5.4 for all three simulations and the two-dimensional distribu-

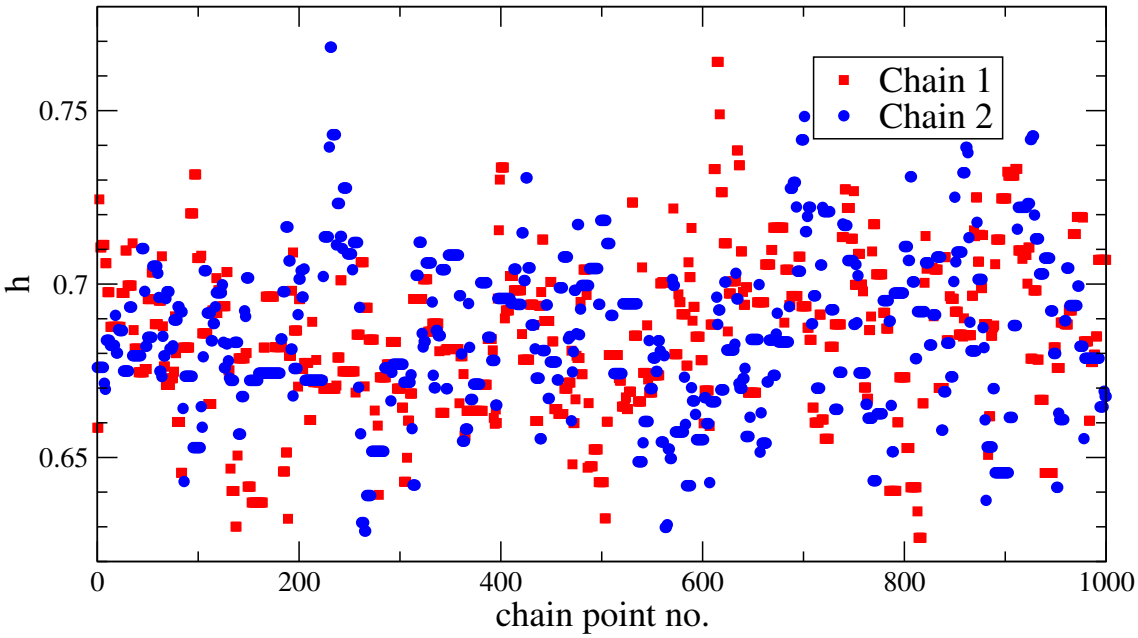

Figure 5.3: The value of parameter h for the first thousand models of chains one (squares, red) and two (circles, blue) of the five-parameter ΛCDM example run using CMB + SNe Ia + LSS data (see text). Even though the chains start in completely different regions of parameter space, they quickly sample from the same distribution. Convergence diagnostics indicate that all chains have converged after $\approx$ 1000 steps.

tions for the full set simulation are shown in figure 5.5. The resulting confidence regions for each parameter are displayed in table 5.2.

We will now discuss the impact of the different observational data sets on the parameters. Consider figure 5.4. The CMB-only data set does not well constrain $\Omega_m h^2$. Adding supernovae improves the bounds on the total matter content considerably, because the lumiosity distance depends sensitively on Ω_m. Adding large scale structure data breaks the degeneracy between matter contribution and initial power spectrum amplitude, hence we obtain still tighter bounds. Note that the distribution of $\Omega_m h^2$ obtained from CMB-only and CMB + SNe Ia + LSS data sets differ somewhat. This has already been noted in [29]. Even from CMB measurements alone we can infer the presence of dark matter at high significance. In contrast, the baryon contribution $\Omega_b h^2$ is already well constrained by the CMB alone, adding SNe Ia and LSS data only improves the bounds slightly. The CMB is most sensitive to this parameter since what one observes are essentially oscillations in a photon-baryon plasma, the density of baryons is a critical parameter for the shape of the CMB spectrum. SNe Ia and LSS measurements are more or less insensitive to this parameter, though hints at oscillations in the power spectrum

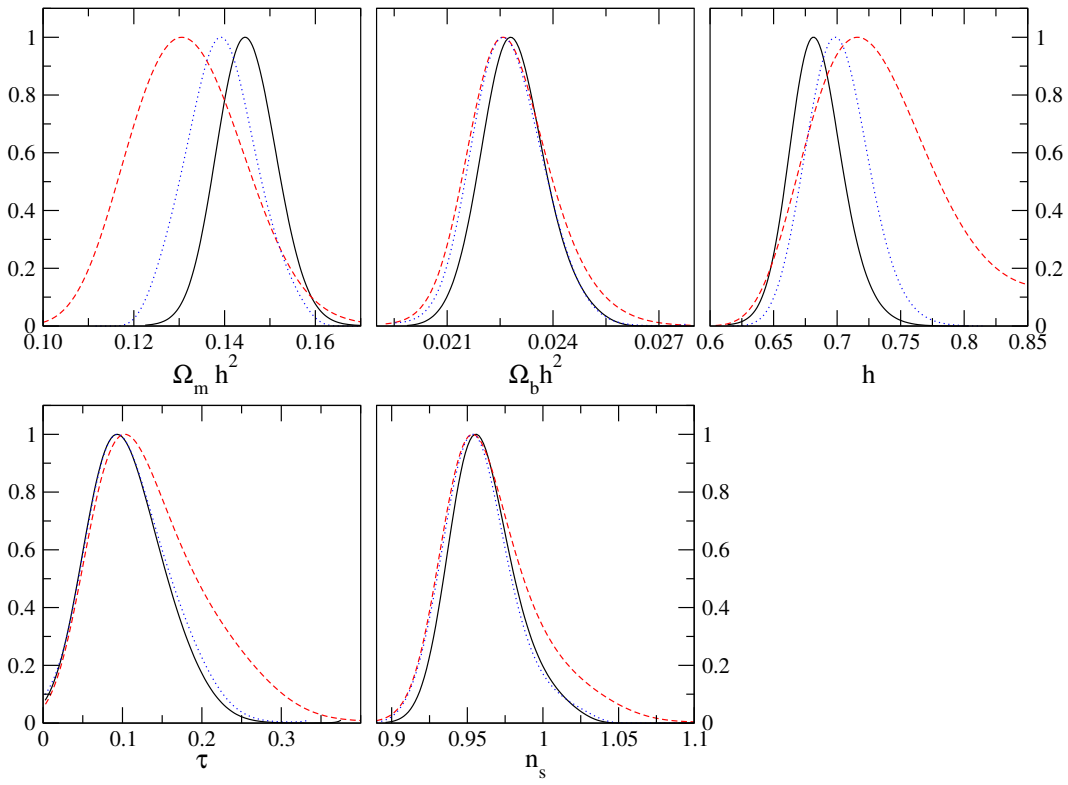

Figure 5.4: One-dimensional marginalized distributions for the five parameters. Constraints from CMB only (dashed, red), CMB + SNe Ia (dotted, blue) and CMB + SNe Ia + LSS (straight, black).

Parameter	CMB only	CMB + SNe Ia	CMB+ SNe Ia + LSS
$\Omega_b h^2$	$0.02261^{+0.0012}_{-0.0011}$	$0.02257^{+0.0011}_{-0.0009}$	$0.02278^{+0.0009}_{-0.0009}$
$\Omega_m h^2$	$0.1306^{+0.013}_{-0.012}$	$0.1393^{+0.0076}_{-0.008}$	$0.144^{+0.0063}_{-0.0066}$
h	$0.716^{+0.053}_{-0.041}$	$0.699^{+0.024}_{-0.024}$	$0.682^{+0.021}_{-0.021}$
τ	$0.1019^{+0.081}_{-0.052}$	$0.0941^{+0.058}_{-0.043}$	$0.0938^{+0.051}_{-0.043}$
n_s	$0.954^{+0.032}_{-0.024}$	$0.953^{+0.024}_{-0.021}$	$0.956^{+0.023}_{-0.019}$

Table 5.2: Constraints on the parameters of the ΛCDM model from a combination of data sets. These confidence intervals were generated from the one-dimensional marginalized distributions (errors are given at 68.3 % confidence level).

have been detected [8].

The Hubble parameter h, is only slightly constrained by CMB measurements alone. Adding SNe Ia data considerably improves the bounds, adding large scale structure data does not improve the bounds very much. The bounds obtained for the Hubble parameter for the full data set are consistent with the HST key project value $h = 0.72 \pm 0.08$ [7] derived from measuring the local Hubble flow or the results from the SNe Ia Hubble diagram $h = 0.73 \pm 0.04$ (statistical) $\pm$ 0.05 (systematic) [165]. Even though the optical depth does not directly influence SNe Ia predictions, adding SNe Ia data tightens the bound on the optical depth τ as seen in figure 5.4. The mechanism is somewhat indirect: SNe Ia data tightens the bound on Ω_m and thus limits the range of allowed values for τ, h and n_s from CMB measurements. As we marginalize over the bias of the SDSS data, large scale structure does not add further to the bounds on τ. This concludes our discussion of MCMC simulation.

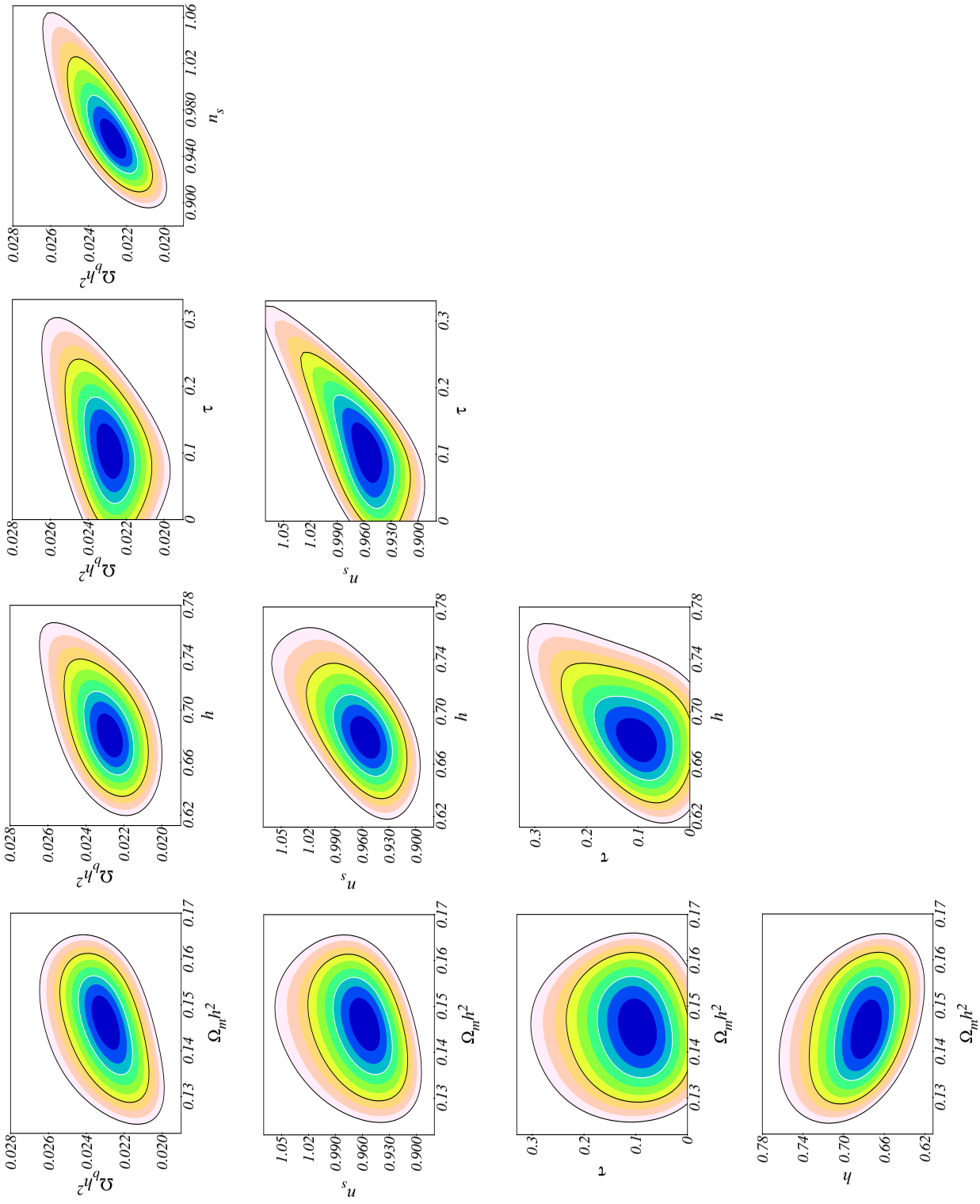

Figure 5.5: Two-dimensional marginalized likelihoods for the five cosmological parameters of the ΛCDM example using CMB + SNe Ia + LSS data. The contours are one, two and three sigma confidence regions, respectively.

6

Constraining the Equation of State of Dark Matter

Space is big. You just won't believe how vastly, hugely, mind-bogglingly big it is. I mean, you may think it's a long way down the road to the chemist's, but that's just peanuts to space.

Douglas Adams, The Hitchhiker's Guide to the Galaxy

In this chapter we would like to constrain the dark matter equation of state using cosmological observations and Markov Chain Monte Carlo simulation [166]. The question we want to answer is: given the information from present cosmological observations, how sure can we be that the equation of state of dark matter is $w_{DM} = 0$? Or, phrased differently: how cold is cold dark matter?

In this context, we do not want to limit ourselves to a non-negative equation of state since the nature of dark matter is not yet clear. There are a number of particle dark matter candidates and numerous experiments attempting to detect dark matter particles (see section 2.2.4 and references therein). However, dark matter may not be a particle at all, it may be something different, such as non-linear fluctuations of a scalar field [167]. We will try to keep an open mind and check if a significantly negative or positive equation of state can be ruled out by cosmological observations. Previous studies focused on the power spectrum properties of warm dark matter [168] and mixed dark matter models [169], but we would like to emphasize that the present work does not consider the bounds on warm dark matter since there, w_{DM} changes over time whereas we keep w_{DM} fixed. We will consider both positive and negative equations of state w_{DM} and show that the equation of state of dark matter is already strongly constrained by current observations of the CMB, SNe Ia and LSS. We will not concern ourselves with bounds from other than cosmological observations.

This is meant as an exploratory study, not as rigid modeling of dark matter, and we will therefore work only from a fluid perspective and leave the question open how one could obtain a negative equation of state of dark matter. For clarity, we will only allow for a constant equation of state w_{DM}. We have chosen this approach as there is no possibility to give a model-independent formulation of the temporal evolution of w_{DM}.

In models where dark matter interacts with other components of the universe, such as in coupled quintessence models [57], one may obtain a negative equation of state for dark matter. It may be possible to obtain $w_{DM} < 0$ by other methods as well, but we are not aware of any such model. We will consider only gravitationally interacting dark matter here.

We will discuss two simple models for dark matter: one with no entropy production and one with vanishing adiabatic sound speed, both with fixed equation of state. For this investigation we will assume that the universe is spatially flat and contains a cosmological constant type dark energy component with equation of state $w_{DE} = -1$, dark matter with an equation of state $w_{DM} \neq 0$, baryons, photons and massless neutrinos. We do not include the tensor part in our analysis. Following our investigation we will address the issue what will change if we relax the flatness assumption and if the dark energy has an equation of state different from -1.

6.1 Model I: Dark Matter with No Entropy Production

In this section, we will assume that the dark matter component does not produce entropy, $\Gamma_{DM} = 0$. For a constant equation of state of dark matter, the background sound speed is given by

$$c_s^2 = p'/\rho' = w_{DM}. \tag{6.1}$$

If we allow for negative equation of state the square of the background sound speed may thus become negative and, through $\Gamma_{DM} = 0$, this means c_{ad}^2 will also be negative. There is of course a question whether or not this assumption is reasonable, but given the unknown nature of dark matter we may consider this case and see how well constrained w_{DM} is. Before we discuss the numerical solutions of the perturbation equations, it will be helpful to consider the solutions for a universe filled only with dark matter in the sub-horizon limit, $k^2 \gg \mathcal{H}^2$. Equations (3.45)-(3.47) may be combined to eliminate V_{DM} (we will suppress the index DM in what follows for notational simplicity):

$$\Delta'' - (3w-1)\mathcal{H}\Delta' + wk^2\Delta + k^2(1+w)(\Psi - 3w\Phi) = 0, \tag{6.2}$$

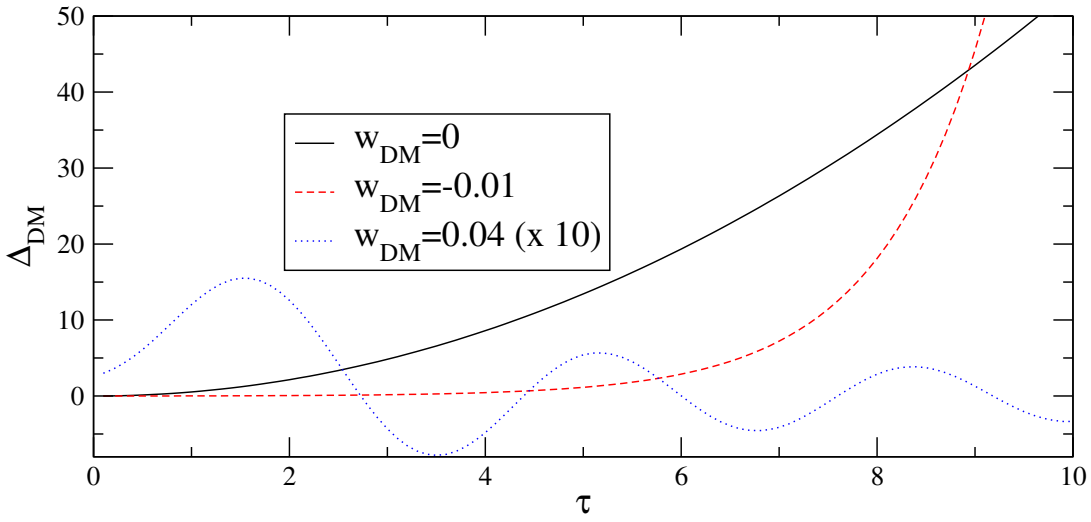

Figure 6.1: Evolution of the energy density perturbation of dark matter Δ_{DM} in the sub-horizon regime for several equations of state in a universe containing only dark matter with $\Gamma_{DM} = 0$. In the case of $w_{DM} = 0$, the energy density perturbation grows $\propto \tau^2$ (straight, black). For $0 < w_{DM} < 1/3$ (dotted, blue) one obtains decaying oscillations while for $w_{DM} < 0$ the density perturbation grows rapidly (dashed, red).

$$\Phi'\mathcal{H} + \left(\frac{5}{2} + \frac{3}{2}w\right)\mathcal{H}^2\Phi + \frac{k^2}{3}\Phi = \frac{\Delta}{2}\mathcal{H}^2. \tag{6.3}$$

The background solution for a universe filled only with a modified dark matter component yields

$$\mathcal{H} = \frac{2}{\tau + 3\tau w_{DM}}. \tag{6.4}$$

For $w_{DM} = 0$ the solution of (6.2) and (6.3) in the sub-horizon limit is $\Delta_{DM} = a(\tau) = \tau^2$ and $\Phi =$ const., as is well known. For the super-horizon regime, $\Delta_{DM} =$ const. The solutions to these equations in the sub-horizon limit if $w_{DM} \neq 0$ are plotted in figure 6.1. It can be seen that for $0 < w_{DM} < 1/3$ we obtain decaying oscillations for Δ_{DM} while for $w_{DM} = 1/3$ one gets oscillations with constant amplitude. For $w_{DM} < 0$ we find that Δ_{DM} increases rapidly. This is obviously due to the negative sound speed, which leads to a growing gravitational potential. We can thus already see that the equation of state will be strongly constrained in the regime $w_{DM} < 0$ since we do not observe this excess or lack of power on small scales. Also, the growing gravitational potential would lead to excessive lensing on small scales, which is not observed. At super-horizon scales, $\Delta_{DM} =$ const., regardless of the equation of state.

We have computed the resulting CMB and power spectrum in figure 6.2 using the parameters of a ΛCDM model with the following parameters: $\Omega_b h^2 = 0.230$,

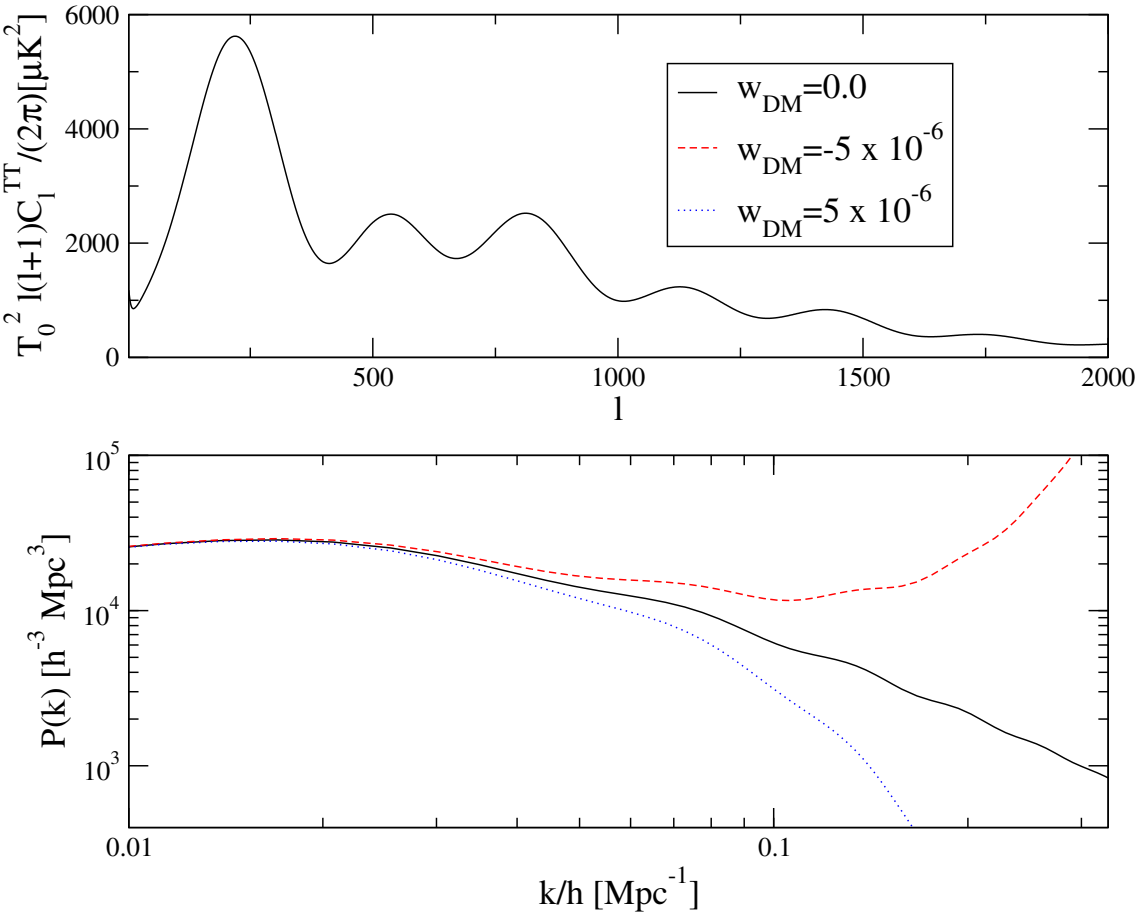

Figure 6.2: CMB and matter power spectra for a ΛCDM model with modified dark matter, $\Gamma_{DM} = 0$. The power on small scales is much larger than in the $w_{DM} = 0$ case (straight, black) if the equation of state is negative (dashed, red). One can see the decaying oscillations for the case of $w_{DM} > 0$ (dotted, blue). As expected, there is no difference in the power spectra at very large scales. The impact on the CMB spectrum is not noticable at this level.

$\Omega_m h^2 = 0.144$, $n_s = 0.961$, $\tau = 0.114$, $h = 0.69$. As one can verify the impact of varying w_{DM} on the power spectrum is very marked on small scales. We therefore expect to obtain tight constraints on w_{DM}. There is hardly any impact on the CMB spectrum at this level so constraining power cannot come from the CMB data sets.

6.2 Model II: Dark Matter with Vanishing Adiabatic Sound Speed

Given the results of the last section and the problematic assumption of negative sound speed, we now choose a different model. As mentioned previously, Γ_{DM}

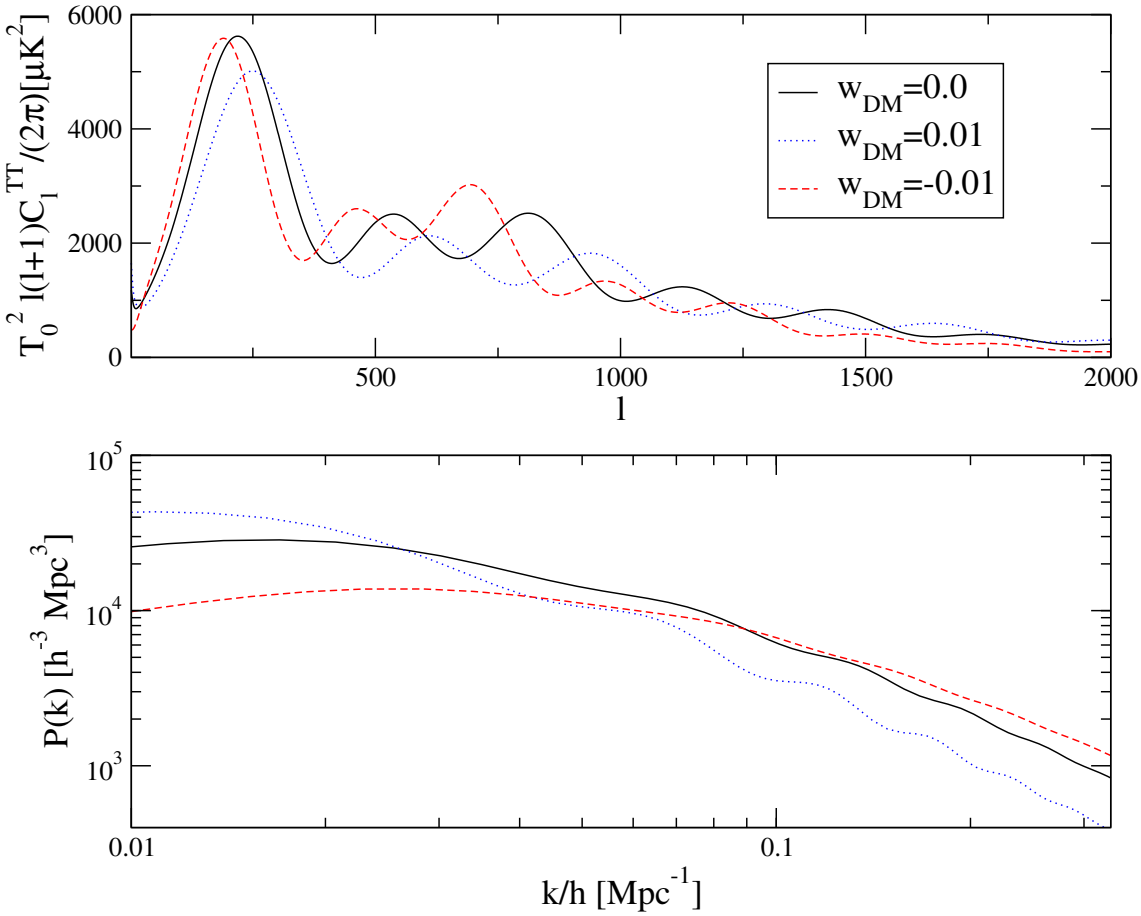

Figure 6.3: CMB and power spectrum for a ΛCDM model with modified dark matter, $c_{ad}^2 = 0$. For a positive equation of state (dotted, blue) the peak positions of the CMB are shifted to smaller scales and have less power than in the $w_{DM} = 0$ case (straight, black). For a negative w_{DM} (dashed, red), the peak positions are shifted to smaller l. Note also the different peak ratios in these cases. The shapes of the matter power spectrum are different in each case, but in contrast to $\Gamma_{DM} = 0$, there is no dramatic difference at small scales with respect to the $w_{DM} = 0$ spectrum. The power spectra at very large scales are different with respect to each other, indicating evolution of super-horizon sized modes.

measures the 'difference' between adiabatic sound speed c_{ad}^2 and background sound speed c_s^2. In the previous example, we enforced $c_{ad}^2 \approx c_s^2$ by the requirement $\Gamma_{DM} = 0$. A different requirement would be that the adiabatic sound speed vanishes. The first problem that arises is that c_{ad}^2 is not gauge-invariant. We must therefore first specify what we mean by vanishing adiabatic sound speed. We may choose a hypersurface such that $c_{ad}^2 = 0$ has a definite meaning. Since $c_{ad}^2 = 0$ implies $p\pi_L = 0$ this leads to the requirement that $\pi_L = 0$ on a certain set of hy-

persurfaces. For simplicity, we choose the Newtonian slicing, giving the shear free hypersurfaces, $\sigma_g = 0$. We therefore require $\pi_L^{(newt)} = 0$, which with the equation for P_L (3.30) gives

$$P_L = 0. \tag{6.5}$$

This is true in any gauge because P_L is gauge-invariant. Hence choosing

$$\Gamma_{DM} = 3(1 + w_{DM})\Phi - \Delta_{DM}, \tag{6.6}$$

we enforce that the adiabatic sound speed vanishes on hypersurfaces of isotropic expansion rate. Of course, this choice is by no means preferred over any other choice of hypersurfaces; we have chosen this one merely for computational simplicity.

Solving the perturbation equations for a universe filled only with modified dark matter, we obtain evolution of super-horizon modes if $w_{DM} \neq 0$. There is no exponential growth for sub-horizon modes if $w_{DM} < 0$. We may conclude that this model is well-behaved compared to the $\Gamma_{DM} = 0$ case. We have plotted the power and CMB spectra in figure 6.3 (model parameters as for the $\Gamma_{DM} = 0$ case). As expected, the modification has a huge impact on the growth behaviour of fluctuations.

6.3 MCMC Simulation Results

In order to quantify the bounds on the equation of state of dark matter we run a MCMC simulation for the $\Gamma_{DM} = 0$ and $c_{ad}^2 = 0$ model with the ANALYZETHIS! package using WMAP TT and TE spectra, VSA, CBI and ACBAR data as well as the SDSS power spectrum and SNe Ia data just as in the ΛCDM example in section 5.4. Each run contained $\sim 50,000$ points after burn-in removal. The model used was a ΛCDM cosmology with modified dark matter and parameter priors as shown in table 5.1 with $-4 \times 10^{-6} < w_{DM} < 5 \times 10^{-6}$ for the $\Gamma_{DM} = 0$ model and $-0.02 < w_{DM} < 0.02$ for the $c_{ad}^2 = 0$ model. The resulting one-dimensional marginalized likelihoods are displayed in Figure 6.4. The confidence intervals for the equation of state are displayed in table 6.1.

The equation of state is quite strongly constrained if $\Gamma_{DM} = 0$, at a level of 10^{-6}. What is somewhat surprising is that the likelihood is centered not on $w_{DM} = 0$ but on a slightly negative equation of state. This may be traced to the fact that the SDSS data set we used does not encompass very small scales and therefore the observations are blind to the very strong increase in power at very small scales if $w_{DM} < 0$. The constraints for the $c_{ad}^2 = 0$ case are less stringent, in line with our expectations. Here, w_{DM} is only constrained at a level of 10^{-3}.

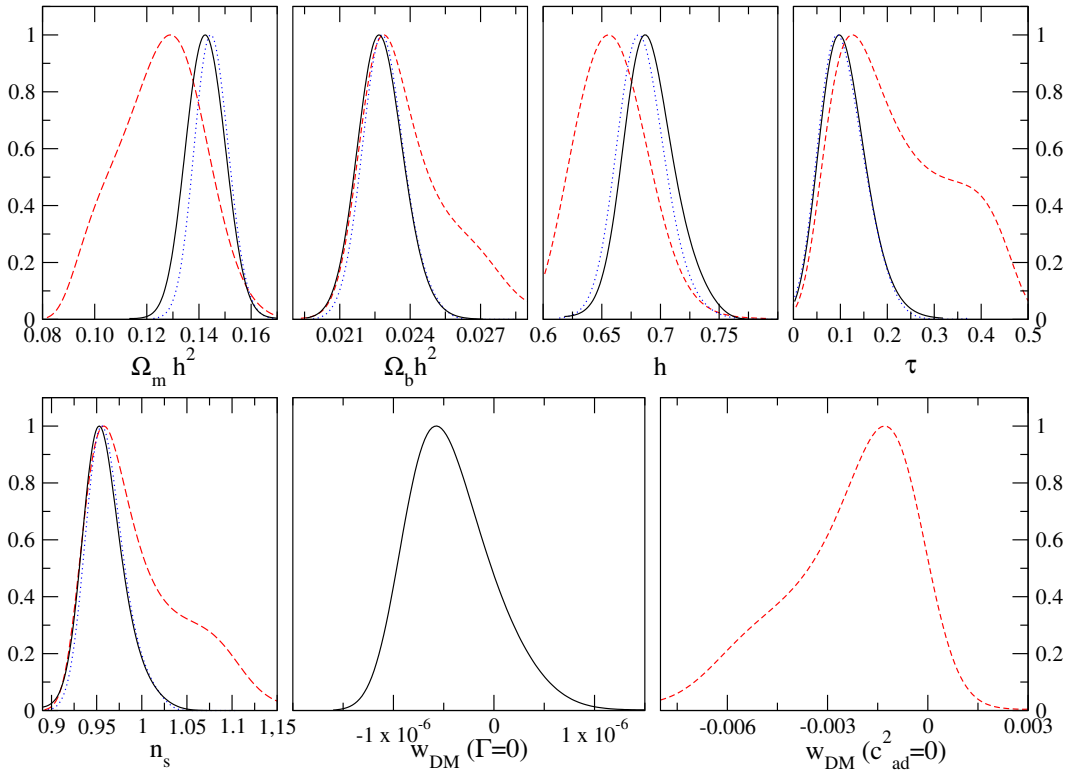

Figure 6.4: One-dimensional marginalized likelihoods of the MCMC simulation for the model parameters, using CMB, SNe Ia and LSS data. The results are for the $\Gamma_{DM} = 0$ (straight, black) and the $c^2_{ad} = 0$ (dashed, red) model. We have plotted the results for a pure ΛCDM model with $w_{DM} = 0$ for comparison (dotted, blue). Note the large difference in constraints on w_{DM} for the two models. Also, the $\Gamma_{DM} = 0$ model has nearly the same parameter distributions as a pure ΛCDM model.

	68.3 %	95.4 %	99.7%
w_{DM} for $\Gamma = 0$ $(\times 10^{-6})$	-0.114 -0.929	$+0.462$ -1.19	$+1.133$ -1.50
w_{DM} for $c^2_{ad} = 0$ $(\times 10^{-3})$	$+0.098$ -3.59	$+0.890$ -6.58	$+1.86$ -8.78

Table 6.1: Confidence intervals for the equation of state of dark matter for the two models discussed in the text.

6.4 Discussion of Results

Since this was an exploratory study we have not attempted to formulate a model with realistic variation in the equation of state but chose to show the main effects and bounds derived from current observations using a constant equation of

state. For the $\Gamma_{DM} = 0$ model, it is clear that the main constraint comes from the matter power spectrum. If we would include measurements at smaller scales, the constraints on the equation of state would be even more restrictive. We may conclude that the $\Gamma_{DM} = 0$ model is unlikely to be realistic. Since it is so strongly constrained we could just assume that $w_{DM} = 0$, so we have the standard CDM model. The situation is not so clear for the $c_{ad}^2 = 0$ model. More accurate measurements of the CMB, especially in the large multipole region, should give tighter constraints. Based on the data we cannot conclude that this model is ruled out. It would be necessary for formulate a specific model before more progress can be made concerning the question of a possible negative equation of state of dark matter. How strongly dependent are these results on our assumption of flatness and dark energy equation of state $w_{DE} = -1$? From fig. 6.2 we can readily see that the main constraint on the $\Gamma_{DM} = 0$ model comes from the large scale structure data; since the CMB spectrum does not change much in the allowed parameter range, we may conclude that relaxing the flatness assumption would not make much difference on the constraints. The same is true for an equation of state of dark energy different from -1. From previous studies it is known that for $w_{DE} > -1$, structure growth is suppressed at small scales [61, 170, 171]. But for the $\Gamma_{DM} = 0$ model, this can only make a small difference, since the growth suppression cannot ameliorate the strong deviation from the LSS measurements at small scales as is readily apparent in figure 6.2.

The situation for the $c_{ad}^2 = 0$ case is different. Here, relaxing the flatness assumption and allowing for open or closed universes will lead to a weaker constraint on w_{DM}. The first peak position is sensitive to the geometry of the universe, but increasing or decreasing w_{DM} can in principle shift this peak to be in agreement with the WMAP data, as may be seen in Fig. 6.3. We therefore expect also that the constraint on the total energy Ω_{tot} will be weaker than in the standard ΛCDM case. Concerning the possibility that the equation of state of dark energy may be $w_{DE} > -1$ we can say that here, too, the constraints on the dark energy equation of state and w_{DM} will be less stringent. As mentioned above, the main impact of $w_{DE} > -1$ is through a suppression of structure growth at small scales, but this may be compensated by decreasing w_{DM} (see figure 6.3). It is therefore apparent that allowing for $w_{DE} \neq -1$ will result in weaker constraints on w_{DM}. Relaxing the flatness and $w_{DE} = -1$ assumption will therefore have a negligible impact for the $\Gamma_{DM} = 0$ model but may lead to a significant relaxation of constraints for the $c_{ad}^2 = 0$ model.

7

BBN and the Variation of Fundamental Couplings

For my ally is the Force. And a powerful ally it is. Its energy surrounds us and binds us. [...] You must feel the Force around you. Here, between you, me, the tree, the rock ... everywhere!

Yoda, The Empire Strikes Back

We mentioned in section 4.7 that there is some disagreement between theory and experiment concerning primordial element abundances. In this chapter we will discuss an issue that may be related to this problem: the variation of fundamental couplings [172]. On the theoretical side, the variation of fundamental couplings has been investigated early on [173–175]. It is a characteristic feature for cosmological models of quintessence. A dependence of fundamental couplings on the value of the scalar field χ induces a time variation of couplings if χ is time dependent. Unfortunately this coupling is of unknown strength [44, 176, 177].

On the experimental side, recent observations of quasi stellar object (QSO) absorption spectra by Webb et al. [178–180] have suggested that the electromagnetic fine structure 'constant' might vary over cosmological timescales, $\Delta\alpha_{\rm em}/\alpha_{\rm em} = -0.54(12) \times 10^{-5}$ for $z \approx 2$. However, other groups excluded such a variation with high statistical significance [181–186]. Also, systematic effects such as the evolution of isotope ratios [187, 188] could have an impact on these measurements. The variability of the fundamental couplings has also been investigated using ${}^{187}_{75}\mathrm{Re} \rightarrow {}^{187}_{76}\mathrm{Os}$ decay in the Oklo natural reactor [189–191]. So far, the only measurement that indicate a variation in fundamental couplings are the QSO absorption line observations by Webb et al. mentioned above. Even though this claim of a variation in $\alpha_{\rm em}$ is in dispute, it is nevertheless instructive to investigate

other possible effects of a variation of the fundamental couplings on cosmological observables.

While the reality of a variation of $\alpha_{\rm em}$ in QSO absorption lines is still in dispute we need to gain an overview of other possible effects of a variation of the fundamental couplings on cosmological observations.

In this chapter we will investigate the effect of a variation in the fundamental couplings on the big bang nucleosynthesis (BBN) of light elements, specifically ^{4}He. In this context, the bounds on the variation of $\alpha_{\rm em}$ at $z \sim 3$ do not say much about the possible size of a variation $\Delta\alpha_{\rm em}/\alpha_{\rm em}$ at the time of BBN, around $z \sim 10^{10}$. A major issue when considering BBN is the complex interplay of the variation of several couplings on the outcome of the element synthesis. A number of recent papers [177,192–198] investigated the bounds on a variation of $\alpha_{\rm em}$ or other single parameters from BBN. However, we will follow a different approach which determines element abundances as a function of nuclear physics parameters without specifying a model in which the fundamental constants change. For a review of current limits on fundamental couplings see [199], a semi-analytic treatment for constraining varying fundamental couplings from light element abundances can be found in [200].

7.1 Constraints on Fundamental Couplings from BBN

To determine light element abundances in the absence of time varying couplings, one needs to know the particle masses and the reaction rates of the relevant nuclear processes from laboratory experiments. Numerical codes for this kind of BBN abundance computation were first created by Wagoner, Fowler and Hoyle [201,202], for a more recent version see [203,204].

An essential parameter for these computations is the baryon to photon ratio η. Taking the value from WMAP measurements [5], $\eta = 6.14 \pm 0.25 \times 10^{-10}$, yields a prediction of the helium abundance $Y_{\rm He} = 0.2484^{+0.0004}_{-0.0005}$ [151], significantly higher than determinations from experiments [151]. Using the experimental values, one obtains $\eta \approx 3 - 5 \times 10^{-10}$, depending on the set of observations used. This discrepancy is likely due to systematic errors which are not fully understood. Increasing the number of light species which are effective at BBN (e.g. more neutrinos) would enhance $Y_{\rm He}$ and only worsen the discrepancy. This also holds for the possible presence of early dark energy [14,61]. If a mechanism for decreasing$Y_{\rm He}$ has to be found the time variation of fundamental couplings seems to be a particularly plausible candidate [177]. Effects of the variation of the weak and strong scales or some dimensionless coupling on BBN have been discussed long ago [44,205,206]. One may therefore try to estimate the allowed variation of couplings at a very early time in cosmology.

Confidence limits on the variation of couplings or parameters in the framework of BBN always assume an underlying model. However, the confidence regions determined from a model where only $\alpha_{\rm em}$ varies are meaningless if one wants to employ a model where other couplings, such as the weak scale, are allowed to change. In a Grand Unified Theory (GUT) framework, not only does the electromagnetic interaction vary, but also weak and strong interactions. The details of how these are connected depend on the specific GUT and the variation of the unified couplings and mass scales of spontaneous symmetry breaking. The present BBN limits on time varying couplings are difficult to compare due to this strong implicit model dependence. It is therefore essential to formulate the BBN estimates in a way that is as model independent as possible. This should facilitate the comparison between different assumptions on the time variation of fundamental couplings. With this one may then discuss specific models which relate the standard model parameters to the GUT parameters [177, 207–210].

We will present such a model-independent formulation below and present an example for illustration. Since computation of the helium abundance can be done with a simple semi-analytical approximation, we will restrict ourselves to considering the helium abundance only.

7.2 Model-Independent Formulation

The success of BBN motivates our main assumption for the model-independent treatment, namely that the relative time variation of the fundamental constants between nucleosynthesis and the present epoch is small. We can then linearize in the relative variation of the fundamental parameters $\Delta G_k/G_k$ and use values extracted from laboratory experiments for G_k. We express the relative change of the helium abundance as

$$\frac{\Delta Y_{\rm He}}{Y_{\rm He}} = \frac{Y_{\rm He}(G+\Delta G) - Y_{\rm He}}{Y_{\rm He}} = \sum_k c_k^{(G)} \frac{\Delta G_k}{G_k}. \tag{7.1}$$

Here $Y_{\rm He}$ corresponds to the helium abundance computed in absence of a cosmological time variation of couplings, assuming that only standard model particles (with three neutrinos) contribute to the energy density at BBN. Our aim is to determine the coefficients $c_k^{(G)}$ which relate the fundamental parameters to the change in $Y_{\rm He}$. We emphasize that relative errors for the relative variation below 10 % are acceptable in contrast to the much higher required precision for the total abundance.

We will consider the effects of the variation of six dimensionless quantities

$$G_k = (M_{\bar{p}}/\Lambda_{QCD},\ \alpha_{\rm em},\ \langle\phi\rangle/\Lambda_{QCD}, m_e/\Lambda_{QCD},\ m_q/\Lambda_{QCD},\ \Delta m/\Lambda_{QCD}). \tag{7.2}$$

Here Λ_{QCD} is the characteristic mass scale of the strong interactions which dominates the mass of the nucleons and the strong interaction rates. The quantity $\langle\phi\rangle$ is the Fermi scale (vacuum expectation value of the Higgs field) relevant for the weak interactions. The strength of the gravitational interactions is given by the reduced Planck mass $M_{\bar{p}}$ and m_e is the electron mass. The up- and down-quark masses m_u, m_d are reflected in $m_q = (m_u + m_d)/2$ and $\Delta m = m_d - m_u$. In combination with $\langle\phi\rangle/\Lambda_{QCD}$ the three last mass ratios could be replaced by the relevant Yukawa couplings h_e, h_u, h_d. We emphasize that only ratios of mass scales are observable and have cosmological significance [14, 44, 177].

For a given model for the time variation of the fundamental couplings the variations $\Delta G_k/G_k$ are typically related to each other. For example, we may assume a unified theory (GUT) and vary only the gauge coupling at the unification scale M_{GUT}, while keeping $G_{3,4,5,6}$ fixed. This results in [177]($\Delta G_{3,4,5,6} = 0$)

$$\frac{\Delta(M_{\bar{p}}/\Lambda_{QCD})}{M_{\bar{p}}/\Lambda_{QCD}} = -\frac{\pi}{11}\frac{\Delta\alpha_{\rm em}}{\alpha_{\rm em}^2} = -\frac{\pi}{11}\frac{\alpha_{\rm em}^{BBN} - \alpha_{\rm em}}{\alpha_{\rm em}^2}. \tag{7.3}$$

Then only a single independent varying coupling is left that we may choose as $\Delta\alpha_{\rm em}/\alpha_{\rm em}$.

For practical reasons we will work in a frame where we keep the strong scale Λ_{QCD} fixed. This can be achieved by an appropriate Weyl scaling [14, 44] and will result in a time dependence of the reduced Planck mass $M_{\bar{p}}$. This particular frame can be understood as a rescaling of the cosmological 'clock' $M_{\bar{p}}$ which compensates for the constant strong interactions. In a frame with fixed $M_{\bar{p}}$ the strong interaction scale Λ_{QCD} would vary with time.

Our computation of the coefficients $c_k^{(G)}$ proceeds in two steps. We first consider the dependence of $Y_{\rm He}$ on the characteristic quantities for nuclear decays and reactions, also referred to as 'nuclear physics parameters'

$$X_i = (M_{\bar{p}},\ \alpha_{\rm em},\ \langle\phi\rangle,\ m_e,\ \tau_n,\ Q,\ B_d), \tag{7.4}$$

according to

$$\frac{\Delta Y_{\rm He}}{Y_{\rm He}} = \sum_i c_i^{(X)}\frac{\Delta X_i}{X_i}. \tag{7.5}$$

Here, τ_n is the neutron lifetime, Q the neutron-proton mass difference and B_d the deuteron binding energy. We keep Λ_{QCD} fixed – otherwise the dimensionful parameters have to be multiplied by appropriate powers of Λ_{QCD}. We emphasize that at this stage the effect of the variation of, say, $\alpha_{\rm em}$ is computed at fixed values of $X_{1,3,4,5,6,7}$. The computation of the coefficients $c_i^{(X)}$ involves the details of nuclear physics, e.g. reaction rates.

Then we translate $\Delta X_i / X_i$ into the variation of the fundamental couplings via

$$\frac{\Delta X_i}{X_i} = \sum_k f_{ik} \frac{\Delta G_k}{G_k}, \tag{7.6}$$

with

$$f_{ik} = \frac{\partial \, lnX_i}{\partial \, lnG_k}. \tag{7.7}$$

This step involves the connection between nuclear physics and particle physics, namely the dependence of τ_n, Q and B_d on the couplings $G_{2,3,4,5,6}$. Obviously, one has $f_{ik} = \delta_{ik}$ for $i = 1...4$ and $k = 1...6$. For known f_{ik} the coefficients $c_k^{(G)}$ follow from $c_i^{(X)}$ as

$$c_k^{(G)} = \sum_i c_i^{(X)} f_{ik}. \tag{7.8}$$

So the connection between fundamental particle physics and nuclear physics parameters is formulated in the form of a 'transfer matrix' f_{ik}. The advantage of this separation is the possibility to compute f_{ik} without invoking BBN wheras computing the coefficients $c_i^{(X)}$ does not use any assumptions about the particle physics-nuclear physics connection. These two issues can therefore be dealt with independently. Any improvement on the estimate of the coefficients $c_i^{(X)}$ can be propagated to the fundamental couplings by equation (7.8) without repeating the whole calculation. A specific GUT model then gives relations between the fundamental couplings and may be constrained by using the coefficients $c_i^{(G)}$ and equation (7.1).

7.3 Helium Abundance

In this section we will compute the coefficients $c_i^{(X)}$ of equation (7.5). For this we need to determine the dependence of the helium abundance on the nuclear physics parameters. We will use the semi-analytic approach of Esmailzadeh, Starkman and Dimopoulos (ESD) [211] – estimating the primordial helium abundance via quasi static equilibrium and fixed point conditions. This approach should be sufficient for a computation of the small relative variations. Of course, a full numerical investigation using BBN codes would improve our analysis considerably. Big bang nucleosynthesis may be split into two distinct epochs. In the first phase protons and neutrons are converted into each other via weak interactions. These reactions cease ('freeze out') as soon as the weak rate becomes comparable to the expansion rate, $\Gamma_{weak} \backsimeq H$. Then, the neutrons decay freely until they are absorbed by nuclear reactions.

7.3.1 Weak Reaction Freeze Out

Let us compute the abundance of neutrons left once the weak reactions freeze out. The rate for the reactions

$$n + \nu_e \longrightarrow p + e^-, \tag{7.9}$$
$$n + e^+ \longrightarrow p + \bar{\nu}_e, \tag{7.10}$$
$$n \longrightarrow p + \bar{\nu}_e + e^-, \tag{7.11}$$

is given by [21]

$$\Gamma_{n\to p} = A\int dx \left(1 - \frac{m_e^2}{(Q+x)^2}\right)^{\frac{1}{2}} (Q+x)^2 (1+e^{(x/T)})^{-1} (1+e^{-(Q+x)/T})^{-1} x^2 \tag{7.12}$$

Here, Q is the neutron-proton mass difference, m_e the electron mass and A the transition amplitude. The integral runs from $-\infty$ to $+\infty$ with an energy gap between $-Q - m_e$ and $-Q + m_e$. $A \propto \langle \phi^{-4} \rangle$ is the four point transition probability in Fermi-theory which depends on the axial and vector couplings c_V and c_A. For simplicity we will keep c_V and c_A constant. We assume that this reaction freezes out at a temperature T_n^* when the Hubble expansion is comparable to this reaction rate[1]

$$\Gamma_{n\to p} = b\ H(T_n^*). \tag{7.13}$$

The shortcomings of our simple approach is accounted for by the factor b. We will fix b such that we obtain the same $Y_{\rm He}$ as predicted by the full numerical code[2].

Big bang nucleosynthesis takes place at $T \sim 0.1 - 1$ MeV, deep in the radiation dominated era. To compute the expansion rate we may therefore ignore all but the relativistic species in the Friedmann equation (2.11). Ignoring effects of changing baryon or electron mass on the expansion rate, the Hubble parameter is given by

$$H^2 = \frac{1}{3M_{\bar{p}}} \frac{\pi^2}{30} g_* T^4, \tag{7.14}$$

where g_* counts the total number of effectively massless degrees of freedom [22],

$$g_* = \sum_{i=\text{bosons}} g_i \left(\frac{T_i}{T}\right)^4 + \frac{7}{8} \sum_{i=\text{fermions}} g_i \left(\frac{T_i}{T}\right)^4, \tag{7.15}$$

[1] Note that an equally well justified assumption would be to include the reaction rate $\Gamma_{p\to n}$ in this condition.

[2] For $b = 1$ we obtain a ^{4}He abundance that deviates by about 10 percent from the value $Y_{\rm He} = 0.2484$ found with a full numerical computation using the WMAP value for η [151]. In order for our analytic approximation to yield the $Y_{\rm He}$ predicted numerically we use $b = 1.22$.

with T_i the temperature and g_i the multiplicity of the respective particle species. Before positron-electron annihilation $g_* = 10.75$. The freeze out temperature of the neutrons with no change in fundamental couplings can then be determined by combining equations (7.12) – (7.14) as $T_n^* = 0.77$ Mev and the freeze out neutron concentration $Y_{\rm n}^*$ at this temperature is

$$Y_{\rm n}^* = \frac{1}{1 + e^{Q/T_n^*}} = 0.158 \, . \tag{7.16}$$

This ends our discussion of the weak reaction freeze out.

7.3.2 Light Element Synthesis

Following the 'freeze out' of the neutron to proton ratio the free neutrons decay, thereby further reducing Y_n for $T < T_n^*$. After a short time the synthesis of deuterium and tritium starts which subsequently leads to the production of helium. Since almost all existing neutrons end up in helium[3], we need to know how many neutrons remained when helium was synthesized in appreciable amounts.

We will assume that the neutrons decay freely until a time t_f when helium formation starts to dominate over the neutron decay process, since then helium is formed fast relative to the neutron lifetime:

$$2\dot{Y}_{\rm He}(t_f) = -\dot{Y}_{\rm n}(t_f). \tag{7.17}$$

The final ^{4}He abundance is then estimated by

$$Y_{\rm He} = \frac{1}{2} Y_{\rm n}(t_f) = \frac{1}{2} Y_{\rm n}^* e^{-(t_f/\tau_n)}. \tag{7.18}$$

It depends on the couplings via Q, T_n^*, τ_n and t_f. In turn, T_n^* depends on $A \propto \langle\phi\rangle^{-4}$, Q, m_e and $M_{\bar{p}}$ via equations (7.12), (7.13) and (7.14).

The equation governing the abundance $Y_i = n_i/n_b$ of element i has the simple form

$$\dot{Y}_i(t) = J(t) - \Gamma(t) Y_i(t), \tag{7.19}$$

where $J(t)$ and $\Gamma(t)$ are the time-dependent source and sink terms which depend on the abundance of other elements and the nuclear reaction rates. As long as the sink term is much larger than the expansion rate, $\Gamma \gg H$, Y_i follows a time-dependent static solution (the element is then in quasi static equilibrium)

$$Y_i = \frac{J(t)}{\Gamma(t)}, \tag{7.20}$$

[3]The final abundances of elements other than ^{1}H and ^{4}He are at a level of $\sim 10^{-4}$ or less after BBN.

where source and sink terms cancel each other such that $\dot{Y}_i \approx 0$. Our task now is to find the dominant source and sink terms for each element, check for quasi static equilibrium and solve the resulting set of algebraic equations for $Y_{\rm He}$. In figure 7.1 we demonstrate that the destruction rates for tritium and ^{3}He are much larger than the expansion rate and these two elements are therefore in quasi static equilibrium. One may also check from numerical calculations [212] that deuterium is in nuclear thermal equilibrium until $T \approx 0.07$ MeV. The reaction network is displayed in figure 7.2 to illustrate the most important reactions involved in ^{4}He production [213].

We will now compute the time t_f at which the helium production rate exceeds the neutron decay rate. The by far most dominant process for ^{4}He production is the reaction [214]

$$d + t \rightarrow n + {}^4\mathrm{He}\,. \tag{7.21}$$

To write down the equations governing the abundances comprised of several reactions we will adopt the notation of ESD who abbreviate a reaction rate

$$a + b \rightarrow c + d, \tag{7.22}$$

as $[abcd]$. Taking into account the reaction (7.21) we have then[4]

$$\dot{Y}_{\rm He} = Y_{\rm d} Y_{\rm t} [dtn\alpha]. \tag{7.23}$$

The condition for the time until which the neutrons decay can be obtained by using equation (7.17) and the helium production rate (7.23) as

$$2 Y_{\rm d} Y_{\rm t} [dtn\alpha] = \frac{1}{\tau_n} Y_{\rm n}^* e^{-t_f/\tau_n}. \tag{7.24}$$

To compute the freezeout time t_f when this relation is satisfied we need to know the abundance of deuterium $Y_{\rm d}$ and tritium $Y_{\rm t}$ as well as the reaction rate $[dtn\alpha]$. In the temperature range we are considering, deuterium can be assumed to be in thermal equilibrium and hence its abundance is given by the Saha equation [22]

$$Y_{\rm d} = 8.15 \left(\frac{T}{m_n}\right)^{3/2} \eta\, e^{B_d/T}\, Y_n Y_p, \tag{7.25}$$

with the proton abundance being $Y_p \approx (1 - Y_{\rm n})$ and m_n the neutron mass.

The estimate of $Y_{\rm t}$ is more involved and also requires knowledge of the abundance Y_3 for ^{3}He. We employ the quasi static equilibrium condition (7.20) for determining $Y_{\rm t}$ and Y_3. For this, we need to find the dominant source and sink terms. The tritium concentration is established by the reactions

$$\begin{aligned} n + {}^3\mathrm{He} &\rightarrow p + t, \\ d + d &\rightarrow p + t, \end{aligned} \tag{7.26}$$

[4] In the reaction rate notation we abbreviate ^{4}He with α and ^{3}He with 3.

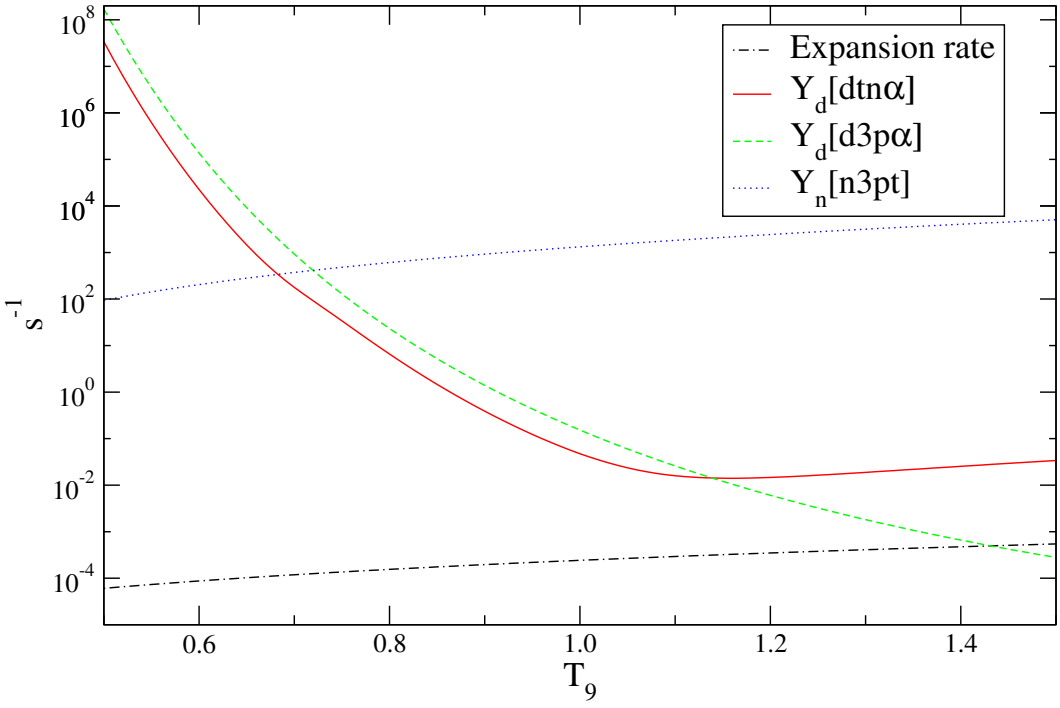

Figure 7.1: Destruction rates of tritium (straight, red) and ^{3}He (dashed, green & dotted, blue) compared with the expansion rate (dash-dot, black) as a function of temperature in units of 10^9 K, with $T_9 = 1.0$ corresponding to $T = 0.086$ MeV (see appendix B.3 for conversion factors). The rates displayed here are given in appendix A.

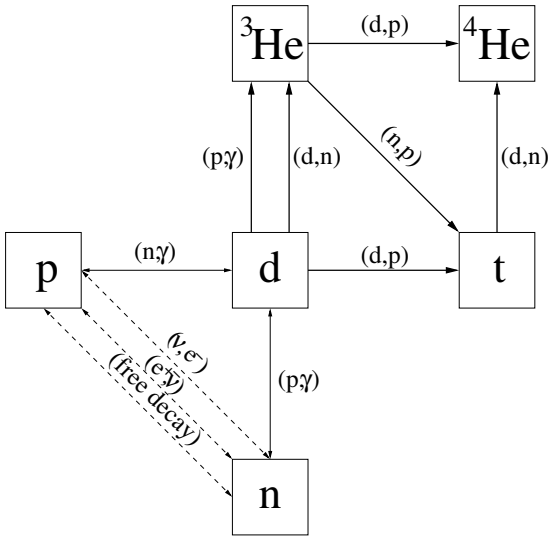

Figure 7.2: Network of the included reactions. We consider weak rates (dashed) and the most important nuclear reaction rates for the lightest elements.

creating and

$$d + t \rightarrow n + {}^4\mathrm{He}, \tag{7.27}$$

annihilating tritium. Other reactions are subdominant by at least 2 orders of magnitude [214] and are therefore neglected. Using the fixed point condition (7.20) leads us to an equation for Y_t of the form

$$Y_\mathrm{t} = \frac{Y_\mathrm{n}\, Y_3\, [n3pt] + Y_\mathrm{d}\, Y_\mathrm{d}\, [ddpt]}{Y_\mathrm{d}\, [dtn\alpha]}. \tag{7.28}$$

The dominant processes for the ^{3}He abundance are the creation reactions

$$p + d \rightarrow {}^3\mathrm{He} + \gamma, \tag{7.29}$$
$$d + d \rightarrow n + {}^3\mathrm{He}, \tag{7.30}$$

and the destruction reactions[5]

$$d + {}^3\mathrm{He} \rightarrow p + {}^4\mathrm{He}, \tag{7.31}$$
$$n + {}^3\mathrm{He} \rightarrow p + t. \tag{7.32}$$

Invoking the fixed point condition yields

$$Y_3 = \frac{Y_\mathrm{d}\, Y_\mathrm{p}[pd3\gamma] + Y_\mathrm{d}\, Y_\mathrm{d}[ddn3]}{Y_\mathrm{d}\, [d3p\alpha] + Y_\mathrm{n}\, [n3pt]}. \tag{7.33}$$

From equations (7.25), (7.28) and (7.33) we can determine the abundance of deuterium, tritium and ^{3}He as a function of T and Y_n. In turn, temperature and time are related by the background cosmology and $Y_\mathrm{n} = Y_\mathrm{n}^*\, e^{-t/\tau_n}$. Equation (7.24) now determines t_f.

The dependence of Y_He on the various parameters cannot be solved analytically. In the linear approximation, however, the computation of the response coefficients $c^{(X)}$ is straightforward. For this purpose we assume that all strong interaction rates are determined by the strong interaction scale Λ_{QCD}. At this point we benefit from our particular frame with constant Λ_{QCD} which implies that we can use constant rates $[dtn\alpha]$ etc., except for small electromagnetic effects which we have incorporated. The rates needed in equations (7.24), (7.28) and (7.33) are given in appendix A along with an explanation of the modifications due to changes in the electromagnetic coupling α_em.

When we carry through the whole analysis we obtain the 'nuclear physics' coefficients $c_i^{(X)}$ displayed in table 7.1. They are plausible in the sense that they resemble what one would expect from simple arguments. Increasing the Planck

[5] We have not included the reaction $[d3p\alpha]$ in the ^{4}He production computation because it is subdominant, but for determining the ^{3}He abdundance this is an important sink term.

variable	$M_{\bar{p}}$	$\alpha_{\rm em}$	$\langle\phi\rangle$	m_e	τ_n	Q	B_d
$c_i^{(X)}$	-0.81	-0.043	2.4	0.024	0.24	-1.8	0.53

Table 7.1: Coefficients $c_i^{(X)}$ for nuclear physics parameters.

mass $M_{\bar{p}}$ gives a slower expansion rate, resulting in a later freeze out of weak interactions, hence less neutrons are available for helium production. Increasing the decay time τ_n of the free neutrons leaves more neutrons to be converted into helium since effectively all neutrons are bound in helium. Increasing $\langle\phi\rangle$ results in a decrease of the Fermi interaction G_F, hence weak interactions freeze out earlier resulting in an increase in $Y_{\rm He}$. Changing Q results in a different neutron-proton ratio at freeze out and also in modified weak rates due to changes in the available phase space. If we exclude the changes in phase space volume, the coefficient is -1.4 instead of -1.8. Thus, helium abundance is a decreasing function of the proton-neutron mass difference Q as anticipated. Increasing the binding energy of the deuteron, B_d, results in earlier formation of helium and reduces the amount of neutrons decaying into protons. The influence of the electron mass is only through the phase space volume in the weak rates which is a very small effect for our purposes.

Changes in $\alpha_{\rm em}$ affect the nuclear reaction rates with the main effects being variations in the Coulomb barrier for charge-induced reactions, final-state interactions, radiative capture and mass differences (see appendix A). Except for electromagnetic effects we have not taken into account any other effect that may change the reaction rates.

7.4 Determining the Transfer Matrix f_{ik}

In this section we describe the relation between the fundamental couplings G_k and the nuclear physics parameters X_i. This relation was expressed in the form of a matrix equation with a transition matrix f_{ik} (7.7). We will now discuss what effects we took into account by going through each row of the matrix f_{ik} given in table 7.2. To quantify the relation between nuclear and particle physics parameters we have to make some model dependent assumptions. Because of the modular character of our analysis, this model dependence is clearly identifiable and can easily be replaced with different estimates, the coefficients $c_i^{(X)}$ will not change as a result of an update on f_{ik}. Each entry in f_{ik} describes the response of the 'nuclear physics parameter' X_i when one varies a single parameter G_k, while keeping the other $G_{l\neq k}$ fixed. When there is no contribution at all a zero is written. For some relations between the G_k and the X_i small effects are present but

parameter	$M_{\bar{p}}$	$\alpha_{\rm em}$	$\langle\phi\rangle$	m_e	m_q	Δm
$M_{\bar{p}}$	1	0	0	0	0	0
$\alpha_{\rm em}$	0	1	0	0	0	0
$\langle\phi\rangle$	0	0	1	0	0	0
m_e	0	0	0	1	0	0
τ_n	0	3.86	4	1.52	–	−10.4
Q	0	−0.59	–	–	–	1.59
B_d	0	−0.0081	–	–	$-r/2$	–

Table 7.2: The transfer matrix f_{ik}, corresponding to the coefficients relating relative changes in G_k to relative changes in X_i. The parameters are dimensionless, but we omitted the scaling by Λ_{QCD}.

with negligible coefficients. To distinguish those from the others, we have left the matrix entry empty. For $i = 1 \ldots 4$ the parameters appear both in the lists of X_i and G_k, so that $f_{ik} = \delta_{ik}$ by virtue of our definition. Also τ_n, Q and B_d do not depend on $M_{\bar{p}}$ implying $f_{1k} = \delta_{1k}$. The nontrivial coefficients f_{ik} for $i = 5, 6, 7$ account for the dependence of τ_n, Q and B_d on $\alpha_{\rm em}$, $\langle\phi\rangle$, m_e, m_q and Δm.

The nucleon masses and nuclear binding energies depend on the quark masses and $\alpha_{\rm em}$. The dependence of the neutron-proton mass difference on the fundamental couplings was given by Gasser and Leutwyler [215] as

$$Q = \left[-0.76\left(1 + \frac{\Delta\alpha_{\rm em}}{\alpha_{\rm em}}\right) + 2.05\left(1 + \frac{\Delta(\Delta m)}{\Delta m}\right)\right] \text{ MeV} . \tag{7.34}$$

From this we can determine f_{62} and f_{66}.

When we consider the deuteron binding energy B_d recent studies have suggested that it may increase with decreasing pion mass [216,217]. We may parametrize the dependence of B_d on m_π at fixed $\langle\phi\rangle$ by a linear fit [194] and neglect the dependence on $\langle\phi\rangle$ at fixed m_q, Δm. For the electromagnetic part we use the Monte Carlo simulation data of Pudliner et al. [218]. Hence the deuteron binding energy may be expressed in terms of the pion mass $m_\pi \propto m_q^{1/2}$ and $\alpha_{\rm em}$ as

$$B_d = B_d^0\left[(r+1) - r\frac{m_\pi}{m_\pi^0}\right] - 0.018\frac{\Delta\alpha_{\rm em}}{\alpha_{\rm em}} \text{ MeV} , \tag{7.35}$$

where r is a parameter that varies between 6 and 10 and $B_d^0 = 2.225$ MeV is the deuteron binding energy as measured in the laboratory today.

The neutron lifetime is changed due to variations in the weak scale $\tau_n \propto G_F^{-2} \propto \langle\phi\rangle^4$. Furthermore, a change in the phase space volume f of free neutron decay

$$f = \int_{m_e}^{Q} dq\ q^2(Q-q)^2\left(1 - \frac{m_e^2}{q^2}\right)^{1/2} , \tag{7.36}$$

results in a dependence of τ_n on Q and the electron mass m_e. Because Q also depends on $\alpha_{\rm em}$ and Δm, $\Delta\tau_n$ will also have contributions from the variation of those parameters. A linear analysis then yields the corresponding entries for τ_n:

$$\frac{\Delta\tau_n}{\tau_n} = 3.86\frac{\Delta\alpha_{\rm em}}{\alpha_{\rm em}} + 4\frac{\Delta\langle\phi\rangle}{\langle\phi\rangle} + 1.52\frac{\Delta m_e}{m_e} - 10.4\frac{\Delta(\Delta m)}{\Delta m}. \tag{7.37}$$

Having determined the transfer matrix we can calculate the dependence of $\Delta Y_{\rm He}/Y_{\rm He}$ on the fundamental parameters using equation (7.8). The results are shown in table 7.3.

variable	$M_{\bar{p}}$	$\alpha_{\rm em}$	$\langle\phi\rangle$	m_e	m_q	Δm
$c_i^{(G)}$	-0.81	1.94	3.36	0.389	-1.59	-5.358

Table 7.3: Coefficients $c_k^{(G)}$ for fundamental couplings.

7.5 A GUT Example

To illustrate the procedure how to obtain limits on the variation of fundamental couplings we will present a short example. We will give a model for which we have expressed the changes in the fundamental parameters by the variation of only one independent coupling and computed the resulting change in $Y_{\rm He}$. The variation of the couplings is assumed to be due to a scalar field χ [14, 44]. It is possible that this field plays the role of quintessence [177], but here we will not need any particular details of the evolution of the scalar field χ, except that its value at the time of nucleosynthesis was different from its present value. For the details of the derivation of how the fundamental constants change in a GUT scheme we refer the reader to [177, 219]. Merely quoting the results, to one loop order the fundamental couplings as functions of the scalar field χ are given by [177]

$$\alpha_s^{-1}(M_W) = \frac{4\pi Z_F(\chi)}{\bar{g}^2} + \frac{7}{2\pi}\ln\zeta_w(\chi), \tag{7.38}$$

$$\alpha_w^{-1}(M_W) = \frac{4\pi Z_F(\chi)}{\bar{g}^2} + \frac{5}{3\pi}\ln\zeta_w(\chi), \tag{7.39}$$

$$\alpha_{em}^{-1}(M_W) = \frac{32\pi Z_F(\chi)}{3\bar{g}^2} - \frac{5}{3\pi}\ln\zeta_w(\chi), \tag{7.40}$$

where the W-Boson mass is $M_W(\chi) = \zeta_w(\chi)\chi$ and $Z_F(\chi)$ determines the renormalized grand unified gauge coupling ($g_R^2 = \bar{g}^2/Z_F$, $\bar{g}$ fixed). We normalize

χ such that $M_{GUT}(\chi) = \chi$. In equations (7.38) – (7.40) we can replace $M_W = g_w\langle\phi\rangle/\sqrt{2}$ by $\langle\phi\rangle$. The relative variation of g_w (or α_w) induces only a correction of higher order in these relations.

As mentioned before, we will work in a frame in which the scale of the strong interaction is fixed such that the strong interaction rates are constant for our BBN estimate. We will consider a particularly simple scenario where

$$M_{\bar{p}}(\chi)/M_{GUT}(\chi) = \text{const.}. \tag{7.41}$$

Performing the Weyl scaling such that $m_n \approx \Lambda_{QCD}$ is kept fixed we find

$$\frac{\Delta M_{\bar{p}}/\Lambda_{QCD}}{M_{\bar{p}}/\Lambda_{QCD}} = -\Delta\ln\zeta_w + \Delta\ln\left(\langle\phi\rangle/\Lambda_{QCD}\right). \tag{7.42}$$

Furthermore, we also neglect the variation of the Yukawa couplings and hence the variations in m_e, m_q and Δm obey

$$\frac{\Delta m_e}{m_e} = \frac{\Delta(\Delta m)}{\Delta m} = \frac{\Delta m_q}{m_q} = \frac{\Delta\langle\phi\rangle}{\langle\phi\rangle}. \tag{7.43}$$

The effect of the variation of the field χ can now be expressed as a varation in the renormalized grand unified gauge coupling expressed by Z_F and a variation in $\ln\zeta_w$.

At this stage the two unknown quantities $\Delta\ln Z_F$ and $\Delta\ln\zeta_w$ contain all relevant information about the unknown coupling of the scalar field χ to matter and radiation. For the present investigation we can simply use the relative variation of the GUT-coupling $\Delta\ln Z_F$ and the ratio between weak and GUT scale $\Delta\ln\zeta_w$ as free parameters. We need to determine $\alpha_{\rm em}$ at the energy scale μ for nuclear reactions $\mu \approx m_e$. For the running of $\alpha_{\rm em}$ at $\mu < M_W$ we have the relation

$$\alpha_{\rm em}(\mu)^{-1} = \alpha_{\rm em}(M_W)^{-1} + \frac{2}{3\pi}\sum_i Q_i^2\ \ln\frac{M_W}{\mu}, \tag{7.44}$$

where the Q_i are the charges of the particles with masses in the range between M_W and μ. In our case this is given by five quarks (top lies above M_W) in three colours plus 3 leptons, i.e. $\sum_i Q_i^2 = 3\times(8/9+3/9)+3$. For $\mu = m_e$ this takes the form

$$\frac{\Delta\alpha_{\rm em}(m_e)}{\alpha_{\rm em}^2(m_e)} = \frac{\Delta\alpha_{\rm em}(M_W)}{\alpha_{\rm em}^2(M_W)}\left[1+\frac{1}{18}\sum_i\tilde{Q}_i^2\right], \tag{7.45}$$

where $\sum_i\tilde{Q}_i^2 = 2$ runs only over the three light quarks whose effect on the running of $\alpha_{\rm em}$ is cut off at $\mu\sim\Lambda_{QCD}$. Similarly, for the running of α_s below M_W we include five quarks and associate Λ_{QCD} with the scale where the one loop expression for $\alpha_s(\mu)$ diverges.

We can now express $\alpha_{\rm em} = \alpha_{\rm em}(m_e)$ and Λ_{QCD} in terms of $\alpha_{\rm em}(M_W)$ and $\alpha_s(M_W)$. Thus they relate Λ_{QCD}/χ and $\alpha_{\rm em}$ to Z_F and $\ln\zeta_w$. The specific relation between the variations of $\Lambda_{QCD}/M_{\bar{p}}$ and $\alpha_{\rm em}$ depends on the variation of the weak scale $\ln\zeta_w$. In our example we will keep the relative variation between the weak and the GUT scale fixed,

$$\Delta \ln \zeta_w = 0. \tag{7.46}$$

This corresponds to $\langle\phi\rangle/\chi = \text{const}$. For this we obtain

$$\frac{\Delta\alpha_{\rm em}(M_W)}{\alpha^2_{\rm em}(M_W)} = -\frac{32\pi}{3}\frac{\Delta Z_F}{\bar{g}^2}, \tag{7.47}$$

and from equation (7.42)

$$\frac{\Delta M_{\bar{p}}/\Lambda_{QCD}}{M_{\bar{p}}/\Lambda_{QCD}} = \frac{\Delta\langle\phi\rangle}{\langle\phi\rangle} = -\frac{\pi}{12}\ \frac{\Delta\alpha_{\rm em}(M_W)}{\alpha^2_{\rm em}(M_W)}. \tag{7.48}$$

In equation (7.1) we now have nonvanishing entries from $\Delta G_{3,4,5,6}$ related by equations (7.43) and (7.48) to $\Delta\alpha_{\rm em}/\alpha_{\rm em}$ giving with (7.45)

$$\frac{\Delta(M_{\bar{p}}/\Lambda_{QCD})}{M_{\bar{p}}/\Lambda_{QCD}} = \frac{\Delta\langle\phi\rangle}{\langle\phi\rangle} = -32.3\ \frac{\Delta\alpha_{\rm em}(m_e)}{\alpha_{\rm em}(m_e)}. \tag{7.49}$$

In order to get an idea of the sensitivity we compute the value $\Delta\alpha_{\rm em}/\alpha_{\rm em}$ which would be needed in order to obtain a helium abuncance $Y_{\rm He} = 0.24$ for η corresponding to the central WMAP value. We obtain

$$\frac{\Delta\alpha_{\rm em}(m_e)}{\alpha_{\rm em}(m_e)} = -2.7\ \times 10^{-4}. \tag{7.50}$$

7.6 Some Remarks

In this chapter we have constructed a way how to separate BBN abundance prediction and the dependence of the 'nuclear physics parameters' from the 'particle physics parameters' and the underlying GUT model. The benefit is that improvements on the BBN predictions only change the coefficients $c_i^{(X)}$. The $c_i^{(G)}$ can then be recomputed via equation (7.8). Likewise, if we have a new theory relating the deuteron binding energy to the particle physics parameters this will change the entries in the matrix f_{ik}, but not the $c_i^{(X)}$. Constraining GUT models with primordial element abundances is now fairly simple and can be adapted quickly once new information is available.

Excluding very particular cancellations we may infer from the approximate agreement between the WMAP-prediction and the observations of $Y_{\rm He}$ a bound

$|\Delta\alpha_{\rm em}/\alpha_{\rm em}(z = 10^{10})| <$ a few times 10^{-3}. A typical size of a coupling variation that could explain the present discrepancy between WMAP and the observed $Y_{\rm He}$ would be in a range $\Delta\alpha_{\rm em}/\alpha_{\rm em} \approx (2 - 10) \times 10^{-4}$.

Our scheme would of course greatly benefit from a full numerical computation of the 'nuclear physics coefficients' in table 7.1 using a numerical BBN code. In this case, an extension of this analysis to the other light elements deuterium, ^{3}He and lithium would become possible and be able to break possible degeneracies and constraints on models would improve significantly.

– 8 –

Conclusions

The most exciting phrase to hear in science, the one that heralds new discoveries, is not "Eureka!" but rather "hmm... that's funny..."

Isaac Asimov

We hope that we have convinced the reader that cosmology has entered the era of precision measurements and can no longer be termed a 'field of physics with logarithmic error bars'. Even though each cosmological probe has its own systematics, the picture when all available data is combined is surprisingly consistent. The statistical errors grow less and less as the sample sizes of supernovae, galaxies and CMB measurements increase. A number of experiments is planned or currently taking data to improve our knowledge of the universe. Some of these experiments are using new approaches to determine cosmological quantities, such as weak lensing studies. Considering past experience it is possible that our view of the universe may change dramatically in the future. The nature of dark energy is yet unknown, and though all the data is consistent with a cosmological constant, this situation could change in a moment with new experimental data. An equation of state different from -1 would instantly rule out the cosmological constant as the dark energy and point to something else. Quintessence is a good candidate, as there are a lot less theoretical problems associated with it and it also fits all present data. Another equally mysterious component is dark matter, which has eluded direct detection to this day. Even though there are good theoretical arguments that dark matter is a WIMP this need not mean that nature has chosen this option. It could be something quite different.

Considering the fact that we don't know what 95 % of the energy density of the universe are one might be tempted to say that our model is completely wrong and we need to look for something else. However, it is unlikely that

we are on the completely wrong path. Current experiments probe very different epochs and quantities. Big bang nucleosynthesis involves mainly nuclear physics at very early times $z \sim 10^{10}$ and very high energy density. Cosmic microwave background anisotropy experiments are concerned with atomic physics at early times $z \sim 1100$ and moderately high temperatures. Lyman-α forest data probes gravitational physics at $z \sim 3$. The supernovae Ia measurements determine the expansion history up to $z \sim 1.7$. Galaxy surveys test our understanding of gravitational collapse and structure growth at times close to today $z \sim 0.1$. The Hubble flow has been measured in the local universe, at $z \sim 0$. And all of these different observations can be accomodated with only one model. It would be a cruel trick of nature indeed if this was just a coincidence. However, what is to be desired is a more fundamental understanding of dark energy and dark matter. In this respect we need to be on the lookout in order not to value one model above the other without good reason. The popularity of the ΛCDM model is mainly due to its simplicity and goodness of fit, but, as we emphasized previously, a cosmological constant is difficult to put into a fundamental framework. One needs to be able to compare new models with experiments and constantly check if old models are consistent with new data. Quintessence cosmology can also be accomodated with the data. A very good way to decide whether the dark energy is due to a cosmological constant or something else is by measuring the equation of state. This may be determined by observations of the expansion history by taking 'snapshots' of the large scale structure power spectrum at different redshifts via weak lensing or supernovae observations. Especially weak lensing studies can place stringent constraints on the equation of state and will therefore most likely be a very important cosmological probe in the future. Measurements of B-mode polarization in the CMB would enable us to determine the spectrum of primordial gravitational waves and allow to constrain models of inflation and their energy scale.

In this work we have presented one way how to constrain models. We introduced the CMBEASY software which can compute model predictions for a number of cosmological models quickly and accurately. It is written in the object-oriented C++ programming language and its modular structure lends itself to easy modifications of the code for new models and observable quantities. The code is constantly upgraded and improved. In addition, the ANALYZETHIS! package included in CMBEASY contains a number of the latest data sets. We have discussed an implementation of Markov Chain Monte Carlo simulation and the basic theory behind it. As an illustration we discussed a ΛCDM cosmology and showed the constraints on its five parameters, along with two-dimensional marginalized likelihoods. But we should also mention that the CMBEASY code is only concerned with the linear regime. A lot of information can be extracted from

non-linear observations. For this one uses N-body codes and hydrodynamical simulations, but the computing time required makes it impractical to determine statistical properties of model parameters. Usually one gives a fitting formula with a number of coefficients as result, but these are model dependent. But the linear regime may be used to first find model parameter values and use these in the N-body code. If there is then any strong disagreement with the simulation results and observational data one may rule out the model.

Turning to the investigation of cosmological models we used these tools to investigate a dark matter model. We cannot be sure that dark matter is a WIMP unless it has been directly measured. Therefore we investigated a model where we wanted to see whether the equation of state of dark matter is tightly constrained by cosmological observations. In this respect we did not exclude a negative equation of state from our considerations. It turned out that there is no unique way to model this and we had to construct two models which are more or less ad-hoc. The model without entropy production is tightly constrained and unlikely to be realistic. For a negative equation of state it lead to excessive growth of structures at small scales and this is inconsistent with measurements. The reason why a negative equation of state was allowed in this model was due to the fact that we only used the linear part of the galaxy power spectrum. Had we taken into account the nonlinear part as well the constraints would be much tighter. But we also found that the model with vanishing adiabatic sound speed can be accomodated with present data, and so one should be careful when one assumes that the equation of state of dark matter has to be zero. It would be interesting to find a motivation how the equation of state of dark matter can be negative. This could be possible with non-linear scalar field fluctuations.

The disagreement between theory and experiment concerning primordial element abundances, though most likely due to systematics, may indicate something deeper. There is also a (disputed) claim of an observation of a variation in the fine structure constant over cosmological timescales. This led us to considering the effect in a variation in the fundamental couplings on predictions of light element abundances. Since constraints on the variation of fundamental couplings depend on the model chosen we have developed a model-independent approach that may be readily used to determine the BBN prediction for any model relating the fundamental couplings to each other. For illustration we considered a simple GUT model where we kept the variation between the weak and GUT scale fixed. Our approach can be easily modified once new data becomes available or from improved estimates on the nuclear physics-fundamental physics parameters connection.

To sum up, the future of cosmology will be very interesting given the present problems and upcoming experiments. What the true nature of dark energy and

dark matter is remains to be seen. It may be that our view of the universe will be quite different in ten years, and yet we consider it unlikely that the basic picture will change very much. Even though we will be looking deeper and deeper into space, observing ever fainter objects, cosmology's future will most likely be a very bright one.

A

Nuclear Reaction Rates

The temperature in nuclear reaction rates for BBN computation is given in units of 10^9 K which we will label here with T_9. Rates are from a number of sources: NACRE [220], Cyburt, Fields and Olive (CFO) [151] and Smith, Kawano and Malaney (SKM) [212].

We employ the scheme of Bergström, Iguri and Rubinstein (BIR) [221] to find the change in reaction rates with a variation of $\alpha_{\rm em}$ and we include the improvements of Nollett and Lopez [222]; modification factors are labled according to the following scheme, where $\delta \equiv \Delta\alpha_{\rm em}/\alpha_{\rm em}$:
(a) Coulomb normalization $(1+\delta)$,
(b) Radiative capture process $(1+\delta)$,
(c) Final-state Coulomb interactions $(1+n\,\delta)$,
with n depending on the specific process. Since the NACRE rates have a polynomial expansion in terms of T_9 while BIR use an expansion in terms of $T_9^{1/3}$, we first fit the NACRE polynomial $p_{\rm NACRE}(T_9)$ to a BIR polynomial $p_{\rm BIR}(T_9)$ in order to be able to use the BIR treatment. We minimize the relative differences, that is the ratio

$$\left(p_{\rm NACRE}(T_9) - p_{\rm BIR}(T_9)\right)/p_{\rm NACRE}(T_9). \tag{A.1}$$

For the neutron-induced reaction $n + {}^3He \longrightarrow p + t$ there is no need for the BIR treatment, hence we do not have to fit the polynomial.
Reaction rates are given in units of $\mathrm{cm}^{-3}\mathrm{s}^{-1}\mathrm{mole}^{-1}$.

1. $n + {}^3He \longrightarrow p + t$

$$7.35\times10^8\,(1+0.3\,\delta)\left(1-0.776\,T_9^{1/2}+0.538\,T_9-0.102\,T_9^{3/2}\right). \tag{A.2}$$

source: CFO
corrections: c

2. $d + t \longrightarrow n + {}^4He$

$$
\begin{aligned}
&8.12 \times 10^8 \, (1+\delta)^2 \, T_9^{-0.712} \exp[-0.506/T_9] + \\
&8.29 \times 10^{10} \, (1+\delta)^{7/3} \, T_9^{-2/3} \exp\left[-4.524 \, (1+\delta)^{2/3} \, T_9^{-1/3}\right. \\
&\left.-156.25 \, (1+\delta)^2 \, T_9^2\right] \Big(1 + 19.76 \, (1+\delta)^{-2/3} \, T_9^{1/3} - 204.4 \, (1+\delta)^{2/3} \, T_9^{2/3} \\
&+745.3 \, T_9 - 1120.5 \, (1+\delta)^{4/3} \, T_9^{4/3} + 748.1 \, (1+\delta)^{2/3} \, T_9^{5/3}\Big). \qquad \text{(A.3)}
\end{aligned}
$$

source: NACRE
corrections: a, b

3. $p + d \longrightarrow {}^3He + \gamma$

$$
\begin{aligned}
&2.58 \times 10^3 \, (1+\delta)^{7/3} \, T_9^{-2/3} \exp\left[-3.721 \, (1+\delta)^{2/3} \, T_9^{-1/3}\right] \times \\
&\Big(1 + 0.107 \, (1+\delta)^{-2/3} \, T_9^{1/3} - 0.674 \, (1+\delta)^{2/3} \, T_9^{2/3} + 5.452 \, T_9 \\
&-1.488 \, (1+\delta)^{4/3} \, T_9^{4/3} + 0.681 \, (1+\delta)^{2/3} \, T_9^{5/3}\Big). \qquad \text{(A.4)}
\end{aligned}
$$

source: NACRE
corrections: a, b

4. $d + d \longrightarrow n + {}^3He$

$$
\begin{aligned}
&4.67 \times 10^8 \, (1+\delta)^{4/3} \, T_9^{-2/3} \exp\left[-4.259 \, (1+\delta)^{2/3} \, T_9^{-1/3}\right] \times \\
&\Big(1 + 0.744 \, (1+\delta)^{-2/3} \, T_9^{1/3} - 3.538 \, (1+\delta)^{2/3} \, T_9^{2/3} + 6.770 \, T_9 \\
&-3.663 \, (1+\delta)^{4/3} \, T_9^{4/3} + 0.672 \, (1+\delta)^{2/3} \, T_9^{5/3}\Big). \qquad \text{(A.5)}
\end{aligned}
$$

source: NACRE
corrections: a

5. $d + d \longrightarrow p + t$

$$
\begin{aligned}
&4.66 \times 10^8 \, (1+\delta)^{4/3} (1 - 0.16 \, \delta) \, T_9^{-2/3} \exp\left[-4.259 \, (1+\delta)^{2/3} \, T_9^{-1/3}\right] \times \\
&\Big(1 + 0.383 \, (1+\delta)^{-2/3} \, T_9^{1/3} - 1.781 \, (1+\delta)^{2/3} \, T_9^{2/3} + 3.565 \, T_9 \\
&-1.762 \, (1+\delta)^{4/3} \, T_9^{4/3} + 0.301 \, (1+\delta)^{2/3} \, T_9^{5/3}\Big). \qquad \text{(A.6)}
\end{aligned}
$$

source: NACRE
corrections: a, c

6. $d + {}^3He \longrightarrow p + {}^4He$

$$
\begin{aligned}
& 5.212 \times 10^8 \, T_9^{-1/2} \exp[-1.762/T_9] + \\
& 5.021 \times 10^{10} (1+\delta)^{4/3} (1 - 0.09\,\delta) \, T_9^{-2/3} \times \\
& \exp\left[-7.144\,(1+\delta)^{2/3} \, T_9^{-1/3} - (1+\delta)^2 \, (T_9/0.270)^2 \right] \times \\
& \Big(1 + 0.058\,(1+\delta)^{-2/3} \, T_9^{1/3} + 0.603\,(1+\delta)^{2/3} \, T_9^{2/3} + 0.245\,T_9 \\
& + 6.97\,(1+\delta)^{4/3} \, T_9^{4/3} + 7.19\,(1+\delta)^{2/3} \, T_9^{5/3} \Big).
\end{aligned}
\tag{A.7}
$$

source: SKM
corrections: a, c

B

Conventions, Constants and Symbols

B.1 Conventions

- We use signature $(-,+,+,+)$ for the metric. For particles with non-vanishing mass we have therefore $ds^2 < 0$ and the four-velocity is normalized $u^\mu u_\mu = -1$.
- We only consider spatially flat universes, $K = 0$ and $\Omega_{tot} = 1$.
- $c = \hbar = k_B = 1$ and we take the reduced Planck mass $M_{\bar{p}}^{-2} = 8\pi G_N$.
- We employ the Einstein summation convention. Greek indices run from $0 \ldots 3$ and latin indices (also referred to as spatial indices) run from $1 \ldots 3$.
- Derivatives with respect to conformal time $d\tau = dt/a$ are labled $\frac{df}{d\tau} = f'$ while those with respect to normal time t are labled $\frac{df}{dt} = \dot{f}$.
- Quantities at present time are labled with '(0)' as superscript or '0' as subscript.
- The covariant derivative for a tensor f will be labled by $f_{;\mu}$, partial derivatives by $f_{,\mu}$.
- For derivatives of the quintessence potential $U(\phi)$ with respect to the field we use the shorthand $\frac{dU(\phi)}{d\phi} = U_{,\phi}$.
- The determinant of the metric tensor g is defined by $g = \det g_{\mu\nu}$.
- The Christoffel symbols are

$$\Gamma^\mu_{\alpha\beta} = \frac{1}{2} g^{\mu\sigma} \left(g_{\sigma\beta,\alpha} + g_{\alpha\sigma,\beta} - g_{\alpha\beta,\sigma} \right) , \tag{B.1}$$

and the Riemann tensor is

$$R^{\mu}{}_{\nu\sigma\rho} = \Gamma^{\mu}_{\nu\rho,\sigma} - \Gamma^{\mu}_{\nu\sigma,\rho} + \Gamma^{\lambda}_{\nu\rho}\Gamma^{\mu}_{\lambda\sigma} - \Gamma^{\lambda}_{\nu\sigma}\Gamma^{\mu}_{\lambda\rho}. \tag{B.2}$$

The Einstein equations are given by

$$G_{\mu\nu} = R_{\mu\nu} - \frac{1}{2}g_{\mu\nu}R = M_{\bar{p}}^{-2}T_{\mu\nu}. \tag{B.3}$$

- Except for the gauge-dependent metric quantities A, B, H_T, H_L, gauge-dependent quantities are labled by lower case letters $\delta, v, \chi \ldots$
- Gauge-invariant quantities are denoted by uppercase letters $\Delta, V, X, \ldots$
- The reaction rate for the reaction $a + b \rightarrow c + d$ is denoted by $[abcd]$.

B.2 ΛCDM Concordance Model

We use a reference model ('ΛCDM best fit model', 'concordance model') for illustrative purposes throughout the text. It is a pure ΛCDM cosmology and is taken from Table 4 column 7 of Tegmark et al. [29], except that we take $h = 0.7$ instead of specifying Ω_Λ as a free parameter. For all numerical computations we use the parameters

$$\Omega_b h^2 = 0.0228, \tag{B.4}$$
$$\Omega_{CDM} h^2 = 0.123, \tag{B.5}$$
$$h = 0.7, \tag{B.6}$$
$$\tau = 0.104, \tag{B.7}$$
$$n_s = 0.966. \tag{B.8}$$

The difference in parameter constraints between this reference model and our example discussed in section 5.4 is due to the fact that Tegmark et al. used the SNe Ia compilation of Tonry et al. [223] while we used the newer compilation of Riess et al. [6]. We also use a different CMB data set than Tegmark et al. Nevertheless, there is no reason for concern as both results agree quite well and there is no indication that only one data set has significant impact on the parameter constraints.

B.3 Constants and Conversion Factors

Most of these values are taken from the Particle Data Group [114]:

$$M_{\bar{p}} = 2.436 \times 10^{18}\ \text{GeV}$$

$$
\begin{aligned}
&= 3.809 \times 10^{56}\ \mathrm{Mpc}^{-1} \\
B_d &= 2.225\ \mathrm{MeV} \\
\tau_n &= 885.7\ \mathrm{s} \\
m_n &= 939.565\ \mathrm{MeV} \\
Q &= 1.293\ \mathrm{MeV} \\
G_F &= 1.16639 \times 10^{-11}\ \mathrm{MeV}^{-2} \\
m_e &= 0.5110\ \mathrm{MeV} \\
H_0 &= 3.336 \times 10^{-4} h\ \mathrm{Mpc}^{-1}
\end{aligned}
$$

Conversion factors:

$$
\begin{aligned}
1\ \mathrm{Mpc} &= 3.086 \times 10^{16}\ \mathrm{m} \\
&= 1.0293 \times 10^{14}\ \mathrm{s} \\
&= 3.262 \times 10^{6}\ \mathrm{a} \\
&= 1.5637 \times 10^{38}\ \mathrm{GeV}^{-1} \\
1\ \mathrm{MeV} &= 11.605 \times 10^{9}\ \mathrm{K} \\
10^9\ \mathrm{K} &= 86.173\ \mathrm{keV} \\
1\ \mathrm{s} &= 1.128 \times 10^{19}\ \mathrm{MeV} \\
&= 1.309 \times 10^{29}\ \mathrm{K}
\end{aligned}
$$

B.4 Symbols

Symbol	Meaning
a	scale factor
A	gauge-dependent perturbation in $\tilde{g}_{00}$, see eq. (3.5)
B	gauge-dependent perturbation in $\tilde{g}_{0i}$, see eq. (3.6)
B_d	deuteron binding energy
c^2_{ad}	adiabatic sound speed, see eq. (3.33)
c_s^2	background sound speed $c_s^2 = p'/\rho'$
χ	quintessence field
δ	gauge-dependent energy density perturbation, see eq. (3.11)
Δ	gauge-invariant energy density perturbation, see eq. (3.28)
d_L	luminosity distance, see eq. (2.32)
g	defined by $g \equiv \det(g_{\mu\nu})$
Γ	gauge-invariant entropy production rate, see eq. (3.32)
h	defined by $H_0 \equiv 100\, h$ km sec^{-1} Mpc^{-1}
	…continued on next page…

	…continued from previous page …
H	Hubble parameter $H \equiv \dot{a}/a$
$\mathcal{H}$	conformal Hubble parameter $\mathcal{H} \equiv a'/a$
H_0	Hubble constant
H_L	gauge-dependent perturbation in the trace of $\tilde{g}_{ij}$, see eq. (3.7)
H_T	gauge-dependent traceless part of the perturbation in $\tilde{g}_{ij}$, see eq. (3.7)
$k(\chi)$	kinetic term, see eq. (2.21)
$\mathcal{L}$	Lagrangian
$\mathcal{L}_m$	matter Lagrangian
Λ	cosmological constant
$L(x\|\theta)$	likelihood of measuring x when parameters θ are given
$M_{\bar{p}}$	reduced Planck mass $M_{\bar{p}}^{-2} \equiv 8\pi G_N$
n_s	scalar spectral index, see eq. (3.51)
Ω_x	contribution of species x to the total energy density
p	pressure
$P(\theta)$	prior on the parameters θ
ϕ	homogenous part of the quinessence field χ
Φ	gauge-invariant gravitational potential, see eq. (3.34)
π_L	gauge-dependent pressure perturbation, see eq. (3.14)
π_T	anisotropic stress, see eq. (3.14)
Π	anisotropic stress, $\Pi \equiv \pi_T$
$\tilde{\Pi}$	reduced anisotropic stress, $\tilde{\Pi} = \Pi/x^2$
$\pi(\theta)$	posterior probability distribution of θ
P_L	gauge-invariant pressure perturbation, see eq. (3.30)
Ψ	gauge-invariant gravitational potential, see eq. (3.35)
Q	neutron-proton mass difference
ρ	energy density
t	normal time
τ	conformal time defined by $d\tau \equiv dt/a$; also optical depth
τ_n	neutron decay constant
$U(\chi)$	quintessence field self-interaction potential
v	gauge-dependent velocity perturbation, see eq. (3.13)
V	gauge-invariant velocity perturbation, see eq. (3.27)
$\tilde{V}$	reduced velocity perturbation $\tilde{V} \equiv V/x$
w	equation of state $w \equiv p/\rho$
X	gauge-invariant scalar field perturbation, see eq. (3.42)
Y	harmonic function satisfying $\Delta Y = -k^2 Y$
Y_i	abundance of element i
z	redshift, see eq. (2.14)

Bibliography

[1] A. Einstein, Sitzungsber. Preuss. Akad. Wiss. Berlin (Math. Phys.) **1917**, 142 (1917).

[2] A. Friedmann, Z. Phys. **10**, 377 (1922).

[3] E. Hubble, Proc. Nat. Acad. Sci. **15**, 168 (1929).

[4] G. F. Smoot *et al.*, Astrophys. J. **396**, L1 (1992).

[5] D. N. Spergel *et al.*, Astrophys. J. Suppl. **148**, 175 (2003), [astro-ph/0302209].

[6] Supernova Search Team, A. G. Riess *et al.*, Astrophys. J. **607**, 665 (2004), [astro-ph/0402512].

[7] W. L. Freedman *et al.*, Astrophys. J. **553**, 47 (2001), [astro-ph/0012376].

[8] W. J. Percival *et al.*, Mon. Not. Roy. Astron. Soc. **327**, 1297 (2001), [astro-ph/0105252].

[9] SDSS, M. Tegmark *et al.*, Astrophys. J. **606**, 702 (2004), [astro-ph/0310725].

[10] Supernova Cosmology Project, S. Perlmutter *et al.*, Astrophys. J. **517**, 565 (1999), [astro-ph/9812133].

[11] Supernova Search Team, A. G. Riess *et al.*, Astron. J. **116**, 1009 (1998), [astro-ph/9805201].

[12] Supernova Search Team, P. M. Garnavich *et al.*, Astrophys. J. **509**, 74 (1998), [astro-ph/9806396].

[13] Supernova Search Team, B. P. Schmidt *et al.*, Astrophys. J. **507**, 46 (1998), [astro-ph/9805200].

[14] C. Wetterich, Nucl. Phys. **B302**, 668 (1988).

[15] B. Ratra and P. J. E. Peebles, Phys. Rev. **D37**, 3406 (1988).

[16] U. Seljak and M. Zaldarriaga, Astrophys. J. **469**, 437 (1996), [astro-ph/9603033].

[17] A. Lewis, A. Challinor, and A. Lasenby, Astrophys. J. **538**, 473 (2000), [astro-ph/9911177].

[18] M. Doran, (2003), [astro-ph/0302138].

[19] N. Christensen, R. Meyer, L. Knox, and B. Luey, Class. Quant. Grav. **18**, 2677 (2001), [astro-ph/0103134].

[20] M. Doran and C. M. Mueller, JCAP **09**, 003 (2004), [astro-ph/0311311].

[21] S. Weinberg, *Gravitation and Cosmology* (John Wiley and Sons, New York, 1972).

[22] E. W. Kolb and M. S. Turner, *The Early Universe* (Addison-Wesley, 1990), Frontiers in physics, 69.

[23] L. D. Landau and E. M. Lifshitz, *Lehrbuch der Theoretischen Physik, Bd. II: Klassische Feldtheorie* (Akademie-Verlag, Berlin, 1987).

[24] C. W. Misner, K. Thorne, and J. Wheeler, *Gravitation* (W. H. Freeman, New York, 1973).

[25] A. R. Liddle and D. H. Lyth, *Cosmological inflation and large-scale structure* (Cambridge University Press, Cambridge, 2000).

[26] D. J. Fixsen *et al.*, Astrophys. J. **473**, 576 (1996), [astro-ph/9605054].

[27] C. L. Bennett *et al.*, Astrophys. J. Suppl. **148**, 1 (2003), [astro-ph/0302207].

[28] M. Fukugita and P. J. E. Peebles, Astrophys. J. **616**, 643 (2004), [astro-ph/0406095].

[29] SDSS, M. Tegmark *et al.*, Phys. Rev. **D69**, 103501 (2004), [astro-ph/0310723].

[30] J. C. Mather *et al.*, ApJ **512**, 511 (1999).

[31] V. Barger, D. Marfatia, and A. Tregre, Phys. Lett. **B595**, 55 (2004), [hep-ph/0312065].

[32] K. Ichikawa, M. Fukugita, and M. Kawasaki, Phys. Rev. **D71**, 043001 (2005), [astro-ph/0409768].

[33] S. W. Allen, R. W. Schmidt, and S. L. Bridle, Mon. Not. Roy. Astron. Soc. **346**, 593 (2003), [astro-ph/0306386].

[34] S. Hannestad, JCAP **0305**, 004 (2003), [astro-ph/0303076].

[35] R. H. Brandenberger, A. Mazumdar, and M. Yamaguchi, Phys. Rev. **D69**, 081301 (2004), [hep-ph/0401239].

[36] P. Crotty, J. Lesgourgues, and S. Pastor, Phys. Rev. **D69**, 123007 (2004), [hep-ph/0402049].

[37] F. Zwicky, Helv. Phys. Acta **6**, 110 (1933).

[38] G. Bertone, D. Hooper, and J. Silk, Phys. Rept. **405**, 279 (2005), [hep-ph/0404175].

[39] The EDELWEISS, V. Sanglard *et al.*, (2005), [astro-ph/0503265].

[40] G. Angloher *et al.*, Astropart. Phys. **23**, 325 (2005), [astro-ph/0408006].

[41] CDMS, D. S. Akerib *et al.*, Phys. Rev. Lett. **93**, 211301 (2004), [astro-ph/0405033].

[42] R. Bernabei *et al.*, Riv. Nuovo Cim. **26N1**, 1 (2003), [astro-ph/0307403].

[43] S. Weinberg, Rev. Mod. Phys. **61**, 1 (1989).

[44] C. Wetterich, Nucl. Phys. **B302**, 645 (1988).

[45] A. Vilenkin, Phys. Rept. **121**, 263 (1985).

[46] A. A. Starobinsky, Phys. Lett. **B91**, 99 (1980).

[47] S. M. Carroll, V. Duvvuri, M. Trodden, and M. S. Turner, Phys. Rev. **D70**, 043528 (2004), [astro-ph/0306438].

[48] R. R. Caldwell, Phys. Lett. **B545**, 23 (2002), [astro-ph/9908168].

[49] P. J. E. Peebles and B. Ratra, Rev. Mod. Phys. **75**, 559 (2003), [astro-ph/0207347].

[50] L. P. Grishchuk, (2005), [gr-qc/0504018].

[51] K. M. Smith, W. Hu, and M. Kaplinghat, Phys. Rev. **D70**, 043002 (2004), [astro-ph/0402442].

[52] J. Delabrouille, Astrophys. Space Sci. **290**, 87 (2004), [astro-ph/0307549].

[53] C. Wetterich, Astron. Astrophys. **301**, 321 (1995), [hep-th/9408025].

[54] R. R. Caldwell, R. Dave, and P. J. Steinhardt, Phys. Rev. Lett. **80**, 1582 (1998), [astro-ph/9708069].

[55] I. Zlatev, L.-M. Wang, and P. J. Steinhardt, Phys. Rev. Lett. **82**, 896 (1999), [astro-ph/9807002].

[56] P. J. Steinhardt, L.-M. Wang, and I. Zlatev, Phys. Rev. **D59**, 123504 (1999), [astro-ph/9812313].

[57] L. Amendola, Phys. Rev. **D62**, 043511 (2000), [astro-ph/9908023].

[58] C. Brans and R. H. Dicke, Phys. Rev. **124**, 925 (1961).

[59] C. Armendariz-Picon, V. Mukhanov, and P. J. Steinhardt, Phys. Rev. **D63**, 103510 (2001), [astro-ph/0006373].

[60] A. Hebecker and C. Wetterich, Phys. Lett. **B497**, 281 (2001), [hep-ph/0008205].

[61] R. R. Caldwell, M. Doran, C. M. Mueller, G. Schaefer, and C. Wetterich, Astrophys. J. **591**, L75 (2003), [astro-ph/0302505].

[62] P. J. E. Peebles and B. Ratra, Astrophys. J. **325**, L17 (1988).

[63] R. R. Caldwell and M. Doran, Phys. Rev. **D69**, 103517 (2004), [astro-ph/0305334].

[64] A. Albrecht and C. Skordis, Phys. Rev. Lett. **84**, 2076 (2000), [astro-ph/9908085].

[65] C. Skordis and A. Albrecht, Phys. Rev. **D66**, 043523 (2002), [astro-ph/0012195].

[66] P. Brax and J. Martin, Phys. Lett. **B468**, 40 (1999), [astro-ph/9905040].

[67] T. Barreiro, E. J. Copeland, and N. J. Nunes, Phys. Rev. **D61**, 127301 (2000), [astro-ph/9910214].

[68] S. C. C. Ng, N. J. Nunes, and F. Rosati, Phys. Rev. **D64**, 083510 (2001), [astro-ph/0107321].

[69] V. Sahni and L.-M. Wang, Phys. Rev. **D62**, 103517 (2000), [astro-ph/9910097].

[70] J. Weller and A. Albrecht, Phys. Rev. **D65**, 103512 (2002), [astro-ph/0106079].

[71] J. Weller and A. Albrecht, Phys. Rev. Lett. **86**, 1939 (2001), [astro-ph/0008314].

[72] B. F. Gerke and G. Efstathiou, Mon. Not. Roy. Astron. Soc. **335**, 33 (2002), [astro-ph/0201336].

[73] P. S. Corasaniti and E. J. Copeland, Phys. Rev. **D67**, 063521 (2003), [astro-ph/0205544].

[74] C. Wetterich, Phys. Lett. **B594**, 17 (2004), [astro-ph/0403289].

[75] J. M. Bardeen, Phys. Rev. **D22**, 1882 (1980).

[76] H. Kodama and M. Sasaki, Prog. Theor. Phys. Suppl. **78**, 1 (1984).

[77] V. F. Mukhanov, H. A. Feldman, and R. H. Brandenberger, Phys. Rept. **215**, 203 (1992).

[78] R. Durrer, J. Phys. Stud. **5**, 177 (2001), [astro-ph/0109522].

[79] A. Lewis, Phys. Rev. **D70**, 043518 (2004), [astro-ph/0403583].

[80] R. Durrer, *Gauge-invariant cosmological perturbation theory*, PhD thesis, Universität Zürich, 1988.

[81] Y.-T. Lin and B. D. Wandelt, (2004), [astro-ph/0409734].

[82] A. Kosowsky, Ann. Phys. **246**, 49 (1996).

[83] J. M. Stewart, *Non-equilibrium relativistic kinetic theory* (Springer, Berlin, 1971), Lecture Notes in Physics, Vol.10.

[84] W. Hu and M. J. White, Phys. Rev. **D56**, 596 (1997), [astro-ph/9702170].

[85] W. Hu, U. Seljak, M. J. White, and M. Zaldarriaga, Phys. Rev. **D57**, 3290 (1998), [astro-ph/9709066].

[86] C.-P. Ma and E. Bertschinger, Astrophys. J. **455**, 7 (1995), [astro-ph/9506072].

[87] M. Zaldarriaga and U. Seljak, Phys. Rev. **D55**, 1830 (1997), [astro-ph/9609170].

[88] R. A. Frewin, A. G. Polnarev, and P. Coles, Mon. Not. Roy. Astron. Soc. **266**, L 21 (1994), [astro-ph/9310045].

[89] R. Crittenden, J. R. Bond, R. L. Davis, G. Efstathiou, and P. J. Steinhardt, Phys. Rev. Lett. **71**, 324 (1993), [astro-ph/9303014].

[90] R. G. Crittenden, D. Coulson, and N. G. Turok, Phys. Rev. **D52**, 5402 (1995), [astro-ph/9411107].

[91] Y. B. Zeldovich, Astron. Astrophys. **5**, 84 (1970).

[92] E. R. Harrison, Phys. Rev. **D1**, 2726 (1970).

[93] U. Seljak, N. Sugiyama, M. J. White, and M. Zaldarriaga, Phys. Rev. **D68**, 083507 (2003), [astro-ph/0306052].

[94] M. Doran, C. M. Muller, G. Schafer, and C. Wetterich, Phys. Rev. **D68**, 063505 (2003), [astro-ph/0304212].

[95] G. Schäfer, *Quintessence Cosmology*, PhD thesis, Universität Heidelberg, 2004.

[96] M. Doran, *Theory and Phenomenology of Quintessence*, PhD thesis, Universität Heidelberg, 2002.

[97] R. Durrer, Fund. Cosmic Phys. **15**, 209 (1994).

[98] P. J. E. Peebles and J. T. Yu, Astrophys. J. **162**, 815 (1970).

[99] J. M. Bardeen, P. J. Steinhardt, and M. S. Turner, Phys. Rev. **D28**, 679 (1983).

[100] D. H. Lyth, C. Ungarelli, and D. Wands, Phys. Rev. **D67**, 023503 (2003), [astro-ph/0208055].

[101] D. Wands, K. A. Malik, D. H. Lyth, and A. R. Liddle, Phys. Rev. **D62**, 043527 (2000), [astro-ph/0003278].

[102] J. Martin and D. J. Schwarz, Phys. Rev. **D57**, 3302 (1998), [gr-qc/9704049].

[103] M. Bucher, K. Moodley, and N. Turok, Phys. Rev. **D62**, 083508 (2000), [astro-ph/9904231].

[104] D. Langlois and A. Riazuelo, Phys. Rev. **D62**, 043504 (2000), [astro-ph/9912497].

[105] F. Perrotta and C. Baccigalupi, Phys. Rev. **D59**, 123508 (1999), [astro-ph/9811156].

[106] L. R. W. Abramo and F. Finelli, Phys. Rev. **D64**, 083513 (2001), [astro-ph/0101014].

[107] M. Malquarti and A. R. Liddle, Phys. Rev. **D66**, 123506 (2002), [astro-ph/0208562].

[108] S. Gupta, K. A. Malik, and D. Wands, Phys. Rev. **D69**, 063513 (2004), [astro-ph/0311562].

[109] M. Bucher, K. Moodley, and N. Turok, Phys. Rev. Lett. **87**, 191301 (2001), [astro-ph/0012141].

[110] K. Enqvist, H. Kurki-Suonio, and J. Valiviita, Phys. Rev. **D62**, 103003 (2000), [astro-ph/0006429].

[111] L. Amendola, C. Gordon, D. Wands, and M. Sasaki, Phys. Rev. Lett. **88**, 211302 (2002), [astro-ph/0107089].

[112] R. Trotta, A. Riazuelo, and R. Durrer, Phys. Rev. **D67**, 063520 (2003), [astro-ph/0211600].

[113] K. Moodley, M. Bucher, J. Dunkley, P. G. Ferreira, and C. Skordis, Phys. Rev. **D70**, 103520 (2004), [astro-ph/0407304].

[114] Particle Data Group, S. Eidelman *et al.*, Phys. Lett. **B592**, 1 (2004).

[115] Boomerang, P. de Bernardis *et al.*, Nature **404**, 955 (2000), [astro-ph/0004404].

[116] Boomerang, A. E. Lange *et al.*, Phys. Rev. **D63**, 042001 (2001), [astro-ph/0005004].

[117] A. Balbi *et al.*, Astrophys. J. **545**, L1 (2000), [astro-ph/0005124].

[118] Boomerang, C. B. Netterfield *et al.*, Astrophys. J. **571**, 604 (2002), [astro-ph/0104460].

[119] C. Pryke *et al.*, Astrophys. J. **568**, 46 (2002), [astro-ph/0104490].

[120] J. Kovac *et al.*, Nature **420**, 772 (2002), [astro-ph/0209478].

[121] A. Kogut *et al.*, Astrophys. J. Suppl. **148**, 161 (2003), [astro-ph/0302213].

[122] G. Hinshaw *et al.*, Astrophys. J. Suppl. **148**, 135 (2003), [astro-ph/0302217].

[123] C. Dickinson *et al.*, (2004), [astro-ph/0402498].

[124] A. C. S. Readhead *et al.*, Astrophys. J. **609**, 498 (2004), [astro-ph/0402359].

[125] ACBAR, C.-l. Kuo *et al.*, Astrophys. J. **600**, 32 (2004), [astro-ph/0212289].

[126] W. Hu and N. Sugiyama, Astrophys. J. **444**, 489 (1995), [astro-ph/9407093].

[127] V. Mukhanov, (2003), [astro-ph/0303072].

[128] K. Subramanian, (2004), [astro-ph/0411049].

[129] J. R. Pritchard and M. Kamionkowski, (2004), [astro-ph/0412581].

[130] S. Chandrasekhar, *Radiative Transfer* (Dover, New York, 1960).

[131] M. Zaldarriaga, (2003), [astro-ph/0305272].

[132] W. Hu and M. J. White, New Astron. **2**, 323 (1997), [astro-ph/9706147].

[133] L. Verde *et al.*, Astrophys. J. Suppl. **148**, 195 (2003), [astro-ph/0302218].

[134] http://lambda.gsfc.nasa.gov.

[135] A. Slosar, U. Seljak, and A. Makarov, Phys. Rev. **D69**, 123003 (2004), [astro-ph/0403073].

[136] F. Bernardeau, S. Colombi, E. Gaztanaga, and R. Scoccimarro, Phys. Rept. **367**, 1 (2002), [astro-ph/0112551].

[137] L. Verde *et al.*, Mon. Not. Roy. Astron. Soc. **335**, 432 (2002), [astro-ph/0112161].

[138] J. A. Peacock *et al.*, Nature **410**, 169 (2001), [astro-ph/0103143].

[139] A. V. Filippenko, (2003), [astro-ph/0307139].

[140] P. McDonald *et al.*, (2004), [astro-ph/0407377].

[141] P. J. Outram *et al.*, Mon. Not. Roy. Astron. Soc. **348**, 745 (2004), [astro-ph/0310873].

[142] U. Seljak *et al.*, (2004), [astro-ph/0407372].

[143] K. Benabed and L. Van Waerbeke, Phys. Rev. **D70**, 123515 (2004), [astro-ph/0306033].

[144] CLASS, S. T. Myers *et al.*, Mon. Not. Roy. Astron. Soc. **334**, 1 (2002), [astro-ph/0211073].

[145] CLASS, I. W. A. Browne *et al.*, Mon. Not. Roy. Astron. Soc. **341**, 13 (2003), [astro-ph/0211069].

[146] I. Tereno, O. Dore, L. van Waerbeke, and Y. Mellier, (2004), [astro-ph/0404317].

[147] M. Bartelmann and P. Schneider, Phys. Rept. **340**, 291 (2001), [astro-ph/9912508].

[148] L. Van Waerbeke and Y. Mellier, (2003), [astro-ph/0305089].

[149] Y. I. Izotov and T. X. Thuan, Astrophys. J. **602**, 200 (2004), [astro-ph/0310421].

[150] B. D. Fields and K. A. Olive, Astrophys. J. **506**, 177 (1998), [astro-ph/9803297].

[151] R. H. Cyburt, B. D. Fields, and K. A. Olive, Phys. Lett. **B567**, 227 (2003), [astro-ph/0302431].

[152] N. Christensen and R. Meyer, (2000), [astro-ph/0006401].

[153] L. Knox, N. Christensen, and C. Skordis, Astrophys. J. **563**, L95 (2001), [astro-ph/0109232].

[154] A. Kosowsky, M. Milosavljevic, and R. Jimenez, Phys. Rev. **D66**, 063007 (2002), [astro-ph/0206014].

[155] A. Lewis and S. Bridle, Phys. Rev. **D66**, 103511 (2002), [astro-ph/0205436].

[156] W. M. Bolstad, *Introduction to Bayesian Statistics* (John Wiley & Sons, Hoboken, NJ, 2004).

[157] D. Gamerman, *Markov Chain Monte Carlo* (Chapman & Hall, London, 1997).

[158] W. R. Gilks, S. Richardson, and D. J. Spiegelhalter, *Markov Chain Monte Carlo in Practice* (Chapman & Hall, London, 1996).

[159] R. M. Neal, (1993), ftp://ftp.cs.utoronto.ca/pub/radford/review.ps.Z.

[160] L. Tierney, Ann. Stat. **22**, 1701 (1994).

[161] W. K. Hastings, Biometrika **57**, 97 (1970).

[162] N. Metropolis, A. W. Rosenbluth, M. N. Rosenbluth, A. H. Teller, and E. Teller, J. Chem. Phys. **21**, 1087 (1953).

[163] A. Gelman and D. B. Rubin, Stat. Sci. **7**, 457 (1992).

[164] A. Slosar and M. Hobson, (2003), [astro-ph/0307219].

[165] A. G. Riess *et al.*, (2005), [astro-ph/0503159].

[166] C. M. Muller, Phys. Rev. **D71**, 047302 (2005), [astro-ph/0410621].

[167] C. Wetterich, Phys. Rev. **D65**, 123512 (2002), [hep-ph/0108266].

[168] S. Colombi, S. Dodelson, and L. M. Widrow, Astrophys. J. **458**, 1 (1996), [astro-ph/9505029].

[169] M. Davis, F. J. Summers, and D. Schlegel, Nature **359**, 393 (1992).

[170] M. Doran, J.-M. Schwindt, and C. Wetterich, Phys. Rev. **D64**, 123520 (2001), [astro-ph/0107525].

[171] P. G. Ferreira and M. Joyce, Phys. Rev. **D58**, 023503 (1998), [astro-ph/9711102].

[172] C. M. Muller, G. Schafer, and C. Wetterich, Phys. Rev. **D70**, 083504 (2004), [astro-ph/0405373].

[173] P. M. Dirac, Nature **192**, 235 (1937).

[174] P. Jordan, Naturwiss. **25**, 513 (1937).

[175] P. Jordan, Z. Phys. **113**, 660 (1939).

[176] G. R. Dvali and M. Zaldarriaga, Phys. Rev. Lett. **88**, 091303 (2002), [hep-ph/0108217].

[177] C. Wetterich, JCAP **0310**, 002 (2003), [hep-ph/0203266].

[178] J. K. Webb, V. V. Flambaum, C. W. Churchill, M. J. Drinkwater, and J. D. Barrow, Phys. Rev. Lett. **82**, 884 (1999), [astro-ph/9803165].

[179] M. T. Murphy *et al.*, Mon. Not. Roy. Astron. Soc. **327**, 1244 (2001), [astro-ph/0101519].

[180] M. T. Murphy, J. K. Webb, and V. V. Flambaum, Mon. Not. Roy. Astron. Soc. **345**, 609 (2003), [astro-ph/0306483].

[181] R. Srianand, H. Chand, P. Petitjean, and B. Aracil, Phys. Rev. Lett. **92**, 121302 (2004), [astro-ph/0402177].

[182] H. Chand, R. Srianand, P. Petitjean, and B. Aracil, Astron. Astrophys. **417**, 853 (2004), [astro-ph/0401094].

[183] R. Quast, D. Reimers, and S. A. Levshakov, Astron. Astrophys. **415**, L7 (2004), [astro-ph/0311280].

[184] J. N. Bahcall, C. L. Steinhardt, and D. Schlegel, Astrophys. J. **600**, 520 (2004), [astro-ph/0301507].

[185] S. A. Levshakov, M. Centurion, P. Molaro, and S. D'Odorico, (2004), [astro-ph/0408188].

[186] H. Chand, P. Petitjean, R. Srianand, and B. Aracil, (2004), [astro-ph/0408200].

[187] T. Ashenfelter, G. J. Mathews, and K. A. Olive, Phys. Rev. Lett. **92**, 041102 (2004), [astro-ph/0309197].

[188] T. P. Ashenfelter, G. J. Mathews, and K. A. Olive, Astrophys. J. **615**, 82 (2004), [astro-ph/0404257].

[189] K. A. Olive *et al.*, Phys. Rev. **D66**, 045022 (2002), [hep-ph/0205269].

[190] Y. Fujii, Phys. Lett. **B573**, 39 (2003), [astro-ph/0307263].

[191] S. K. Lamoreaux, Phys. Rev. **D69**, 121701 (2004), [nucl-th/0309048].

[192] K. Ichikawa and M. Kawasaki, Phys. Rev. **D69**, 123506 (2004), [hep-ph/0401231].

[193] P. P. Avelino *et al.*, Phys. Rev. **D64**, 103505 (2001), [astro-ph/0102144].

[194] J. J. Yoo and R. J. Scherrer, Phys. Rev. **D67**, 043517 (2003), [astro-ph/0211545].

[195] C. J. Copi, A. N. Davis, and L. M. Krauss, Phys. Rev. Lett. **92**, 171301 (2004), [astro-ph/0311334].

[196] K. Ichikawa and M. Kawasaki, Phys. Rev. **D65**, 123511 (2002), [hep-ph/0203006].

[197] V. F. Dmitriev, V. V. Flambaum, and J. K. Webb, Phys. Rev. **D69**, 063506 (2004), [astro-ph/0310892].

[198] J. P. Kneller and G. C. McLaughlin, Phys. Rev. **D68**, 103508 (2003), [nucl-th/0305017].

[199] J.-P. Uzan, Rev. Mod. Phys. **75**, 403 (2003), [hep-ph/0205340].

[200] S. J. Landau, M. E. Mosquera, and H. Vucetich, (2004), [astro-ph/0411150].

[201] R. V. Wagoner, W. A. Fowler, and F. Hoyle, Astrophys. J. **148**, 3 (1967).

[202] R. V. Wagoner, Astrophys. J. **179**, 343 (1973).

[203] L. Kawano, (1988), FERMILAB-PUB-88-034-A.

[204] L. Kawano, (1992), FERMILAB-PUB-92-004-A.

[205] B. A. Campbell and K. A. Olive, Phys. Lett. **B345**, 429 (1995), [hep-ph/9411272].

[206] E. W. Kolb, M. J. Perry, and T. P. Walker, Phys. Rev. **D33**, 869 (1986).

[207] J. R. Ellis, S. Kalara, K. A. Olive, and C. Wetterich, Phys. Lett. **B228**, 264 (1989).

[208] X. Calmet and H. Fritzsch, Eur. Phys. J. **C24**, 639 (2002), [hep-ph/0112110].

[209] X. Calmet and H. Fritzsch, Phys. Lett. **B540**, 173 (2002), [hep-ph/0204258].

[210] P. Langacker, G. Segre, and M. J. Strassler, Phys. Lett. **B528**, 121 (2002), [hep-ph/0112233].

[211] R. Esmailzadeh, G. D. Starkman, and S. Dimopoulos, Astrophys. J. **378**, 504 (1991).

[212] M. S. Smith, L. H. Kawano, and R. A. Malaney, Astrophys. J. Suppl. **85**, 219 (1993).

[213] R. V. Wagoner, W. A. Fowler, and F. Hoyle, Astrophys. J. **148**, 3 (1967).

[214] M. S. Smith, L. H. Kawano, and R. A. Malaney, Astrophys. J. Suppl. **85**, 219 (1993).

[215] J. Gasser and H. Leutwyler, Phys. Rept. **87**, 77 (1982).

[216] E. Epelbaum, U.-G. Meissner, and W. Gloeckle, Nucl. Phys. **A714**, 535 (2003), [nucl-th/0207089].

[217] S. R. Beane and M. J. Savage, Nucl. Phys. **A717**, 91 (2003), [nucl-th/0208021].

[218] B. S. Pudliner, V. R. Pandharipande, J. Carlson, S. C. Pieper, and R. B. Wiringa, Phys. Rev. **C56**, 1720 (1997), [nucl-th/9705009].

[219] C. Wetterich, Phys. Lett. **B561**, 10 (2003), [hep-ph/0301261].

[220] C. Angulo *et al.*, Nucl. Phys. A **656**, 3 (1999).

[221] L. Bergstrom, S. Iguri, and H. Rubinstein, Phys. Rev. **D60**, 045005 (1999), [astro-ph/9902157].

[222] K. M. Nollett and R. E. Lopez, Phys. Rev. **D66**, 063507 (2002), [astro-ph/0204325].

[223] Supernova Search Team, J. L. Tonry *et al.*, Astrophys. J. **594**, 1 (2003), [astro-ph/0305008].

Acknowledgements

I am grateful for having Prof. Christof Wetterich as my supervisor. He gave me the chance to do research in cosmology where I was free to do what I wanted to do. The lively and creative discussions with him and the cosmology group were always a great way to learn. He was always enthusiastic and helpful in every aspect of my work. Thank you very much for everything.
My thanks go also to Prof. Michael G. Schmidt for his support and for being my co-supervisor all these years and who kindly volunteered to referee this thesis.

I am also grateful to the 'hard core' of the cosmology group, Dr. Gregor Schäfer, Dr. Jörg Jäckel and Dr. Michael Doran who were great friends to have around, work and publish with. Thanks to Michael for letting me become the co-author of CMBEASY, Gregor for being such a constantly enthusiastic and supportive colleague who was also willing to waste time with me to conquer the world and Jörg for being able to discuss all issues from GUTs to zombie movies.

I also thank the rest of the people 'under the roof' for making this one of the most enjoyable times of my life: Juliane Behrend for enduring my constant and sarcastic criticism all these years, Dr. Jan Schwindt, Sebastian Diehl, Armin Steinkasserer, Mona Frommert, Jonas Schmidt, Georg Robbers, Tobias Kleischmidt, Christian Krahl, Lala Adueva and Dr. Frank Steffen. Thanks again to Mona, Juliane and Michael for proof reading this thesis and useful comments.

Thanks to Dr. Eduard Thommes for the discussions about cosmology and astrophysics and without whom this Institute would probably fall apart. My thanks go to Prof. Werner Wetzel as well for providing the Institute with all computer resources. This thesis wouldn't have been possible without them.

Finally, a lot of thanks to my parents for encouragement and support and to my love Kristina for being my continuing source of happiness.

Still round the corner there may wait
A new road or a secret gate;
And though I oft have passed them by,
A day will come at last when I
Shall take the hidden paths that run
West of the Moon, East of the Sun.

J. R. R. Tolkien, The Lord of the Rings